BEST AVAILABLE IMAGES

Defective images within this document are accurate representation of The original documents submitted by the applicant.

Defects in the images may include (but are not limited to):

- BLACK BORDERS
- TEXT CUT OFF AT TOP, BOTTOM OR SIDES
- FADED TEXT
- ILLEGIBLE TEXT
- SKEWED/SLANTED IMAGES
- COLORED PHOTOS
- BLACK OR VERY BLACK AND WHITE DARK PHOTOS
- GRAY SCALE DOCUMENTS

IMAGES ARE BEST AVAILABLE COPY.

As rescanning documents *will not* correct images, please do not report the images to the Image Problem Mailbox.

CHAPTER 4

Structure Analysis by Scattered Ultrasonic Radiation†

K. GOEBBELS

Fraunhofer-Gesellschaft, Institut für zerstörungsfreie Prüfverfahren (IzfP)
D-6600 Saarbrücken 11, West Germany

I. INTRODUCTION

A. Elastic and Anelastic Propagation of Ultrasonic Waves

Quality assurance of materials, components, and plant demands increasing knowledge about microscopic and macroscopic materials structure. For

† This chapter is based on work performed with the support of the Bundesministerium für Forschung und Technologie (Reaktorsicherheits-Forschungsprogramm) and the Europäische Gemeinschaft für Kohle und Stahl (Messwesen in der Eisen- und Stahlindustrie).

finished components; in particular this knowledge must be gained through nondestructive evaluation (NDE) methods. The essential parameters are:

(1) chemical composition and phases;
(2) grain size, distribution of inclusions, and segregates;
(3) texture and anisotropy;
(4) residual stresses, fatigue, plastic deformation, and embrittlement;
(5) locally distributed inhomogeneities, latent defects, and structure anomalies.

Interactions of ultrasound with some of these parameters can be used for the structural characterization of materials, for which Table I contains a general statement.

TABLE I

Structural Features and Related Ultrasound Parameters

Structural features	Ultrasound parameters	Examples
Chemical composition	Velocity, attenuation	Steels, ceramics, plastics
Phase composition	Velocity, attenuation, scattering	Steels: mixed structure of, for example, ferrite/bainite, ferrite/pearlite Ceramics: porosity, glassy phases Composites: fibre content
Grain size	Scattering	Metals, alloys, steels, ceramics
Randomly distributed inclusions, segregations	Absorption	Steels
Anisotropy, texture	Velocity, attenuation	Steels, composites
Residual stress, fatigue, deformation, embrittlement	Velocity, absorption	Steels, composites
Locally distributed heterogeneities	Scattering	Steels: inclusions, segregations, microcracks Ceramics: secondary phases, pores

The present chapter treats, in this context, the propagation of ultrasonic pulses of free longitudinal waves and free shear waves. One can distinguish between an elastic and an anelastic interaction between ultrasound waves and the material:

(1) Elastic behaviour influences the sound velocity, which is directly dependent on the elastic constants of the material. Under certain circumstances velocity is also influenced by the interaction of the propagating wave with the excited scattered ultrasound.
(2) Anelastic behaviour contains those interactions by which energy is withdrawn from the ultrasonic pulse during propagation and transformed, via different mechanisms, into heat or different ultrasound, i.e. ultrasound-scattering. Anelastic behaviour is quantitatively linked to ultrasonic attenuation, absorption, and scattering.

It is therefore possible to make statements about some of the structural parameters of materials, as listed in Table I, by measuring velocity, attenuation, absorption, and scattering. After a short general treatment of these interactions in the following section, the chapter concentrates on structure evaluation by means of ultrasound scattering.

B. Velocity, Attenuation, Absorption and Scattering

1. Velocity

In solid materials there are two possible types of free waves: longitudinal waves (L-), and shear waves (T-) which may be polarized. Hooke's law states that the elastic strain ε is proportional to the stress σ. The proportionality is described by the (reduced) elasticity tensor $\{c_{ij}\}$:

$$\sigma_i = c_{ij} \cdot \varepsilon_j,$$

c_{ij} = elastic moduli ($i,j = 1,\ldots,6$ in accordance with the three spatial directions and the two possible wave modes). (In the above, Einstein's summation convention has been used.)

In the cubic system, which for the sake of simplicity will be assumed in the following, three independent moduli appear, c_{11}, c_{12} and c_{44}. These moduli are directly correlated to the sound velocity and its directional dependence in the single crystal (Truell *et al.*, 1969). Longitudinal wave velocity v_L, along the edge of the cube, direction [100] (ρ = density) is

$$v_L^{[100]} = (c_{11}/\rho)^{\frac{1}{2}},$$

v_L, across a face, direction [110]:

$$v_L^{[110]} = [(c_{11} - \tfrac{1}{2}(c_{11} - c_{12} - 2c_{44}))/\rho]^{\frac{1}{2}},$$

v_L, diagonally through the cube, direction [111]:

$$v_L^{[111]} = [(c_{11} - \tfrac{2}{3}(c_{11} - c_{12} - 2c_{44}))/\rho]^{\frac{1}{2}}.$$

Shear-wave, or transversal-wave, velocity v_T along the edge of the cube is

$$v_T^{[100]} = (c_{44}/\rho)^{\frac{1}{2}},$$

v_T across a face, with different polarization:

$$v_T^F[110],[001] = (c_{44}/\rho)^{\frac{1}{2}},$$

$$v_T^F[110],[1\bar{1}0] = [(c_{44}+\tfrac{1}{2}(c_{11}-c_{12}-2c_{44}))/\rho]^{\frac{1}{2}},$$

v_T diagonally through a cube:

$$v_T^D = [(c_{44}+\tfrac{1}{3}(c_{11}-c_{12}-2c_{44}))/\rho]^{\frac{1}{2}}.$$

The chosen notation makes it clear that for $c_{11}-c_{12}=2c_{44}$ the velocities degenerate, independently of the direction of propagation and vibration, to

$$v_L = (c_{11}/\rho)^{\frac{1}{2}},$$

$$v_T = (c_{44}/\rho)^{\frac{1}{2}}.$$

In other words, the elastic anisotropy, i.e. the directional dependence of the sound velocities in single crystals, is described by the anisotropy factor A:

$$A = c_{11}-c_{12}-2c_{44}. \tag{1}$$

For the isotropic case $A = 0$. This is of importance for ultrasound scattering because scattering is based on the change of acoustic impedance ρv, for the propagating pulse, at phase and grain boundaries.

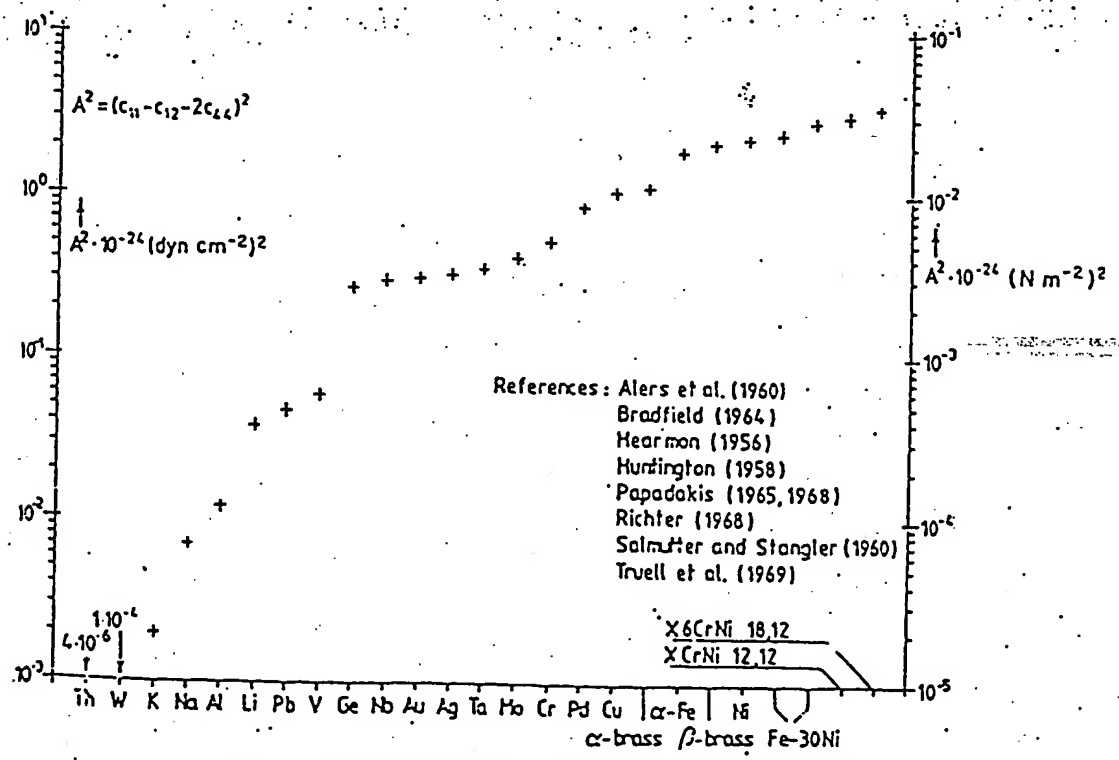

FIG. 1. Anisotropy factors for cubic metals and alloys.

In polycrystalline, quasi-monophasic systems, therefore, there is only scattering excitation when $A \neq 0$. Figure 1 gives values for A^2 for a series

of cubic crystallizing materials. In the literature (e.g. Bhatia, 1967),

$$A' = 2c_{44}/(c_{11}-c_{12})$$

is used alternatively as an anisotropy factor, in this case with the value 1 for isotropic materials. The relation between the sound velocity and the elastic constants of higher order can be neglected with regard to ultrasound scattering. The effect of multiple scattering on the propagation velocity will be treated in a later section.

2. *Attenuation*

The energy loss of a propagating pulse can be described by ultrasonic attenuation. Generally, the attenuation coefficient α for sound pressure is the related parameter, which is composed of the absorption coefficient α_A plus the scattering coefficient α_S (Krautkrämer and Krautkrämer, 1975):

$$\alpha = \alpha_A + \alpha_S. \tag{2}$$

Pulse-echo-measurements show (Fig. 2), for a sequence of backwall echoes

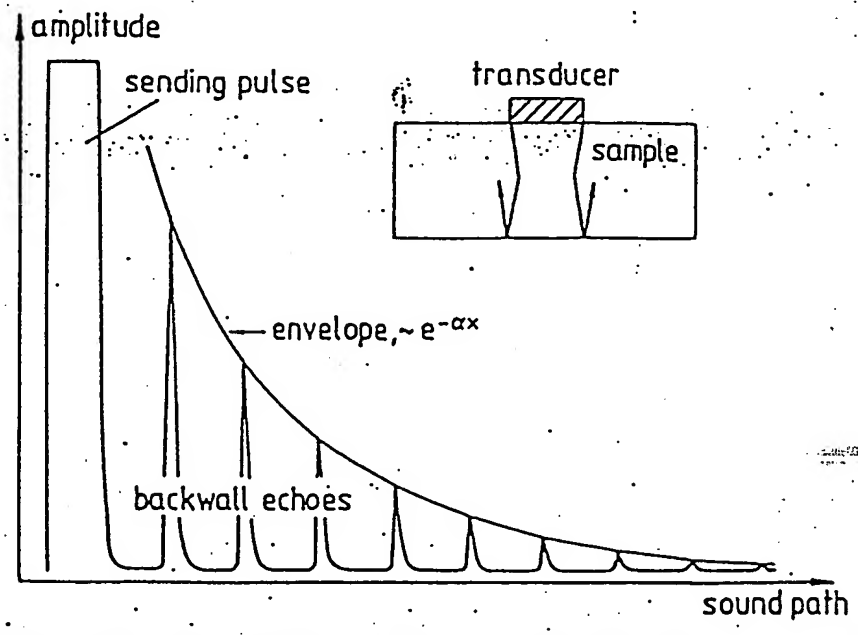

FIG. 2. Determination of attenuation coefficient α by backwall echo sequence, disregarding beam diffraction.

from a homogeneous, parallel-sided material (disregarding beam diffraction), an exponential amplitude function $A(x)$ with increasing sound path x:

$$A(x) = A_0 \exp(-\alpha x). \tag{3}$$

A_0 is the sound amplitude excited in the surface region ($x = 0$).

The necessary correction for diffraction depends on the probe parameters. It is constant in the nearfield and becomes a correction function proportional to $1/x$ in the farfield.

The amplitude of a backwall echo for a locally inhomogeneous structure, i.e. $\alpha = \alpha(x) = \alpha_A(x) + \alpha_S(x)$, measured by a pulse-echo-technique is

$$A(x) = A_0 \exp\left(-2\int_0^{x/2} \alpha(z)\,dz\right). \quad (4)$$

The disadvantages with attenuation measurements are:

(1) Flat, plane-parallel samples are an essential requirement and deviations from plane-parallelism require complex corrections.

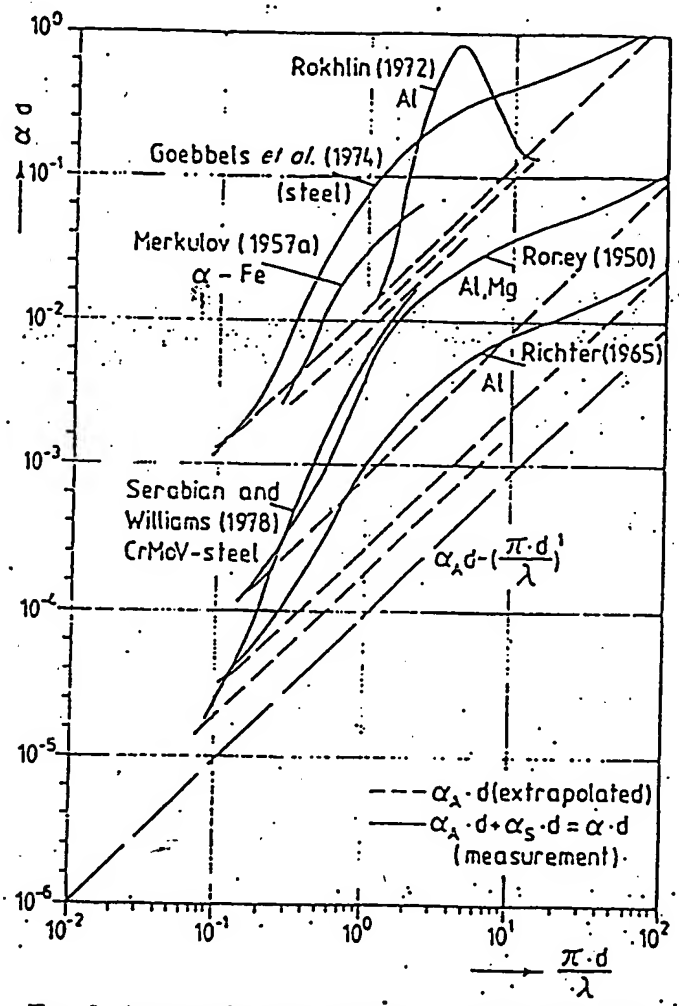

FIG. 3. Attenuation per grains as function of $\pi d/\lambda$.

(2) The measured attenuation coefficient consists of absorption and scattering elements which cannot easily be separated. Figure 3 shows, for various metals, how the absorption, which generally increases

linearly with frequency, is superimposed on the ultrasonic scattering as a function of d/λ (d = mean grain size; λ = ultrasonic wavelength) in the region $0{\cdot}01 \lesssim d/\lambda \lesssim 10$.

(3) The essential disadvantage lies in the fact that such an attenuation coefficient represents an integrated value over the sound path between the upper and lower surface of the sample. Local structure variations, which can greatly influence α, cannot be resolved.

(4) Attenuation measurements depend very much on the coupling between the ultrasonic probe and the sample. Fluctuations in coupling can lead to additional losses which may be greater than the attenuation within the material.

(5) Sound field diffraction represents a further parameter which has to be taken into consideration in attenuation measurements (Krautkrämer and Krautkrämer, 1975). Since in flaw detection with pulse-echo measurements in the farfield the ultrasonic amplitude of a backwall echo is halved with a doubling of the sound path, the beam diffraction correction which is necessary, far exceeds the effect of the attenuation in materials at low frequencies and with fine-grained structures.

Despite these various factors attenuation measurements are widely used in practice since it is possible to find integrated values for structures in a relatively simple manner (Dunegan, 1964; Bratina, 1971; Kopec, 1975; Mercier, 1975; Klinman *et al.*, 1978; Vary, 1978b). Many samples with a different microscopic structure can thus be quickly analysed and qualitatively characterized under constantly maintained experimental conditions. Some of the disadvantages of the technique can be avoided by scattering measurements, as described in Section IIIB, therefore opening ways of differentiated structure studies.

3. Absorption

Many interaction mechanisms, characterized in Table II for metals, contribute to ultrasonic absorption. All of the processes provide important information about solid-state properties in the macroscopic and microscopic regions, down to subatomic dimensions. The supposition here is that the separation and isolation of a single effect is possible through careful choice of experimental conditions such as:

(1) single crystals and polycrystalline materials;
(2) low and high temperatures;
(3) low and high frequencies;
(4) influence of magnetic fields, radiation, or other external factors.

In certain circumstances it is possible to obtain a quantitative description of

the individual absorption effects (see Table II). In practice, however, with polycrystalline metals (such as steels), non-metals (such as ceramics), or organic materials (such as plastics), several of the interaction effects listed in Table II act simultaneously so that quantitative measurements cannot, under normal circumstances, be obtained.

TABLE II

Absorption Processes in Metals and Alloys

Interaction process with	Frequency dependence	Comment
Zero- to three-dimensional lattice defects (e.g. dislocations) (vibration, relaxation, hysteresis with and without amplitude dependence)	$f^2 \ldots f^0$	E.g. Granato–Lücke model (Granato and Lücke, 1956; Seeger and Schiller, 1962)
Magnetic structure (reversible and irreversible Bloch wall movements, reversible rotation processes, change of magnetization by macro-eddy currents)	$f^2 \ldots f^0$	Particularly for ferromagnetic materials (ferritic steel) (Martius and Bratina, 1961) (Franz, 1962)
Thermoelasticity (heat flow from dilatation to compression regions)	f^2	Only for L-waves (Lücke, 1956)
Electrons, phonons		Only for low temperatures and/or high frequencies (GHz) (Truell *et al.*, 1969; Bhatia, 1967)
Electron spin, nucleus spin		Small effect at high frequencies (Truell *et al.*, 1969; Bhatia, 1967)

It can be estimated that at room temperature, and frequencies below 50 MHz, only dislocation damping, thermoelastic and magnetoelastic losses (especially for ferromagnetic materials) influence the measured absorption.

Absorption can be measured quantitatively when the separation of α_A and α_S in the attenuation coefficient α is feasible. This is possible for steels as a result of scattering measurements (see Section IIE). Experience shows that:

(1) A linear dependence on frequency (Mason and McSkimin, 1947; 1948; Roney, 1950; Papadakis and Reed, 1961; Tietz, 1974; Mercier, 1975; Lord *et al.*, 1977; Serabian and Williams, 1978; Vary, 1978a).
(2) A quantitative value for the absorption per wavelength: $\alpha_A \lambda \approx 0{\cdot}007 \pm 0{\cdot}005$ (Goebbels and Höller, 1978).
(3) A dependence of the absorption coefficient on chemical composition (Goebbels and Höller, 1978; Serabian and Williams, 1978).

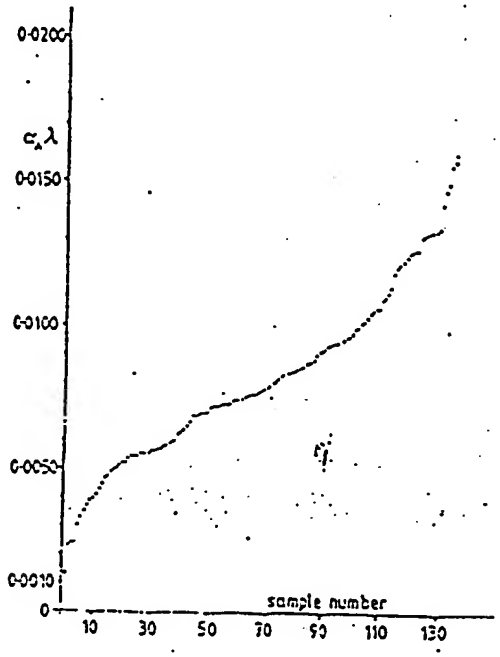

FIG. 4. Absorption per wavelength for 139 different types of steel.

The suppositions under which this experience has been gained are described in Section IIIB. Figure 4 shows $\alpha_A \lambda$ for different types of steel samples, for which the metallurgical data are characterized in Table III (Goebbels *et al.*, 1976). Non-linear connections between absorption and frequency found by other authors (Papadakis, 1964; Aurich and Martin, 1970; Martin and Aurich, 1972) led to unrealistic, partly nonsensical (negative) values for the absorption and scattering coefficients during the evaluation of experimental results. The direct connection with residual stresses, deformation, and embrittlement states makes absorption interesting for further exact investigations. The comparison between the data of $\alpha_A \lambda$ from Fig. 4, on the one hand, and the grain size d and different alloying elements, on the other hand, leads to the following results, disregarding fine details of this analysis:

(1) C, Mn, P ($< 0{\cdot}03\%$), S, N, Al, As, Cu and Pb have no influence on $\alpha_A \lambda$. Nor does grain size.

(2) With increasing content of Si, Cr, Ni (>0·1%, but not for the austenites), Nb, Mo and V (>0·05%) $\alpha_A\lambda$ is shifted to lower values.
(3) Only with increasing P (>0·03%) does $\alpha_A\lambda$ also increase.

TABLE III

Metallurgical Data for Steel Samples Analysed with Ultrasound Backscattering Measurements and Plotted in Figs 4 and 29

Number of steel samples analysed with backscattering:	250 samples
Number plotted in Fig. 4 with increasing $\alpha_A\lambda$:	139 samples
Number plotted in Fig. 29 as grain size comparison:	164 samples

Types of steel: austenitic from X10 CrNi 10·18 to 72 Ni, 16 Cr and 78 Ni, 20 Cr,
ferritic from α-Fe to pearlite and free machining steel

Grain sizes: from martensitic structure to $d \approx 200\ \mu m$.

Alloying elements (weight %):

C	Si	Mn	P
≲ 0·4	≲ 0·6	≲ 1·6	≲ 0·08
S	N	Al	Cu
≲ 0·4	≲ 0·02	≲ 0·10	≲ 0·03
As	Cr	Ni	Mo
≲ 0·08	≲ 2·0	≲ 1·5	≲ 0·4
	(excluding austenites)		
V	Nb	Pb	
≲ 0·2	≲ 0·05	≲ 0·3	

4. *Scattering*

Ultrasonic waves are particularly influenced by phase boundaries, which can be described simply as a jump in acoustic impedance ($\Delta\rho v$). A series of effects on the propagation of the ultrasound wave is possible between reflection, diffraction, and scattering, depending on the geometrical form and spatial extension. Table IV shows this schematically. It is essential that the energy character and the mechanical vibration are maintained by this, so that for further spatial and temporal propagation ultrasound is also present. Ultrasonic scattering appears where small linear dimensions d compared to the wavelength λ prevail, or when d is comparable with λ.

According to Table V, this is the case for relatively simple structures (polycrystalline material) up to complex structures (composites). Thus the two parameters are defined which determine the scattering: $\Delta\rho v$ and d/λ.

The quantitative solution to the scattering problem (scattering cross-section and scattering coefficient, suitably computed from the solution of the

TABLE IV
Influencing Ultrasonic Waves at Phase Boundaries

Shape of phase boundary	Spatial extension	Influence on incident ultrasonic wave	Influence on measured ultrasonic amplitude	Example
Flat	Infinite half space	Geometrical reflection (R)	A_R ($\Delta\rho v$)	Surface, backwall
Flat	Infinite in two dimensions, thickness d	Geometrical reflection, resonance, through-transmission (D)	A_R, A_D ($\Delta\rho v$, d/λ)	Plate, adhesive, lamellar structure
Round	Infinite in one dimension, diameter d	Reflection, diffraction (B), scattering (S)	A_R, A_B, A_S ($\Delta\rho v$, d/λ)	Fibre reinforced structure
Any shape	All dimensions limited $d > \lambda$	Reflection diffraction	A_R, A_B ($\Delta\rho v$, d/λ)	Defect, flaw
Any shape	All dimensions limited $d \lesssim \lambda$	Scattering	A_S ($\Delta\rho v$, d/λ)	Polycrystalline structure, grains, inclusions, pores, segregates

TABLE V
Materials in which Scattering will be Excited

Matrix	Scatterer	Example
Liquid	Gas bubbles, fine dispersed particles	Air in water emulsions
Homogeneous, isotropic solid	Pores, solids with different values for ρ, v	Porosity in plastics, heterogeneities, fibres in plastics
Homogeneous, quasi-isotropic solid	Grains, pores, other solids with different values of ρ, v	Metals, steel, ceramics, inclusions, segregations, pores.
Inhomogeneous, anisotropic solid	Grains, pores, other solids with different values for ρ, v	Texture, anisotropy, lamellar tearing.

wave equation) now depends on the boundary conditions, as can be seen in Table VI. The intensity of the scattering excited in a material's structure is directly proportional to the scattering coefficient α_S, so that the scattering amplitude, generally measured in the experiment, is proportional to $\sqrt{\alpha_S}$.

TABLE VI

Parameters for Ultrasonic Scattering

Elements of scattering	Quasi-monophasic systems	Two-phase systems
$\Delta\rho v$	$\Delta\rho v \ll \langle\rho v\rangle_{\text{matrix}}$	Any value of $\Delta\rho v$
$d \ll \lambda$, Rayleigh-scattering	Theory: Lifshits and Parkhomovskii (1948, 1950), Bhatia (1959, 1967), Bhatia and Moore (1959) valid for any shape of scatterers	Theory: Truell *et al.* (1969) valid for any shape of scatterers, but isotropic matrix and isotropic scatterer
$d \approx \lambda$, stochastic scattering	Theory: Rokhlin (1972) for cubical scatterers	Theory: Truell *et al.* (1969) valid for spherical scatterers, isotropic phases necessary
$d \gg \lambda$, diffuse scattering	Theory: Rokhlin (1972) for cubical scatterers	Theory: Truell *et al.* (1969) valid for spherical scatterers, isotropic phases necessary
Relative volume concentration x of scatterers ($0 \leqslant x \leqslant 1$)	$x = 1$ (e.g. grains)	0, ..., 1·0 (e.g. pores)
Scatterers independent of each other	Single scattering, only linear superposition of the scattering processes	
Scatterers influencing each other	Multiple scattering—velocity dispersion. Theory: Waterman and Truell (1961)	

Analogous to pulse-echo and attenuation measurement, the backscattering amplitude $A_S(x)$ can be measured in this way as a function of the time of flight t, and therefore of the sound path x ($= vt$).

As can be seen in the following section, it follows, for example for homogeneous structures (Fay, 1973; Koppelmann and Fay, 1973), that

$$A_S(x) = A_0 \cdot (\alpha_S \Delta x)^{\frac{1}{2}} \cdot \exp(-\alpha x), \tag{5}$$

and for inhomogeneous structures:

$$A_S(x) = A_0 \cdot (\alpha_S(\tfrac{1}{2}x) \cdot \Delta x)^{\frac{1}{2}} \cdot \exp\left(-2\int_0^{x/2} \alpha(z)\,dz\right), \tag{6}$$

where Δx is pulse length.

The comparison of eqns (3) and (5) or (4) and (6), respectively, shows at once that scattering amplitudes lie by a factor of

$$A_S/A = (\alpha_S \Delta x)^{\frac{1}{2}}$$

below the amplitudes of backwall echoes, i.e. generally 40–60 dB down.

Inversely, the signal-to-noise ratio (S/N-R) is determined, if the scattering by the structure surpasses the electronic noise, by the relation (Ermolov and Pilin, 1976; Goebbels *et al.*, 1978a)

$$\text{S/N-R} \sim A/A_S = (\alpha_S \Delta x)^{-\frac{1}{2}}. \tag{7}$$

This will be dealt with in detail in the following sections.

II. Theory of Scattering

A. Boundary Conditions

The scattering coefficient α_S can be computed quantitatively after the wave equations for the incident and the scattered wave have been established, and after proper consideration of the appropriate boundary conditions.

The scattering cross-section γ (applied to a single, isolated scatterer), the scattering coefficient α_S (applied to the volume concentration of the scatterers) and the angular dependence of the scattering describe the "elastic" interaction between ultrasound and material.

Table VI shows which boundary conditions must be taken into consideration. The variety of the parameter combinations is evident. A general solution (Waterman, 1968, 1976) of the scattering problem represents only the starting point for possibly complex and over-simplified approximations.

The two following combinations of boundary conditions are of importance for the practical use of the scattering coefficient in attenuation and scattering measurements for the characterization of materials structure. They are thoroughly discussed in Sections IIB and IIC.

1. Polycrystalline, Quasi-isotropic and Homogeneous, Quasi-monophasic Systems

These have randomly distributed grain orientations, negligible density fluctuations and small changes in velocity or small elastic anisotropy.

This case corresponds to the scattering not only from polycrystalline, metallic structures (steel, for instance), but also anorganic ones (such as dense-sintered ceramic), where further phases (e.g. segregations and non-metallic inclusions in steel or small porosity in ceramic structures) quite possibly produce negligible contributions to the total stimulated scattering, because of their small concentration and/or their small d/λ-condition.

Lifshits and Parkhomovskii (1948, 1950), Bhatia (1959), and Bhatia and Moore (1959) have computed α_S for this case, restricted to Rayleigh-scattering ($d \ll \lambda$). Other derivations have given comparable results (Mason and McSkimin, 1947, 1948, 1949; Pekeris, 1947; Roney, 1950; Merkulov, 1957a, b, c; Szilard and Bihari, 1965; Truell *et al.*, 1969; Rokhlin, 1974). Since the α_S results according to Lifshits and Parkhomovskii and Bhatia and Moore agree best with corresponding experimental results, their derivation is given in Section IIB.

2. Two-phase Systems

These consist of a homogeneous, isotropic matrix with isotropic spherical scatterers, which are independent of each other and randomly distributed.

The jump $\Delta\rho v$ at the phase boundary can be of any size here. In practice, this parameter combination covers exactly scattering by gas bubbles, pores and solid particles in liquids, plastics, glasses and other materials, where special accent lies on the homogeneous, isotropic matrix (which causes no scattering itself). Two-phase, polycrystalline systems such as: pearlite (ferrite (α-Fe)+cementite (Fe_3C)), cast iron (e.g. ferrite+spherical graphite (C)), free machining steel (ferrite+segregations (MnS)), reaction-bonded ceramic (Si_3N_4 or SiC with each up to 20% porosity), and also local structure anomalies in steel (such as accumulation of segregations, nonmetallic inclusions and others) can be dealt with by a simple extension of the fundamental theory.

The spherical form of the scatterers permits computing α_S for any d/λ-values. Multiple scattering and velocity dispersion ($v(f)$) appear dependent on $\Delta\rho v$ between matrix and scatterers, as well as on the concentration of the scattering particles. The basic work here (including consideration of the multiple scattering) has been pioneered by Truell and his co-workers (Ying and Truell, 1956; Einspruch *et al.*, 1960; Waterman and Truell, 1961), collected in the book by Truell *et al.* (1969). An extension of the work has been carried out by Zimmermann (Goebbels *et al.*, 1978b; Hirsekorn, 1979a, b).

At the present time, especially in the USA (Varadan and Pao, 1976; Gubernatis *et al.*, 1977; Varadan, 1978), intense research is being conducted on the scattering problem of nonspherical particles (cylinder, ellipsoid, disc and strip). The research is limited, however, to the scattering from a single object, not with models which correspond for instance to fibre-reinforced materials (CFRP, GFRP, steel-fibre reinforced Al and others) or texture and lamellar tearing structures.

Section IIC deals with the scattering in two-phase systems according to Truell *et al.* (1969) including the extension to the polycrystalline matrix causing scattering itself, while Section IID deals with multiple scattering.

B. Quasi-monophasic Systems, Rayleigh Scattering

Ultrasound scattering in quasi-monophasic systems, such as polycrystalline metallic materials (steel), is distinguished by the fact that the whole volume is filled with "scatterers", and the scattering itself is caused by the elastic anisotropy of the single crystals of which the material is composed. That is to say the jump $\Delta\rho v$ in the sound impedance ρv is described only by the directional dependence of the sound velocity in the single crystal. Density fluctuations may be neglected here. Lifshits and Parkhomovskii (1948, 1950), and, independently of them, Bhatia (1959) and Bhatia and Moore (1959), have computed for the case of Rayleigh scattering (linear dimension of scatterer, e.g. grain size $d \ll$ ultrasonic wavelength λ), the scattering coefficient α_S (Rayleigh, 1945). We follow mainly Bhatia's derivation.

The starting point is the wave equation

$$\rho \partial^2 s_{i1}/\partial t^2 = c_{ijkl} \cdot \partial^2 s_k/\partial x_j \partial x_l \quad (i,j,k,l = 1,2,3), \tag{8}$$

where ρ = density, c_{ijkl} = elastic moduli of the single crystal, $\mathcal{S} = (s_1, s_2, s_3)$ = displacement vector of the point of mass, whose normal position gives $\mathcal{R} = (x_1, x_2, x_3)$, using Einstein's summation convention.

While ρ_0, $\langle c_{ijkl}\rangle$ (with $\rho_0 v_L{}^2 = \langle c_{11}\rangle$, $\rho_0 v_T{}^2 = \langle c_{44}\rangle$), are the properties of the polycrystalline, quasi-isotropic matrix, with its displacement vector $\mathcal{S}^{(0)}$; $\rho_0 + \rho'$, $\langle c_{ijkl}\rangle + c_{ijkl}'$ are the properties of the scatterer, whose volume is V and displacement vector $\mathcal{S}'$.

If terms of higher order can be neglected in the symbols with a prime $'$, i.e. only small fluctuations of the properties at the phase boundary matrix-scatterer, the wave eqn (8) is modified to include the properties of the scatterer:

$$\rho_0 \partial^2 s_i'/\partial t^2 - \langle c_{ijkl}\rangle \partial^2 s_k'/\partial x_j \partial x_l = -\rho' \partial^2 s_i^{(0)}/\partial t^2 + c_{ijkl}' \partial^2 s_k^{(0)}/\partial x_j \partial x_l$$

and with $\mathcal{S}^{(0)}$, $\mathcal{S}' \sim \exp(i\omega t)$ where $\omega = 2\pi f$ (f = frequency),

$$\langle c_{ijkl}\rangle \partial^2 s_k'/\partial x_j \partial x_1 + \rho_0 \omega^2 s_i' = -c_{ijkl}' \partial^2 s_k^{(0)}/\partial x_j \partial x_l - \rho' \omega^2 s_i^{(0)}. \tag{9}$$

With

$$-B_i = \langle c_{ijkl}\rangle \left(\frac{c_{ijkl}'}{\langle c_{ijkl}\rangle}\right) \partial^2 s_k^{(0)}/\partial x_j\,\partial x_l + \rho_0\,\omega^2\left(\frac{\rho'}{\rho_0}\right) s_i^{(0)}$$

and with divergence- or rotation-formation, respectively, in eqn (9) we obtain

$$[\nabla^2 + (\omega/v_L)^2]\,\mathrm{div}\,\mathcal{S}' = \frac{1}{\langle c_{11}\rangle}\,\mathrm{div}\,\Omega, \tag{10}$$

$$[\nabla^2 + (\omega/v_T)^2]\,\mathrm{rot}\,\mathcal{S}' = \frac{1}{\langle c_{44}\rangle}\,\mathrm{rot}\,\Omega, \tag{11}$$

where eqn (10) implies the stimulation of a scattered L-wave (longitudinal), and eqn. (11) implies the stimulation of a scattered T-wave (shear or transversal), independent of whether the incident wave is an L- or T-wave!

In an example, which uses

$$\mathcal{S}^{(0)} = (s_{1,0}^{(0)} \exp(-ikx_1),\ 0,\ 0),\ k = \frac{\omega}{v_L},$$

we can also represent eqns (10) and (11) in the form

$$[\nabla^2 + (\omega/v_L)^2]\,\mathrm{div}\,\mathcal{S}' = \frac{\omega}{v_L^2}\left(\frac{c_{1111}'}{\langle c_{11}\rangle} - \frac{\rho'}{\rho_0}\right)\mathrm{div}\,\mathcal{S}^{(0)}, \tag{12}$$

$$[\nabla^2 + (\omega/v_T)^2]\,\mathrm{rot}\,\mathcal{S}' = \frac{\omega}{v_L^2}\frac{1}{\langle c_{44}\rangle}\,\tau'\,\mathrm{div}\,\mathcal{S}^{(0)}. \tag{13}$$

where $\tau' = (O_1 c_{3111}' - c_{2111}')$.

In a simplified notation we introduce

$$c'_{ijkl} \approx \langle c_{ijkl}'\rangle \tag{14}$$

which means that the deviations of the elastic moduli are independent of their subscripts.

The exact solution, starting point for $\mathrm{div}\,\mathcal{S}'$, is

$$\mathrm{div}\,\mathcal{S}' = \frac{-1}{4\pi\langle c_{11}\rangle}\int_V \frac{\exp(-ikr)}{r}\,\mathrm{div}\,\Omega\,\mathrm{d}V \tag{15}$$

in which $\exp(ikr)/r$, with $r^2 = (x_1 - x_1')^2 + (x_2 - x_2')^2 + (x_3 - x_3')^2$, takes into account the phase differences in volume V.

When the linear dimensions of the scatterer (and thus the distances inside volume V) are small compared to λ (more exactly $\lambda/(2\pi)$), eqn (15) can be transformed for any form of scattering into

$$\mathrm{div}\,\mathcal{S}' = -\frac{1}{4\pi}\left(\frac{\omega}{v_L}\right)^2\left[\frac{\langle c'_{ijkl}\rangle}{\rho_0 v_L^2} - \frac{\rho'}{\rho_0}\right]\int_V \frac{\exp(-ikr)}{r}\,\mathrm{div}\,\mathcal{S}^{(0)}\,\mathrm{d}V,$$

and finally into

$$\operatorname{div}\mathcal{S}^{i} = -\frac{1}{4\pi}\left(\frac{\omega}{v_L}\right)^2\left[\frac{\langle c_{ijkl}'\rangle}{\rho_0 v_L^2} - \frac{\rho'}{\rho_0}\right]\cdot V\cdot\frac{\exp(-ikr)}{r}\operatorname{div}\mathcal{S}^{(o)}.$$

Thus the following proportionality applies:

$$\operatorname{div}\mathcal{S}^{i},\quad \mathcal{S}^{i}\sim\left(\frac{\omega}{v_L}\right)^2\left[\frac{\langle c_{ijkl}'\rangle}{\rho_0 v_L^2} - \frac{\rho'}{\rho_0}\right]\cdot V. \tag{16}$$

The scattering cross-section γ (ratio of the intensity scattered into unit space angle per unit time to the incident recurring intensity per unit time and unit area) is proportional to the square of the right-hand side in eqn (16), and we obtain, by neglecting the density change ($\rho'\equiv 0$),

$$\gamma\sim V^2\cdot\frac{\omega^4}{v_L^4}\cdot\frac{\langle c_{ijkl}'\rangle^2}{\rho_0^2 v_L^4}$$

and the scattering coefficient (density of scatterers $\sim 1/V$):

$$\alpha_S\sim V\cdot\frac{\omega^4\langle c_{ijkl}'\rangle^2}{\rho_0^2 v_L^8}.$$

Similarly the stimulated scattered shear wave (in eqns (11) and (13)) contributes to the scattering coefficient. The consideration of c_{ijkl}' leads, for cubic crystallizing materials, to

$$\langle c_{ijkl}'\rangle^2 = (c_{11}-c_{12}-2c_{44})^2 = A^2.$$

The scattering coefficient (now referring to the sound pressure) for cubic systems is found, at incident L-wave, to be:

$$\alpha_S^{L}\,(\mathrm{mm}^{-1}) = \alpha_S^{L,L}+\alpha_S^{L,T} = \frac{8\pi^3}{375}\cdot\frac{Vf^4A^2}{\rho_0^2 v_L^8}\left[2+3\left(\frac{v_L}{v_T}\right)^5\right], \tag{17}$$

and, at incident T-wave, to be:

$$\alpha_S^{T}\,(\mathrm{mm}^{-1}) = \alpha_S^{T,T}+\alpha_S^{T,L} = \frac{6\pi^3}{375}\cdot\frac{Vf^4A^2}{\rho_0^2 v_T^8}\left[3+2\left(\frac{v_T}{v_L}\right)^5\right]. \tag{18}$$

From eqns (17) and (18) it can be seen that for any incident wave mode the energy loss by scattering is effected mostly as T-waves; for as $v_L \approx 2v_T$:

$$(v_L/v_T)^5 \approx 32.$$

Here the term in square brackets in eqns (17) and (18) determined for T-waves is greater by a factor 48 than the term determined for L-waves (Wüstenberg *et al.*, 1977).

This consideration of the mode conversion at scattering processes distinguishes the derivations of Lifshits and Parkhomovstii (1948, 1950) or Bhatia and Moore (1959) from previous work. Since they also correspond well to

experimental measurements quantitatively, other computations are not stated here.

For stochastic and diffuse scattering only Rokhlin (1972) has taken into account mode conversion. The anisotropy factor used there, however, cannot simply be described quantitatively, and will therefore not be further considered here.

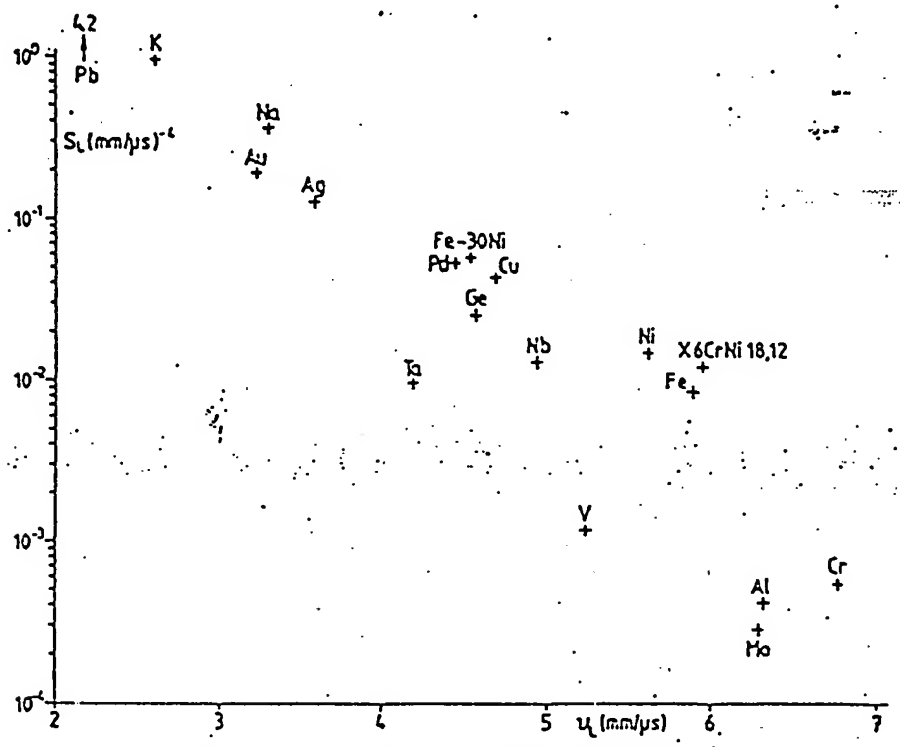

FIG. 5. Scattering parameter for L-waves.

Figures 5 and 6 represent for different substances (partly after Papadakis, 1965, 1968) the scattering factors S_L and S_T, determined from the material properties, according to eqns (17) and (18):

$$S_L = \alpha_S^L/(Vf^4) = \frac{8\pi^3}{375}\cdot\left(\frac{A}{\rho_0 v_L^2}\right)^2\cdot\frac{1}{v_L^4}\left[2+3\left(\frac{v_L}{v_T}\right)^5\right](\mathrm{mm}/\mu\mathrm{s})^{-4}, \qquad (19)$$

$$S_T = \alpha_S^T/(Vf^4) = \frac{6\pi^3}{375}\cdot\left(\frac{A}{\rho_0 v_T^2}\right)^2\cdot\frac{1}{v_T^4}\left[3+2\left(\frac{v_T}{v_L}\right)^5\right](\mathrm{mm}/\mu\mathrm{s})^{-4}. \qquad (20)$$

Figures 5 and 6 show that v essentially determines the value of S, whereas A, $\rho_0 v^2$ and v_L/v_T are responsible only for the deviations.

The suppositions which have been used explicitly and implicitly for the derivations of eqns (17) to (20) are summarized briefly here:

(1) $d \ll \lambda$, more exactly: $d < \lambda/(2\pi)$; $V \sim d^3$ (from eqn (16)).

(2) Small fluctuations of the elastic constants $c_{ijkl}' \ll \langle c_{ijkl}\rangle$ (from eqn (9)).

(3) Continuous change of the stress and strain components at the phase boundary matrix-scatterer (from eqn (15)).
(4) No density fluctuations ($\rho' \equiv 0$) (from eqn (16)).
(5) Scatterers independent from each other, scattering effect exclusively additive (particularly from eqn (17)).
(6) No multiple scattering (particularly from eqn (17)).
(7) Mean scatterer diameter d, mean scatterer volume V respectively, instead of a distribution function $F(d)$, $F(V)$, e.g. Seemann and Bentz (1954) (from eqn (17)).
(8) Mean frequency f instead of a spectrum $A(f)$ (from eqn (17)).

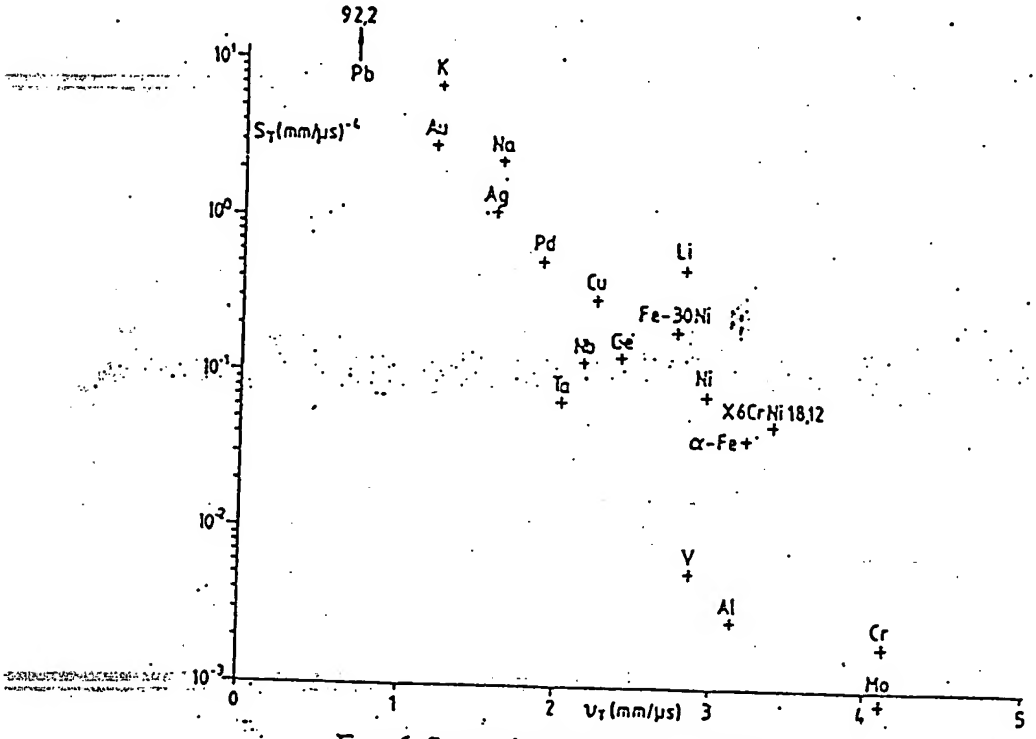

FIG. 6. Scattering parameter for shear waves.

In particular, the last two restrictions have to be considered in quantitative evaluations. From

$$\alpha_S = SVf^4 \approx Sd^3f^4 \tag{21}$$

it follows immediately that, for instance, at a grain size distribution $F(d)$, just as at a frequency spectrum $A(f)$, the high values add overproportionally to α_S.

C. *Two-phase Systems*

Scattering in two-phase systems can be described in a relatively simple way when each of the two phases (matrix, scatterer) is isotropic by itself and thus

causes no scattering. Scattering only arises, then, at the phase boundary matrix–scatterer. Truell and his co-workers (Ying and Truell, 1956; Einspruch *et al.*, 1960), summarized by Truell *et al.* (1969), have computed the scattering cross-section γ and the scattering coefficient α_S for spherical scatterers in any two-phase media and for any d/λ (or $ka = (2\pi/\lambda)(d/2) = \pi d/\lambda$). We follow these derivations. Both phases can be described by three parameters each: ρ, λ, μ (density and Lamé's moduli). The wave equation (see eqn (8))

$$\rho \ddot{s}_i = c_{ijkl}\, \partial^2 s_k / \partial x_j\, \partial x_l$$

is simplified to

$$\rho \ddot{\mathcal{S}} = \mu \nabla^2 \mathcal{S} + (\lambda+\mu)\,\mathrm{grad}\,\mathrm{div}\,\mathcal{S}.$$

With $\mathcal{S} \sim \exp(i\omega t)$ and adequate transfer we obtain

$$-\rho\omega^2 \mathcal{S} = (\lambda+2\mu)\,\mathrm{grad}\,\mathrm{div}\,\mathcal{S} - \mu\,\mathrm{rot}\,\mathrm{rot}\,\mathcal{S}. \tag{22}$$

The splitting into one vector belonging to the L-wave and another vector belonging to the T-wave produces wave equations similar to eqns (10) and (11).

For the L-wave ($\mathrm{rot}\,\mathcal{S} \equiv 0$):

$$\left(\nabla^2 + \frac{\rho\omega^2}{\lambda+2\mu}\right) \mathrm{div}\,\mathcal{S} = 0 \tag{23}$$

and for the T-wave ($\mathrm{div}\,\mathcal{S} \equiv 0$):

$$\left(\nabla^2 + \frac{\rho\omega^2}{\mu}\right) \mathrm{rot}\,\mathcal{S} = 0, \tag{24}$$

where $\rho v_L^2 = \lambda+2\mu$; $\rho v_T^2 = \mu$.

From the linearity of the scattering process with

$$\mathcal{S} = \mathcal{S}_i + \mathcal{S}_s, \quad \mathrm{div}\,\mathcal{S} = \mathrm{div}\,\mathcal{S}_i + \mathrm{div}\,\mathcal{S}_s, \quad \mathrm{rot}\,\mathcal{S} = \mathrm{rot}\,\mathcal{S}_i + \mathrm{rot}\,\mathcal{S}_s$$

(i $\widehat{=}$ incident, s $\widehat{=}$ scattered) we obtain six solution equations:

$$(\nabla^2 + k_n^2)\,\psi_n = 0 \quad (n = 1, \ldots, 6), \tag{25}$$

with

$$k_1 = k_2 = 2\pi/\lambda_{LM}, \quad k_3 = k_4 = 2\pi/\lambda_{TM}, \quad k_5 = 2\pi/\lambda_{LS},$$

$$k_6 = 2\pi/\lambda_{TS}, \quad \psi_1 = \mathrm{div}\,\mathcal{S}_{iM}, \quad \psi_2 = \mathrm{div}\,\mathcal{S}_{sM}, \quad \psi_3 = \mathrm{rot}\,\mathcal{S}_{iM},$$

$$\psi_4 = \mathrm{rot}\,\mathcal{S}_{sM}, \quad \psi_5 = \mathrm{div}\,\mathcal{S}_{sS}, \quad \psi_6 = \mathrm{rot}\,\mathcal{S}_{sS}.$$

(first subscript: i $\widehat{=}$ incident wave, s $\widehat{=}$ scattered wave, second subscript: M $\widehat{=}$ matrix medium, s $\widehat{=}$ scatterer medium).

When the scatterer is a sphere, the solution functions must be H, being symmetrical to an axis through the centre of the scatterer and parallel to the direction of the incident wave: $H(r, \theta, \phi)$ with spherical coordinates.

For an incident L-wave ($\psi_3 = \text{rot}\,\mathcal{S}_{LM} \equiv 0$) the solutions of eqn (25) are ($j = 1, 2, \ldots; 6; j \neq 3$):

$$\psi_j = a \sum_{m=0}^{\infty} (+i)^{m+1} (2m+1)\, P_m(\cos\theta) \cdot C_{m,j} \cdot F_{m,j}(k_j a), \tag{26}$$

where a = radius of scatterer. $C_{m,1} = (-1)^{m+1}/(k_1 a)$, C_2, C_4, C_5, C_6 = constants which result from the boundary conditions (e.g. the scatterer is hard, elastic, a cavity; the boundary condition is in any case the constant change of the stresses and strains at the boundary surface matrix–scatterer). $P_m(\cos\theta)$ = Legendre polynomial of the order m,

$$F_{m,2} = F_{m,4} = B_m(\xi) - i(-1)^{m+1} \cdot B_{-(m+1)}(\xi), F_{m,1} = F_{m,5} = F_{m,6} = B_m(\xi),$$

$B_m(\xi)$ = spherical Bessel function of the order m and the argument ξ.

For an incident L-wave we get the following scattering cross-section:

$$\gamma_L = 4\pi a^2 \sum_{m=0}^{\infty} (2m+1) \left[|C_{m,2}|^2 + m(m+1) \frac{v_{TM}}{v_{LM}} \cdot |C_{m,4}|^2 \right] \tag{27}$$

and for an incident T-wave:

$$\gamma_T = 2\pi a^2 \sum_{m=0}^{\infty} (2m+1) \left[\frac{1}{(k_3 a)^2} \cdot (|Dm|^2 + |E_m|^2) + \frac{k_3 a}{m(m+1)(k_1 a)^3} |G_m|^2 \right], \tag{28}$$

where D_m, E_m, and G_m result from the boundary conditions for an incident T-wave. The second items in the square brackets of eqns (27) and (28) result from mode conversion. The complex calculation of the scattering cross-section (up to approximately 30 orders must be considered ($m = 30$) for the Bessel functions) affords no difficulties with fast computers, so that γ can be computed for any two-phase combinations.

In the Rayleigh region ($ka \ll 1$) these equations can be greatly simplified, and Table VII contains the scattering cross-section in the Rayleigh region for different kinds of scatterers (Ying and Truell, 1956; Einspruch *et al.*, 1960).

The scattering coefficient for a two-phase system under these circumstances is (Truell *et al.*, 1969):

$$\alpha_S = \tfrac{1}{2} n_0 \gamma, \tag{29}$$

where

n_0 = volume density = $x/(4\pi a^3/3)$,

x = volume concentration ($0 \leqslant x \leqslant 1$).

Scattering Cross-section for the Rayleigh-region after Ying and Truell (1956), Einspruch *et al.*, (1960), Truell *et al.*, (1969) and Hirsekorn (1979a).

$\gamma = \text{const} \cdot \pi \cdot a^2 \cdot g \cdot (ka)^4$

Elastic sphere	L	const $= \frac{4}{9}$	$g = \left(\frac{uy^2(4-3/z^2)-4+3/x^2}{4-uy^2(4-3/z^2)}\right)^2 + \frac{40(2+3/x^5)(uy^2-1)^2}{(2uy^2(2+3/x^2)-r/x^2)^2} + \frac{1}{3}(u-1)^2\left(1+\frac{2}{x^3}\right)$
	T	const $= 1$	$g = \frac{4}{15}s(u-1)^2 + 40[1+\frac{2}{3}x^5]\frac{(uy^2-1)^2}{[2uy^2(2x^2+3)-r^2]^2}$
Cavity	L	const $= \frac{4}{9}$	$g = \frac{4}{3} + \frac{40(2+3/x^5)}{(r/x^2)^2} - \frac{1}{x^3}\left[\frac{3}{2} - \frac{1}{x}\left(\frac{2}{3}+\frac{9}{16x}\right)\right]$
	T	const $= 1$	$g = \frac{4}{15}s + 40[1+\frac{2}{3}x^5]\frac{1}{r^2}$
Hard sphere	L	const $= 12(ka)^{-4}$	$g = \left(1+\frac{2}{x^3}\right)\Big/\left(1+\frac{2}{x^2}\right)^2$
	T	const $= 1$	$g = \frac{6s}{t^2} + \frac{4}{3}\cdot\frac{12t+x^4(8+5x)}{(4t-1)^2}$
Fluid-filled sphere	L	const $= \frac{4}{9}$	$g = \left(\frac{3/x^2}{4+3uq^2}-1\right)^2 + \frac{1}{3}\left(1+\frac{2}{x^3}\right)(u-1)^2 + 40\frac{2+3/x^5}{(r/x^2)^2}$
	T	const $= 1$	$g = \frac{4}{15}s(u-1)^2 + 40\frac{1+2/3x^5}{r^2}$

Abbreviations: $r = 4x^2-9$, $s = 1+x^2/2$, $t = 1+x^2$, $u = \rho_2/\rho_1$, $x = v_{T1}/v_{L1}$, $y = v_{T2}/v_{T1}$, $z = v_{T2}/v_{L2}$, $1 \mathrel{\hat{=}}$ matrix, $2 \mathrel{\hat{=}}$ scatterer.

The factor $\frac{1}{2}$ takes into account the amplitude attenuation, while γ was derived from the intensity. Figures 7 to 10 give some examples for scattering cross-sections of two-phase systems, where both phases are taken to be isotropic, i.e. totally described by the values of ka, ρ_i, v_{Li}, v_{Ti} $(i = 1, 2)$.

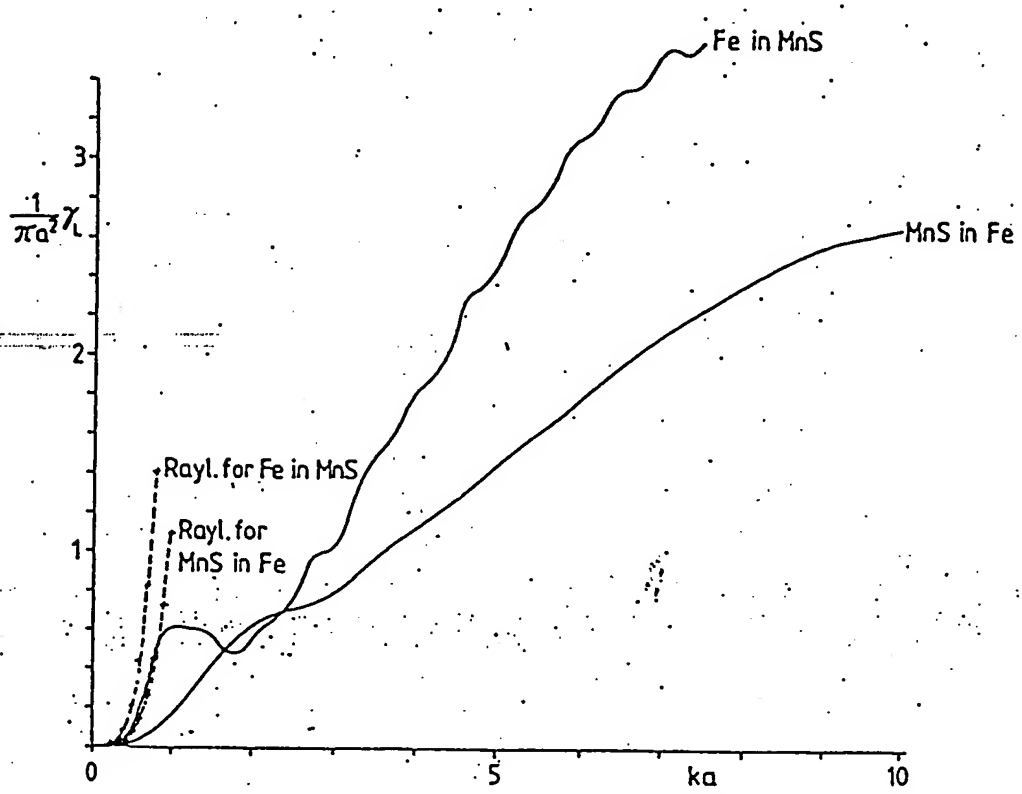

FIG. 7. Scattering cross-sections (L-waves), system Fe, Mns.

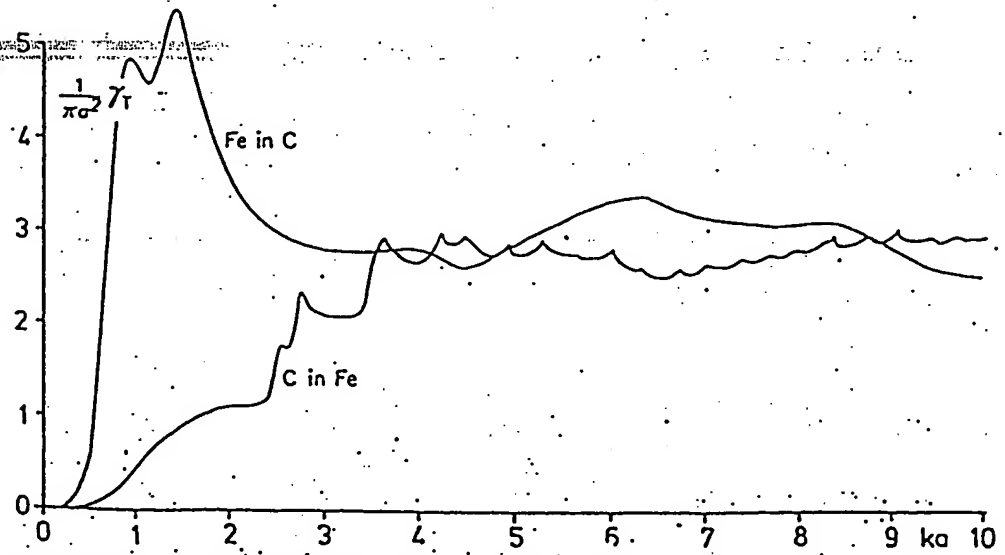

F 8. Scattering cross-sections (shear waves) for elastic scatterers in an elastic medium.

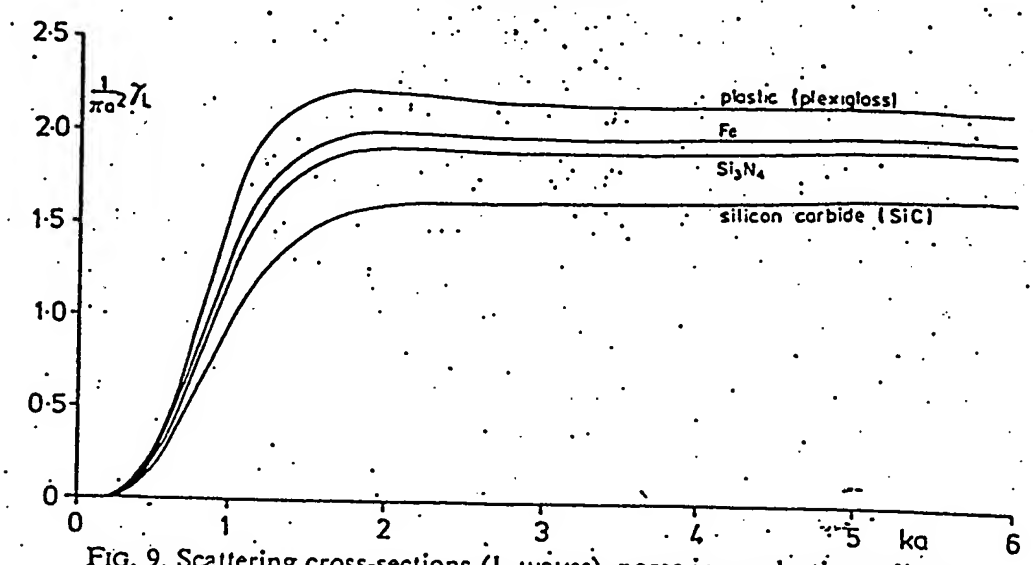

FIG. 9. Scattering cross-sections (L-waves), pores in an elastic medium.

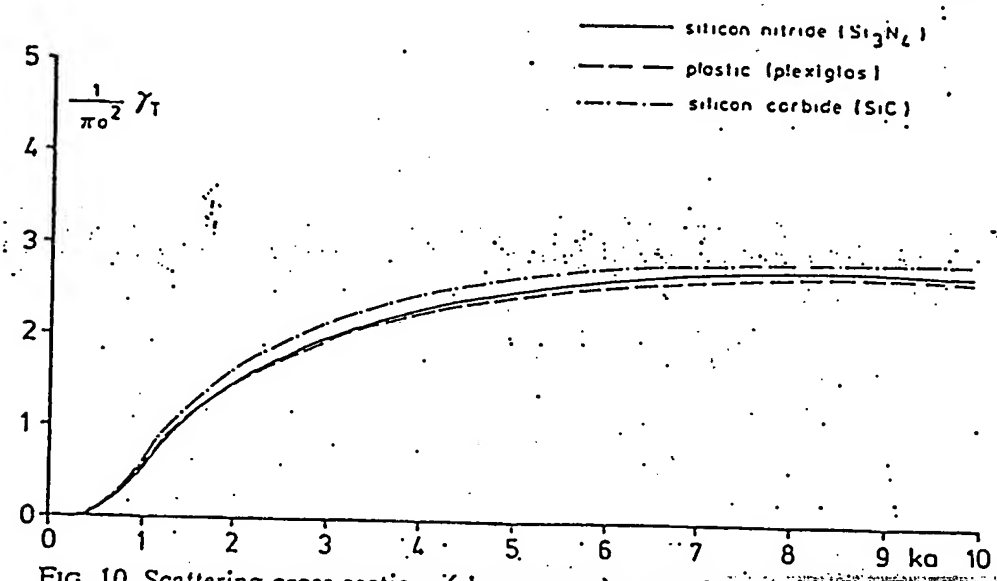

FIG. 10. Scattering cross-sections (shear waves), pores in an elastic medium.

The isotropy of the two phases, especially of the matrix, represents, in practice, an essential limitation on the use of the scattering coefficient, computed after Truell *et al.* (1969). Polycrystalline systems, such as iron and steel as well as non-ferrous metals, oxidic (Al_2O_3) and nonoxidic (SiC, Si_3N_4) ceramics, give one-phase systems scattering as well (Section IIB). The scattering coefficient of a two-phase system must, therefore, consist of several components:

(i) scattering in phase 1 due to elastic anisotropy,
(ii) scattering in phase 2 due to elastic anisotropy,
(iii) scattering at the phase boundary 1 (matrix)–2 (scatterer) and
(iv) scattering at the phase boundary 2 (scatterer)–1 (matrix):

$$\alpha_{S\ \text{resulting}} = x_1^2 \alpha_{S1} + x_2^2 \alpha_{S2} + x_1 \alpha_{S12} + x_2 \alpha_{S21}, \qquad (30)$$

$x_1+x_2=1$, x_i = relative volume concentration,

$$\alpha_{S12}=\tfrac{1}{2}\cdot x_2\cdot\gamma_{12}/V_2,\quad \alpha_{S21}=\tfrac{1}{2}\cdot x_1\cdot\gamma_{21}/V_1.$$

n the Rayleigh region α_{S1} and α_{S2} can, for instance, be obtained from the alculations of Bhatia (1969), (eqns (17) and (18) in Section IIB), while $_{S12}$ and α_{S21} can be computed from eqns (27) and (28) after Truell *et al.* 1969).

Equation (30) represents an approximation for this complex scattering roblem based particularly on the assumption that all scatterers work indeendently of each other. An example of such a system might be pearlite eel, which contains α-Fe and Fe_3C as the two phases.

The present equations refer to spherical scatterers. For cylindrical, elliptic, lanar and other scatterer geometries there are no final calculations known the authors. However, solutions are being pursued (Varadan and Pao, 976; Gubernatis *et al.*, 1977; Varadan, 1978).

D. Multiple Scattering

ll solutions for the wave equations, for instance eqn (8) or (25), have assumed at the single scatterers do not influence each other. Under boundary onditions consisting of densely packed scatterers, strong scattering due to a r. $\Delta\rho v$ jump at the phase boundaries, or strong scattering in the region $\approx\lambda$ this assumption is no longer valid.

In a general formulation of the scattering problem one must assume an fluence on the jth scatterer ($j=1,\ldots,N$ for N scatterers present) through the cident wave and through the excited scattering at all other $N-1$ scatterers well. The complex solution of this problem—here only sketched for an cident L-wave—follows according to Lax (1952), Foldy (1945), Waterman nd Truell (1961), and also Truell *et al.* (1969), from the solution vector ψ qn (25)), which is not only $\sim\exp[i(kx+\omega t)]$, but also (with the attenuation efficient α) proportional to $\exp(-\alpha x)$:

$$\psi\sim\exp(-\alpha x)\cdot\exp[i(\omega t+kx)].$$

ith a complex propagation vector β:

$$\beta=k+i\alpha$$

: obtain

$$\psi\sim\exp[i(\beta x+\omega t)].$$

:cordingly eqn (25) now becomes

$$(\nabla^2+\beta^2)\langle\psi\rangle=0,$$

th an average value $\langle\psi\rangle$, which derives from the consideration of each of scatterers as the jth scatterer.

For isotropic scatterers whose complex scattering function $f(\theta)$ for the forward direction ($\theta = 0$) and the backward direction ($\theta = \pi$) is the same, we then obtain

$$\beta^2 = k^2[1 + (4\pi n_0 f(0)/k^2)] \tag{31}$$

or

$$\beta = k[1 + 4\pi n_0 f(0)/k^2]^{\frac{1}{2}}.$$

$f(0)$ results from the constants of the eqn (26) solution of the wave equation and is given by

$$f(0) = -ai \sum_{m=0}^{\infty} (-1)^m (2m+1) C_{m,2}. \tag{32}$$

At $4\pi n_0 f(0)/k^2 \ll 1$ (see below) is then (expansion of the square root):

$$\beta = k + 2\pi n_0 f(0)/k. \tag{32}$$

The comparison between the coefficients (as $\beta = \omega/v_{\text{phase}} + i\alpha$ applies otherwise) leads to (at incident longitudinal wave $k = \omega/v_{\text{L}} = 2\pi/\lambda_{\text{L}}$):

$$\frac{\omega}{v_{\text{ph}}} = k\left[1 + \frac{2\pi n_0}{k^2} \text{Re} f(0)\right] \tag{33}$$

or

$$v_{\text{ph}} = \omega^2 v_{\text{L}}/[\omega^2 + 2\pi n_0 v_{\text{L}}^2 \text{Re} f(0)],$$

and

$$\alpha = \frac{2\pi n_0}{k} \text{Im} f(0),$$

or, because $\alpha = \frac{1}{2} n_0 \gamma$,

$$\gamma = \frac{4\pi}{k} \text{Im} f(0) = \frac{4\pi v_{\text{L}}}{\omega} \text{Im} f(0). \tag{34}$$

The dispersion (frequency dependence) of the ultrasonic phase velocity v_{ph} can be converted with:

$$v_{\text{group}} = v_{\text{ph}} - \lambda \frac{\partial}{\partial \lambda} v_{\text{ph}}, \tag{35}$$

into the dispersion of the group velocity v_{group}. λ is the resulting wavelength in the two-phase medium (details for eqns (34) and (35) can be seen in Hirsekorn (1979b)).

In order to proceed from eqn (31) to eqn (32), thus enabling the comparison of the coefficient, the item $4\pi n_0 f(0)/k^2$ must be small compared to 1. Since the volume density has the magnitude of 10^5 mm^{-3} (at ≈ 20 µm scatterer diameter and 100 volume %) up to 10^9 mm^{-3} (at ≈ 1 µm scatterer diameter and 100 volume %) it is necessary to examine this assumption in each individual case through the calculation of $f(0)$.

The velocity dispersion according to eqn (33) has been measured for the first time by Latiff and Fiore (1975) for Cu-spheres as scatterers in a plastic matrix. Zimmermann (Goebbels *et al.*, 1978b) has measured the dispersion in free-machining steel (MnS as second phase) and calculated it following the above equations. Examples are given in Figs 11–14. Theory and experiment are in agreement. The phase velocity in free-machining steel has been computed from the average of the two derivations, weighted with the

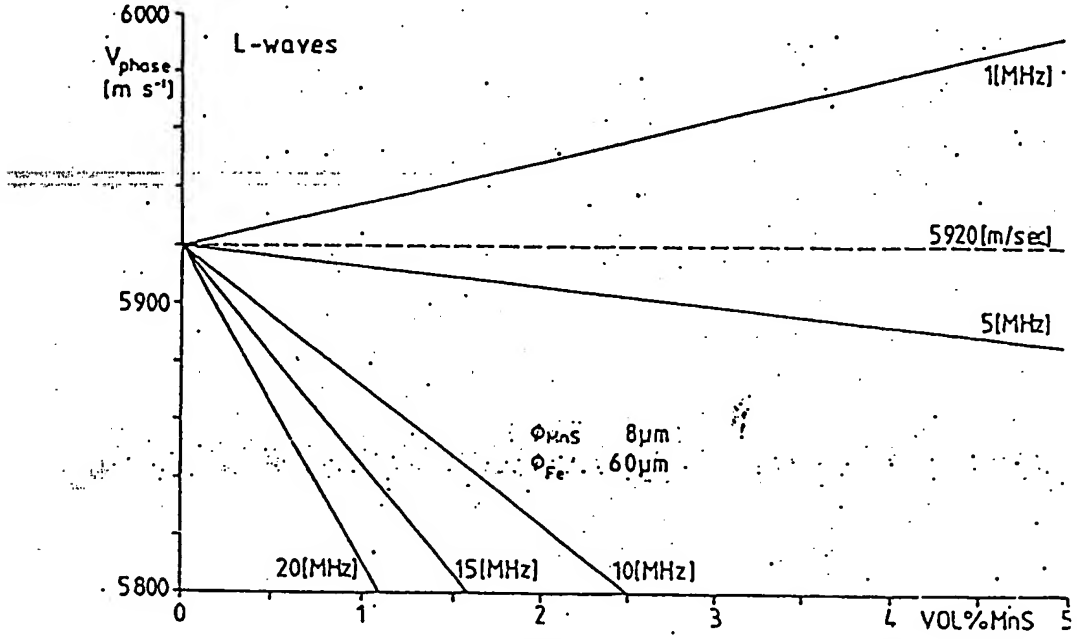

FIG. 11. Velocity dispersion for free machining steel.

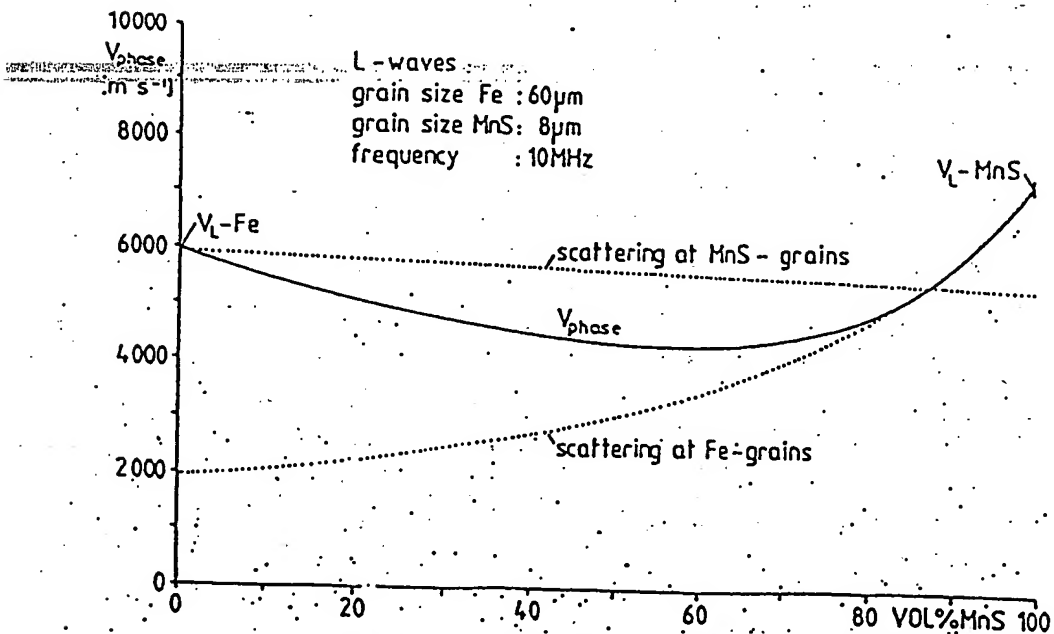

FIG. 12. Dispersion of phase velocity in free machining steel.

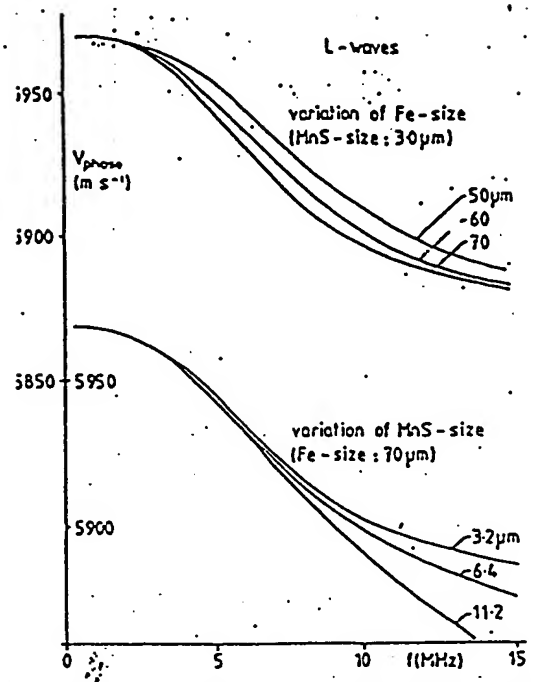

FIG. 13. Velocity dispersion—calculated.

volume concentration x, for α-Fe as matrix and MnS as second phase, and vice versa:

$$v_{ph} = \frac{x_1 \omega^2 v_{L1}}{\omega^2 + 2\pi n_{02} v_{L1}^2 \operatorname{Re} f_2(0)} + \frac{x_2 \omega^2 v_{L2}}{\omega^2 + 2\pi n_{01} v_{L2}^2 \operatorname{Re} f_1(0)}. \tag{36}$$

The connections regarding the experimental measurement of the multiple scattering itself are dealt with in the next section.

E. Fundamentals of Backscattering Measurements

The intensity I_0 at the surface of a material, with sound path $x = 0$, is lowered with increasing sound path, according to

$$I(x) = I_0 \exp(-2\alpha x) \tag{37}$$

assuming homogeneity of the structure ($\alpha \neq \alpha[x]$). Between x and $x+\Delta x$ (where Δx is the pulse length and $2\alpha\Delta x \ll 1$), further intensity is lost through absorption (ΔI_A) and scattering (ΔI_S):

$$\begin{aligned} I(x+\Delta x) &= I_0 \exp[-2\alpha(x+\Delta x)] = I_0 \exp(-2\alpha x) \cdot \exp(-2\alpha \Delta x) \\ &\approx I_0 \exp(-2\alpha x)(1-2\alpha\Delta x) \\ &\approx I(x)(1-2\alpha_A \Delta x - 2\alpha_S \Delta x). \\ I(x+\Delta x) &\approx I(x) - \Delta I_A - \Delta I_S. \end{aligned} \tag{38}$$

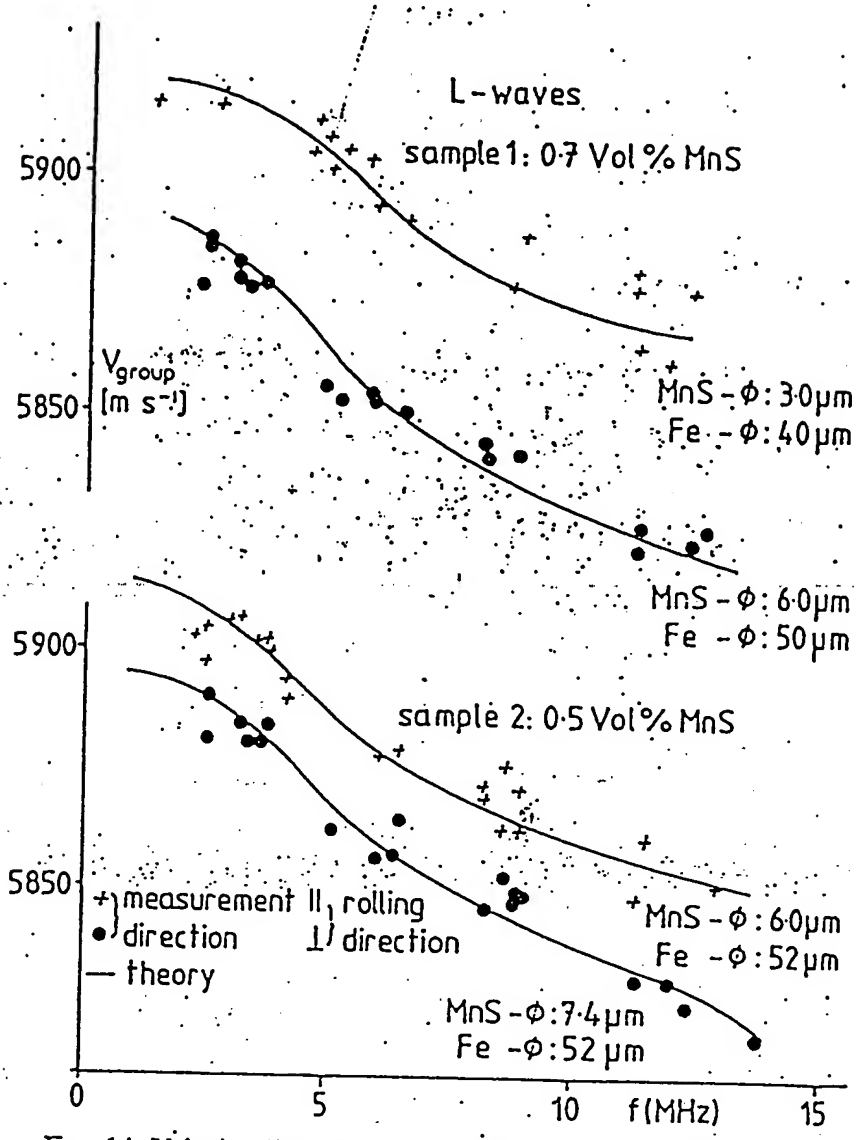

FIG. 14. Velocity dispersion measured in free machining steel.

The energy loss through scattering thus amounts to $\Delta I_S = I(x) \cdot 2\alpha_S \Delta x$. Therefore the scattered ultrasound intensity produced at the point x and radiated into the total space angle is (Beecham, 1966; DiGiacomo *et al.*, 1970; Fay, 1973)

$$I_S(x) = I_0 \cdot 2\alpha_S \Delta x \exp(-2\alpha x). \tag{39}$$

This scattered intensity is distributed over the total space angle, from the position of the scattering volume. Its directivity pattern is of a nearly spherical character in the case of Rayleigh scattering, and distinctive directivity in the case of stochastic and diffuse scattering. While the directivity pattern of a single scatterer can be calculated for any ka, for instance according to Morse and Ingard (1968) and Málecki (1969), little is known about the behaviour in the case of many scatterers with random distribution which

possibly fill the total volume. Various authors state quite different factors for the two wave forms L and T, even in the Rayleigh region.

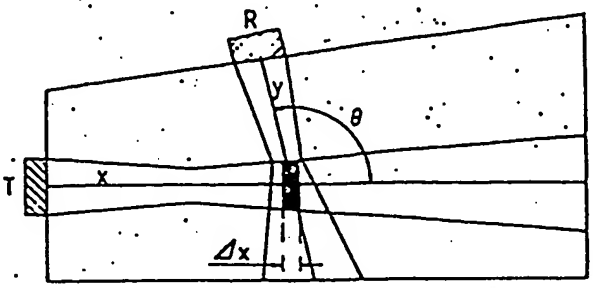

b)

curve	g(θ) normalized to 1 for θ = 0	wave mode	reference
•	$\frac{1}{2}(1-3\cos^2\theta+4\cos^4\theta)$	T	Bhatia (1959)
○	$\frac{1}{2}(1-6\cos^2\theta+9\cos^4\theta)$	L	Beecham (1966)
+	$\frac{1}{2}(1+\cos^2\theta)$	T	Mason and Mc Skimin (1947)
•··	$1+2(ka)^2(1-\cos\theta)$	?	Pekeris (1947)

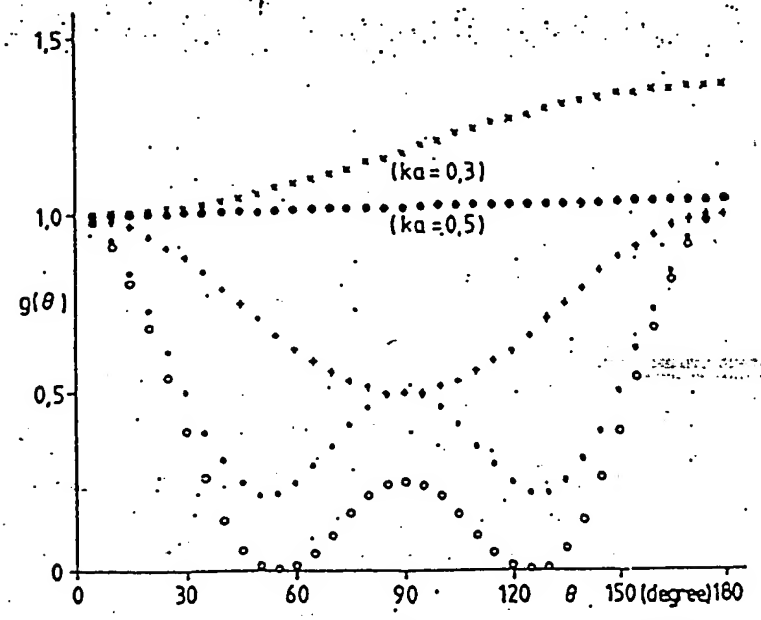

FIG. 15. Directional dependence of Rayleigh scattering according to different concepts.

Figure 15 gives a comparison of the angle functions $g(\theta)$, where θ is the angle between propagation direction and direction of consideration. Most authors working with scattering assume a spherical directivity pattern, $g(\theta) \equiv 1$ in the Rayleigh region (Markgraf, 1963; Szilard and Bihari, 1965; Rokhlin, 1972; Koppelmann and Fay, 1973). Accordingly, a certain amount of the scattering radiated in the space angle returns to the probe ($\theta = 180°$).

The ultrasound scattering produced according to eqn (39) can now be measured with a receiver, e.g. as a function of the angle θ to the propagation direction:

$$I_{S\theta}(x,y) \sim \exp(-2\alpha y) \cdot I_S(x) \cdot g(\theta) \tag{40}$$

where $\exp(-2\alpha y)$ describes the attenuation on the sound path y from the scattering producing volume to the receiver, and $g(\theta)$ the direction characteristic of the scattering. A fraction of the scattered ultrasound also returns to the transmitting transducer—as backscattering ($\theta = 180°$)—which may be switched after a dead time (decay of the transmitting electrical signal) to "receive", as in pulse-echo-testing. However, for $\theta \neq 180°$ scattering can only be measured for times of flight of the beam-crossing region of T- (transmitting) and R-probe (receiving) (Fig. 15), the backscattering is measured as

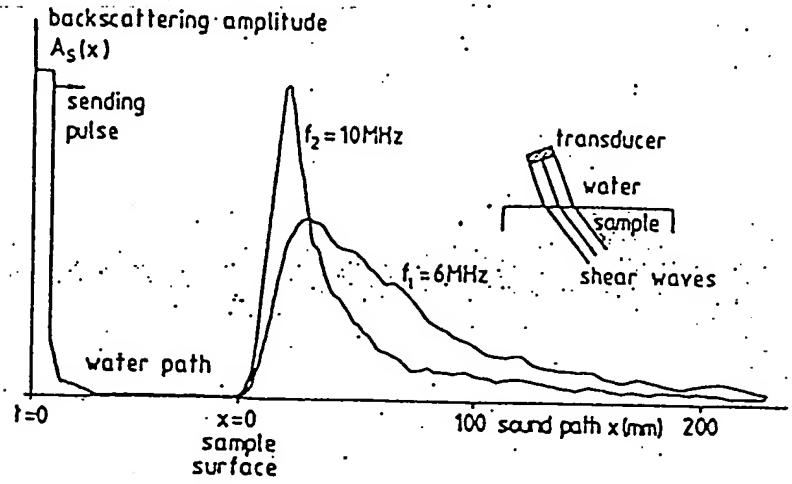

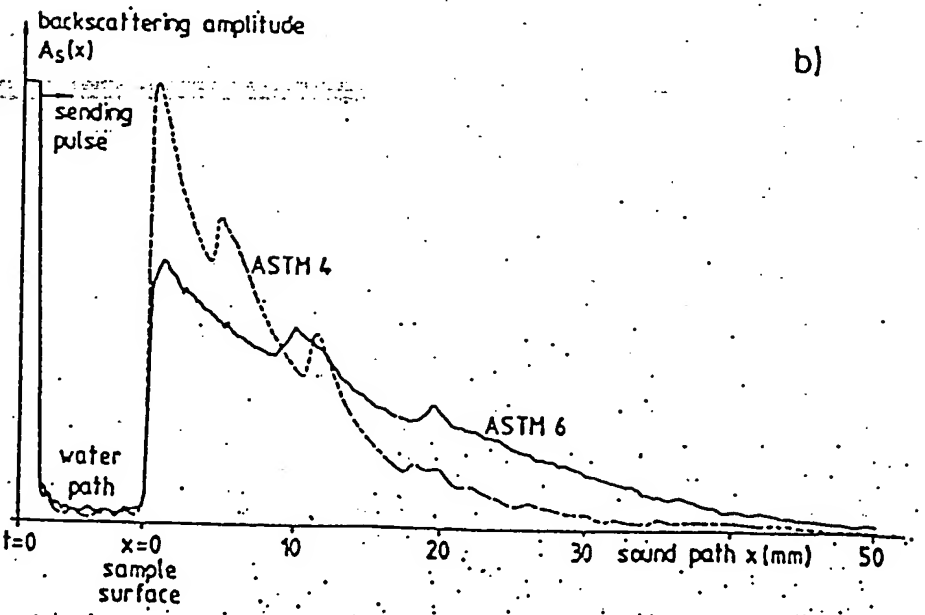

FIG. 16. Backscattering amplitudes by variation of frequency and grain size.

a function of the double sound path $2x$ (to and back) or the double time of flight $2t$ of $t \approx 0$ (minus dead time of the receiver), until the disappearance of the ultrasonic scattering signals in the electrical noise. Backscattering measurements are, therefore, used especially for structure characterization. Figure 16 gives two examples: measurements with two frequencies from one sample and with one frequency from two samples respectively.

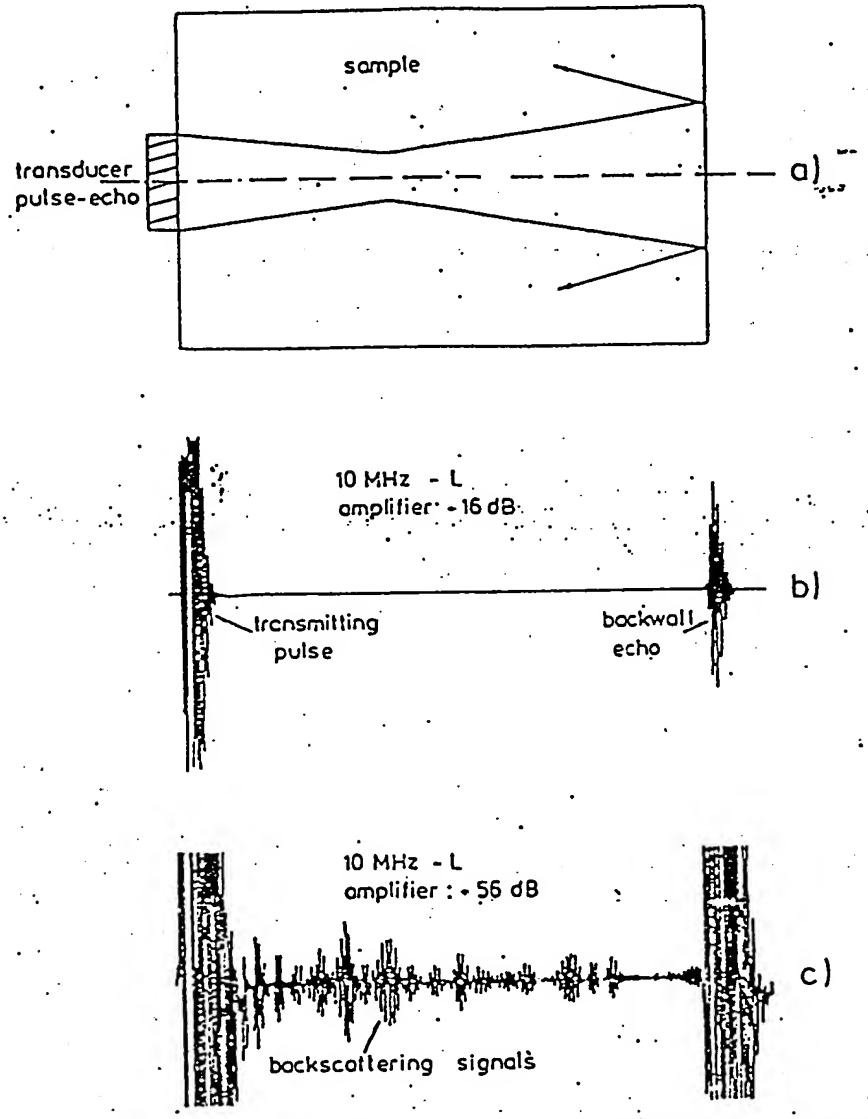

FIG. 17. Austenitic steel, grain size ASTM 4, HF-backwall echo and HF-backscattering signals.

Under the assumption of scatterers being independent of each other and negligible frequency shifts during the scattering processes, the measured backscattering signal consists at first of an amplitude-modulated high frequency (HF) signal amplitude (intensity ~ amplitude squared). An example is given in Fig. 17.

In a similar way to eqn (39), the backscattering amplitude $A_S(x)$ ought to take the course, now with $x = 2x$:

$$A_S(x) = A_0(\alpha_S \Delta x)^{\frac{1}{2}} \cdot \exp(-\alpha x) \tag{41}$$

as shown in Fig. 16, with $A_0 = \sqrt{2I_0}$.

Fay (1973, 1976a, b; Koppelmann and Fay, 1973) has often discussed in which way the sound field diffraction also must be taken into consideration for eqn (41). Fay was able to prove that in the nearfield region, $x \leqslant 4N$, $N = r^2/\lambda$, and $r =$ probe radius, the decrease of the scattering amplitude and the decrease of backwall echo

$$A(x) = A_0 \exp(-\alpha x) \tag{42}$$

run constant. For the farfield region, Fig. 18 shows, on a semi-logarithmic

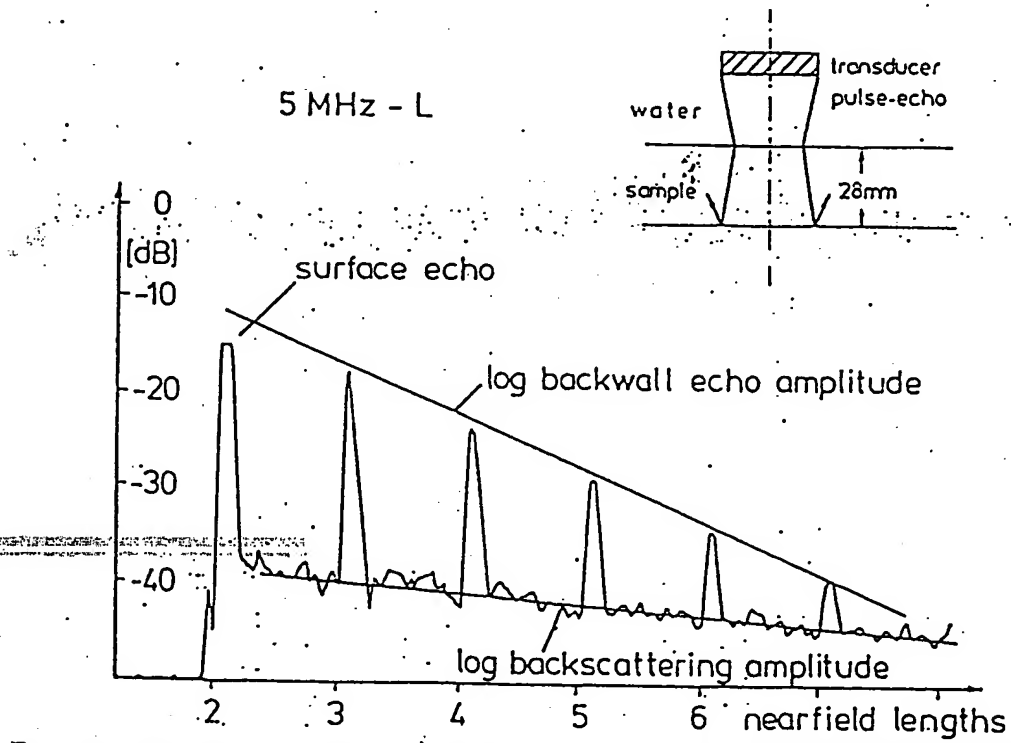

FIG. 18. Attenuation for backscattering signals, attenuation plus diffraction for backwall echoes (Σ 512 rectified signals, half-logarithmic plot).

scale, that the backwall echo sequence corresponding to (Krautkrämer and Krautkrämer, 1975)

$$A(x) = A_0 \cdot \pi \cdot (N/x) \cdot \exp(-\alpha x) \tag{43}$$

decays faster than the scattering amplitude. The difference can be seen in 17(*a*): the beams reflected at the backwall, with the condition that the angle of incidence $\Theta_1 \neq 0$, can no longer contribute to the backwall

echo. The scattering waves starting from under 180°, however, return to the receiver according to the same law. The scattering amplitude $A_S(x)$ in Fig. 17(c) no longer corresponds to eqn (41), i.e. for shorter sound paths we also find smaller amplitudes, and for longer sound paths greater scattering amplitudes. The cause of this lies in the phase sensitivity of the generally used piezoelectric transducer (for instance piston source, rectangular transducer).

The random distribution of the single scattering centres (grain centres) in the volume leads to phase shifts in the result of the sum of all scattering signals which contribute for a certain time of flight t_0 and hence a certain sound path x_0. Koppelmann (1967, 1971a, b, 1972) first succeeded in measuring the scattering amplitude according to eqn (41): a small movement of the probe on the material surface (or in a water path) brings a totally new curve for the function $A_S(x)$, as shown in Fig. 19. A gate, e.g. 1 μs long, that runs with low speed through $A_S(x)$ and records the average amplitude inside the gate as a function of x ("analogue" averaging), or the addition of the particular digitized $A_S(x)$ values (e.g. dividing the time-interval of 100 μs into 2000 points with $\Delta t = 0{\cdot}05$ μs) in an averager ("digital" averaging) lead then to the curve of Fig. 19(f) which is identical to eqn (41). The smallest distance which the movement must take is determined by the magnitude of the grain size (linear scatterer dimension) and wavelength.

In the next section further averaging methods for research studies with the function $A_S(x)$ are described. The development of the phase-insensitive acousto-electric transducer (Busse and Miller, 1978; Heyman *et al.*, 1978) should, however, enable one, at some time, to measure $A_S(x)$ stationary. The considerations leading to eqn (41) assume a homogeneous structure and the neglecting of multiple scattering. With an inhomogeneous structure, where locally α, α_A, and α_S vary ($\alpha = \alpha[x]$), the following expression for the backscattering is valid (with a homogeneous structure eqn (41) again applies):

$$A_S(x) = A_0(\alpha_S(\tfrac{1}{2}x)\,\Delta x)^{\frac{1}{2}} \exp\left(-2\int_0^{x/2}\alpha(z)\,dz\right). \qquad (44$$

This means that the scattering amplitude curve may differ little or much from the exponential behaviour of eqn (41) not only through the $\alpha_S(x)$ term in the prefactor but also through the integral value in the exponent. This results in the possibility of examining structures (in a simple manner by means of backscattering measurements) for their homogeneity and to describe, at least qualitatively, inhomogeneity regions and their size. The next section gives several examples.

Equations (41) and (44) are correspondingly marked in such a way that the ultrasonic pulse with amplitude A_0 on the sound path $x/2$ attenuated by $\exp(-\alpha x/2)$ produces scattering at the location $x/2$ which is proportional

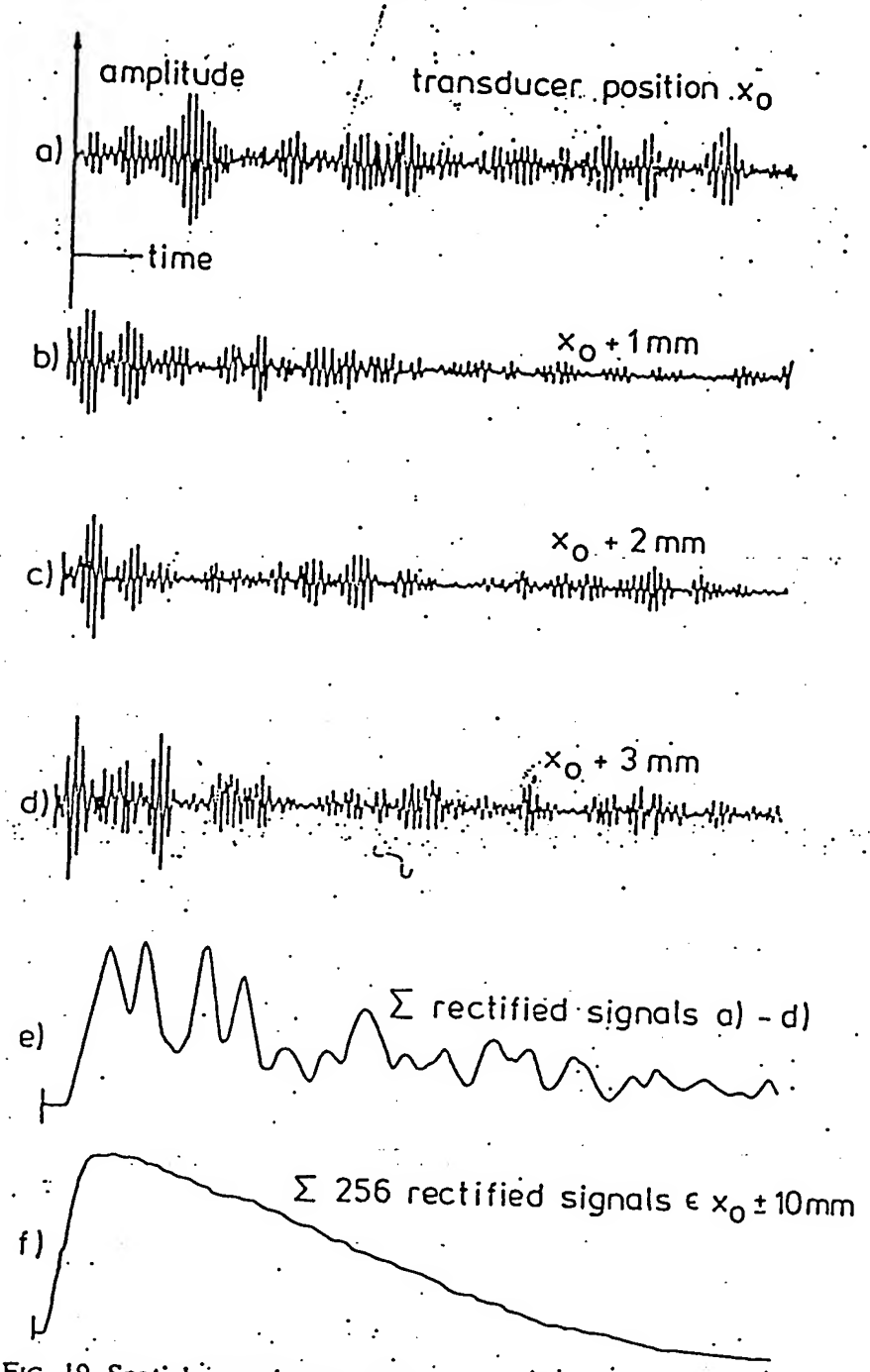

FIG. 19. Spatial averaging (10 MHz), L-waves) backscattering signals.

$(\alpha_S \Delta x)^1$ and will be again attenuated on its return $x/2$ by $\exp(-\alpha x/2)$. Here no account has been taken of the fact that attenuation in both the forward and backward direction results in the generation of further scattering, which first adds to the propagating pulse, then to the backward directed scatter, i.e. scattering of the scattering with terms $(\alpha_S \Delta x)^n$, $n \geq 2$, is neglected. When $\alpha_S \Delta x$ is so large that a measurable additional part results, it becomes necessary to consider this multiple scattering.

An approach exists for the measurement of multiple scattering (Goebbels, 1976). From eqn (39) we see (although we distinguish now between single scattering (index SE) and multiple scattering (index SM)):

$$I_{SE}(0) = 2\alpha_S \Delta x I_0.$$

When considering multiple scattering, a quadratic term must also be included —the scattering of the single scattering:

$$I_{SM}(0) = 2\alpha_S \Delta x I_0 (1 + 2\alpha_S \Delta x)$$

or

$$I_{SM}(0) - I_{SE}(0) = 2\alpha_S \Delta x I_{SE}(0).$$

After a step Δx we obtain

$$I_{SM}(\Delta x) - I_{SE}(\Delta x) = 2\alpha_S \Delta x I_{SE}(0) \exp(-2\alpha \Delta x) + 2\alpha_S \Delta x 2\alpha_S \Delta x I_{SE}(0)$$
$$= 2\alpha_S \Delta x I_{SE}(\Delta x)[1 + 2\alpha_S \Delta x \exp(2\alpha \Delta x)].$$

After n steps of Δx,

$$I_{SM}(n\Delta x) - I_{SE}(n\Delta x) = 2\alpha_S \Delta x I_{SE}(n\Delta x)[1 + 2\alpha_S \Delta x \exp(2\alpha \Delta x)]^n.$$

With $x = n\Delta x$ and $\exp(2x\Delta x) \approx 1$, there results:

$$I_{SM}(x) - I_{SE}(x) = 2\alpha_S \Delta x I_{SE}(x) \left(1 + \frac{2\alpha_S x}{n}\right)^n.$$

With

$$\lim_{n \to \infty} \left(1 + \frac{2\alpha_S x}{n}\right)^n = \exp(2\alpha_S x)$$

it follows that

$$I_{SM}(x) - I_{SE}(x) = 2\alpha_S \Delta x I_{SE}(x) \exp(2\alpha_S x)$$

or

$$I_{SM}(x) = I_{SE}(x)[1 + 2\alpha_S \Delta x \exp(2\alpha_S x)]. \quad (45)$$

When multiple scattering is present the transfer of the measurable back-scattering amplitude corresponds to the step from eqn (39) to eqn (41); we obtain

$$A_{SM}(x) = A_{SE}(x)[1 + 2\alpha_S \Delta x \exp(2\alpha_S x)]^{\frac{1}{2}}; \quad (46)$$

in which $A_{SE}(x)$ results directly from eqn (41).

Experimentally (see also the next section), multiple scattering occurs when α_S has a magnitude of 0·1 mm^{-1} and Δx has a magnitude of several mm. The curve of single- and multiple- scattering is given in Fig. 20 with real values.

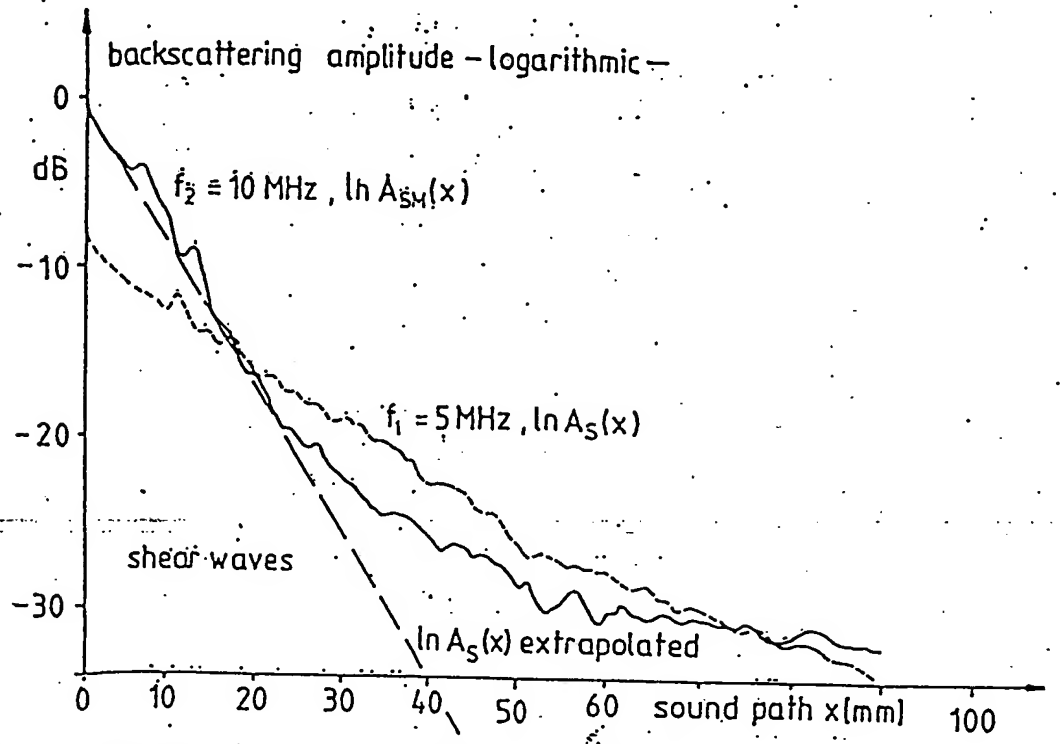

FIG. 20. Backscattering from an austenitic steel (ASTM 2) without multiple scattering (5 MHz) and with multiple scattering (10 MHz).

The importance of eqn (46) lies in the fact that one measurement alone is sufficient for the absolute determination of α_S. The modification of eqn (46) to

$$\ln\left(A_{SM}^2(x)/A_{SE}^2(x)-1\right) = \ln 2\alpha_S \Delta x + 2\alpha_S x \qquad (47)$$

gives, on the left-hand side, a function which can be obtained from the experiment and, on the right-hand side, a straight line with the slope $2\alpha_S$. Figure 21 gives some examples.

The presentation in Fig. 22 of the scattering coefficient, measured by multiple scattering (d being the metallographically determined value of the grain size), confirms the scattering laws in the Rayleigh and stochastic regions of scattering, independently from conditions of frequency- and grain-size dependence of α_A or α_S. Thus, in accordance with eqn (47), a method has been defined for the first time for the determination of the absolute value of α and from this, at least in the Rayleigh region, the determination of grain size d.

A second method for grain-size determination by means of scattering (Goebbels 1975), which is frequently used at present, uses two scattering measurements with two different frequencies, according to eqn (41). In semi-logarithmic presentation we get

$$\ln A_S(x) = \ln\left[A_0(\alpha_S \Delta x)^{\frac{1}{2}}\right] - \alpha x \qquad (48)$$

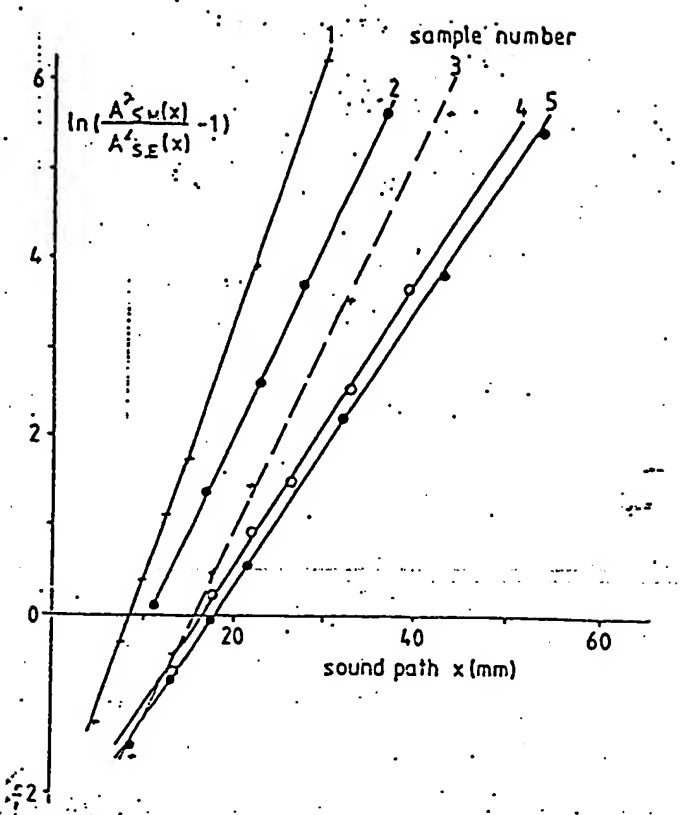

FIG. 21. Normalized multiple scattering curves, half-logarithmic plot.

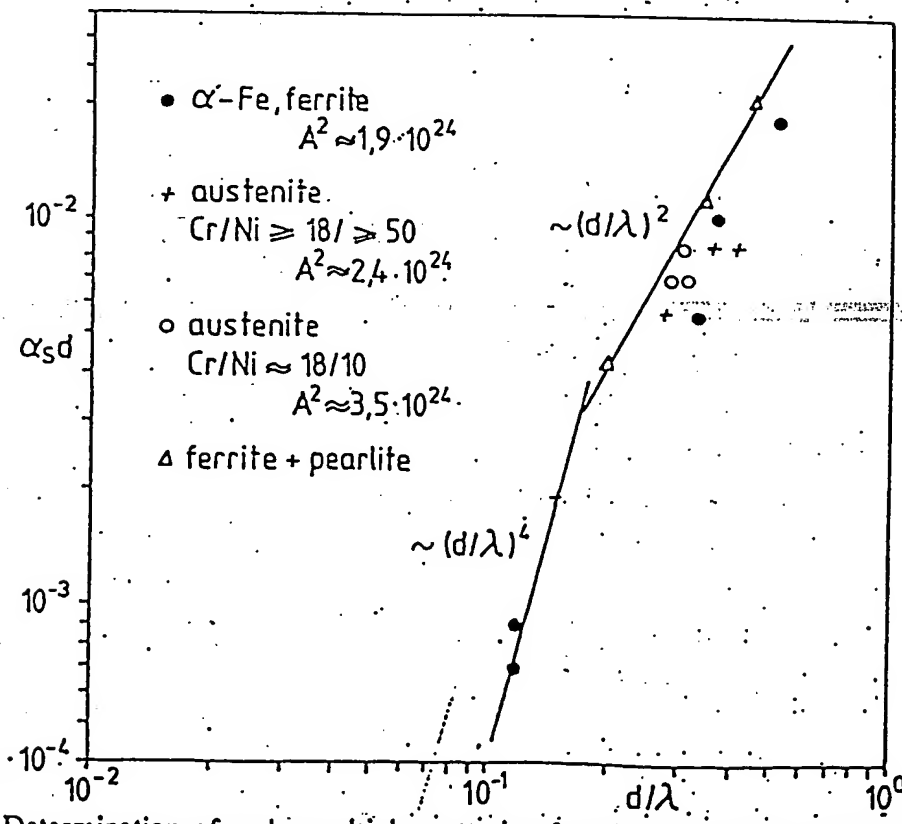

FIG. 22. Determination of α_s by multiple scattering for different types of steel and wi different frequencies.

and thus, from the slope of the straight line, the attenuation coefficient α. In the Rayleigh region, and using eqn (2) with linear frequency dependence of the absorption for the two measurements, we get

$$\alpha_i = a_1 f_i + S d^3 f_i^4 \quad (i = 1, 2).$$

It is then possible to determine d by means of

$$d = \{[\alpha_2 - \alpha_1 f_2/f_1]/[S f_2 (f_2^3 - f_1^3)]\}^{\frac{1}{3}}. \tag{49}$$

The assumption of a linear relationship between α_A and f has been used with good results in several hundred measurements with steel samples (see next section). A squared f-dependence, however, leads in many cases to negative scattering coefficients.

In certain situations another method of nondestructive grain-size determination by means of scattering may be used (Goebbels, 1975), which is based on two measurements on two different samples with a single frequency:

$$A_{Si}(x) = A_0 (\alpha_{Si} \Delta x)^{\frac{1}{2}} \exp(-\alpha_i x) \quad (i = 1, 2),$$

$$\ln A_{Si}(x) = \ln A_{Si}(0) - \alpha_i x. \tag{50}$$

When the absorption is the same in both samples (e.g. same steel from the same cast, but with different heat treatment and hence different grain size), it is possible to determine, by means of eqn (50) and

$$\alpha_i = \alpha_A + S d_i^3 f^4 \quad (i = 1, 2) \tag{51}$$

the two grain sizes to be:

$$d_i = \{(\alpha_i - \alpha_j)/[(1 - A_{Sj}^2(0)/A_{Si}^2(0)) S f^4]\}^{\frac{1}{3}} \quad (i, j = 1, 2;\ i \neq j). \tag{52}$$

The next section gives examples for this technique.

III. Techniques and Applications

A. Backscattering Measurement Techniques

At the present time quantitative backscattering measurements are only possible by means of averaging techniques because phase-sensitive ultrasonic transducers are used. The following signal processing techniques can be used (Kraus and Goebbels, 1977, 1978):

(1) spatial, directional, or frequency averaging;
(2) analogue or digital averaging;
(3) averaging of high frequency (HF) or rectified (DC) signals;
(4) linear or weighted averaging.

They are discussed in the following sections, and the different alternatives are balanced one against another. The measurement procedures used at present will subsequently be shown in detail.

1. Spatial, Directional, or Frequency Averaging

Figure 19 shows that for a fixed position of probe and sample the single high frequency (HF) backscatter signal (A-scan) represents an interference pattern as a result of superimposing all scattering processes from all of the scatterers which lie in the sound beam (for instance, grains in a polycrystalline material). The amplitude-modulated signal has a frequency spectrum quite similar to the spectrum of the transmitted pulse. Backwall echo and scattering signal are coherent signals in this sense. Phase relations between the single scattering centres cause the interference. They can be eliminated by different averaging methods (or by the use of a phase-insensitive receiver).

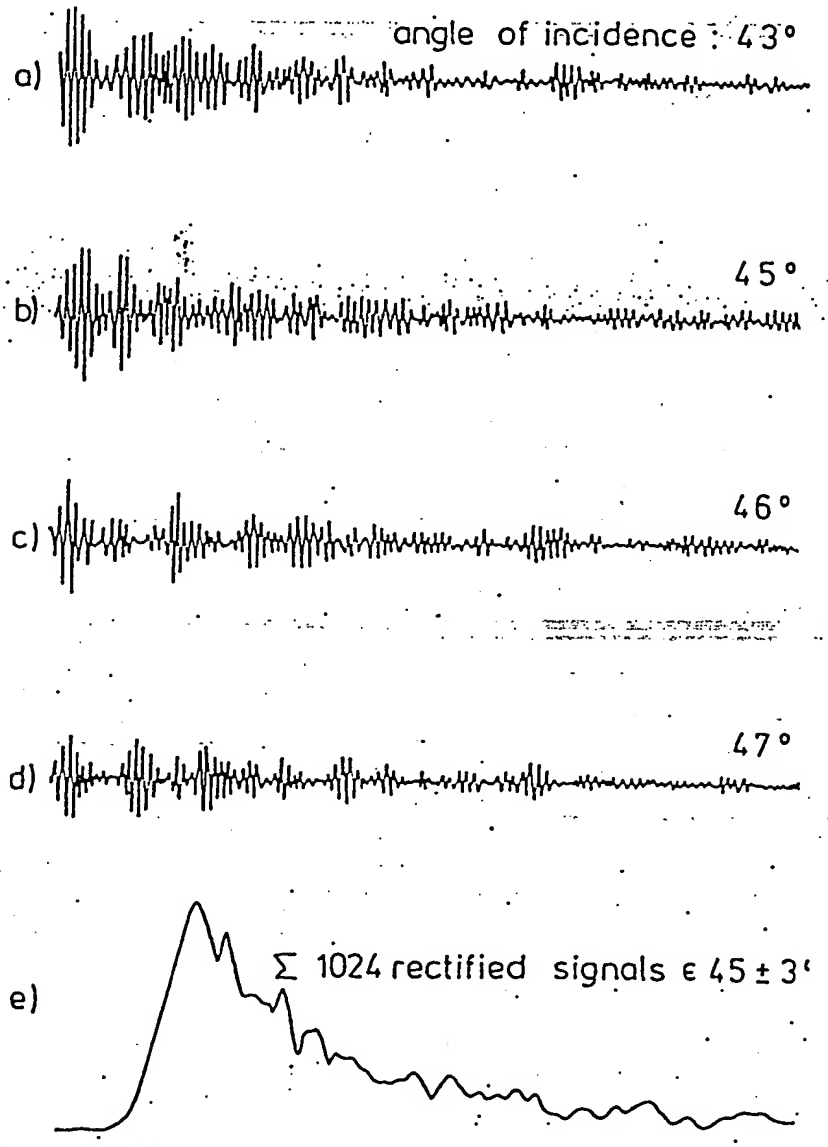

FIG. 23. Directional averaging (6 MHz, T-waves), backscattering signals, austenitic steel, grain size ASTM 4.

For spatial averaging the variation of the position of the probe by approximately one grain diameter or one wavelength suffices to vary drastically the HF signal. Figure 19 shows the averaging of different scattering signals measured in this manner.

The same effect (variation of the volume in which scattering is to be excited) can be achieved by means of directional averaging where the variation of the angle of incidence, for instance by 1°, delivers a new interference result. Figure 23 gives an example of how the averaging by means of scattering signals in the sound angle region $45 \pm 3°$ produces an amplitude curve corresponding to eqn (41).

A third signal averaging method uses wavelength in order to change the phase relations and thus the scattering signal. With this frequency averaging the changing of the central frequency by approximately 0·1 MHz suffices to produce a new interference pattern. Figure 24 gives an example, comparable to Figs 19 and 23. Here the averaging processes have been carried out on signals with electronically excited frequencies of 3·7–5·3 MHz.

For a low-damped piston source with a resonance frequency f_0, pulse lengths of 10λ must be used in order to oscillate it at $f_0 \pm \Delta f$. The transducer used in Fig. 24 was therefore a broadband transducer with about 2λ–3λ pulse lengths. A probe with small bandwidth would, in this small frequency range, result only in an amplitude variation for the single A-scan, but not in a variation of the interference pattern.

2. *Analogue and Digital Averaging*

There is an important difference between the averaging of analogue and digitized signals. In the analogue technique (Koppelmann, 1972) a small gate (for instance 1 μs duration) is slowly moved during the variation of the positioning of the probe, the angle of incidence or the exciting frequency, and the mean amplitude of this gate is registered on an x–y-recorder, i.e. v (gate) $\ll v$ (averaging movement) $\ll v$ (ultrasound). This requires, however, a completely constant coupling during the recording process; variations of the coupling and thus fluctuations of the amplitude excited at $x = 0$ (eqn (41)) directly influence the "plot", but only at the location of the gate at the time of the fluctuations in the coupling. This means that even for a homogeneous structure, $A_S(x)$ can show a curve which differs greatly from an exponential decay.

For this reason the averaging of digitized signals is generally preferred, where each A-scan—whether the coupling is constant or fluctuating—is stored, completely digitized, in a signal averager. Here the fluctuations of the coupling are noticeable only as a constant factor for the complete back-scattering amplitude $A_S(x)$. They are, therefore, only of importance when the

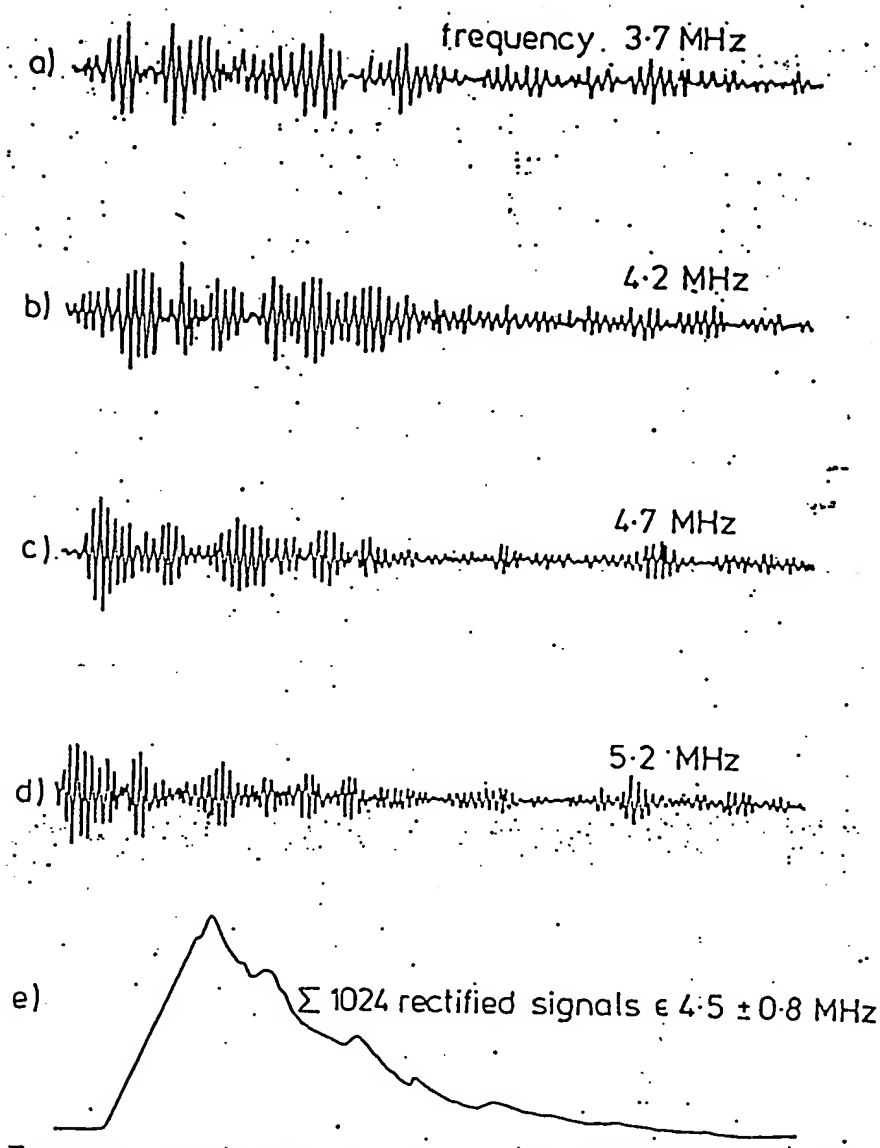

FIG. 24. Frequency averaging (45° T), backscattering signals, austenitic steel, grain size size ASTM 4.

absolute values of the amplitude (particularly $A_S(0)$) of different backscattering measurements are to be compared with each other quantitatively. The same surface quality for different samples therefore reduces this effect to a minimum.

Analogue averaging requires approximately 1 min for the recording process of $A_S(x)$, while for digital averaging, with the present state of the art, the recording in the signal averager requires only a time of 1 μs/address (for an A-scan) and so 1 s/1000 averaging processes. Generally approximately 200 averaging processes are sufficient to receive a suitable function $A_S(x)$, as per eqn. (41). Further developments (Linzer *et al.*, 1978; Kraus *et al.*, 1979) in the averaging electronics further reduce recording times to 0·02 μs/address (50 MHz-rate) and 0·05 μs/address (20 MHz-rate) respectively.

Flaw detection by means of signal averaging in coarse-grained materials (austenitic welds, castings) provides also, with the DC-technique, a better signal-to-noise ratio than for the single A-scan, because the top values of the scattering amplitudes will be reduced by interference to the curve of eqn (41). This reduction can amount to 20 dB, so that signals which are drowned in noise in the single A-scan may be recognized by averaging with sufficient signal-to-noise ratio (see Fig. 26 and also Section IIIB).

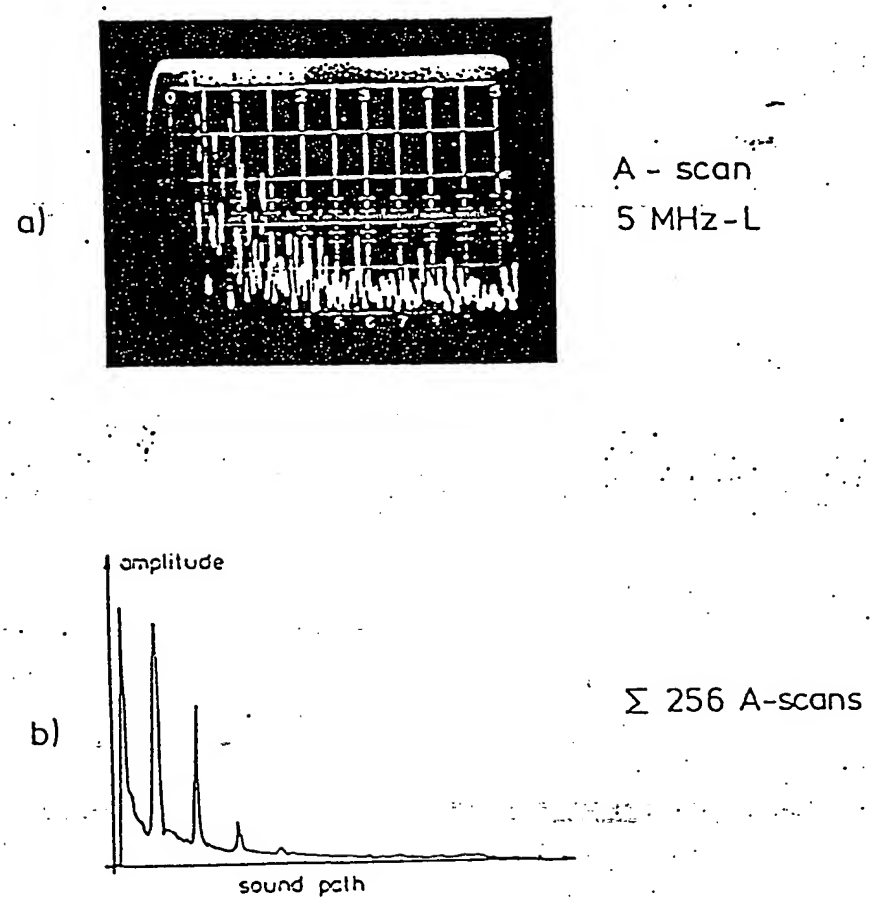

FIG. 26. Signal enhancement by spatial averaging for a backwall echo sequence.

4. Linear and Weighted Averaging

In the digital averaging techniques which we have investigated so far, each A-scan is evaluated with the weighting factor 1 (linear averaging). There are also developments to use different weighting factors for each single A-scan, so that signals from earlier scans have less influence in the averaging process than those from the actual testing time and in the actual testing position (Goebbels *et al.*, 1978a). Particularly, exponential averaging (the Nth signal will be multiplied by the factor e^{-1}, N being selectable) can be of advantage in an automatic inspection because after each A-scan a complete averaging

result is to hand and it is not necessary to wait for the sum of N A-scans. With the high transfer speeds of signal averagers (see above) possible today this advantage disappears. In linear averaging the improvement of the signal-to-noise ratio (S/N-R) is, for HF-averaging, proportional to the square root of the number N of the summed A-scans (through the averaging process, the noise signal in the A-scan coherent to the reflector signal changes to an incoherent, stochastic noise signal):

$$\text{S/N-R} \sim \sqrt{N}, \tag{53}$$

while for DC-averaging the optimum attainable signal-to-noise ratio is given by division of eqn (42) by eqn (41) and is (Ermolov and Pilin, 1976; Goebbels *et al.*, 1978):

$$\text{S/N-R} \sim A(x)/A_S(x) \approx (\alpha_S \Delta x)^{-\frac{1}{2}} \tag{7}$$

(without consideration of sound field diffraction). Exponential averaging does not reach the signal enhancement given by eqns (53) and (7) until $N \to \infty$ (see above).

The connection between materials structure characterization and flaw detection has been stated in an easy way by means of this description of the different possibilities to execute scattering measurements. Equation (7) shows directly that the signal-to-noise ratio increases with decreasing pulse length Δx; physically, this results from the axial reduction of the volume in which scattering can be excited. Part B of this section also contains several examples for the improvement of the signal-to-noise ratio by signal averaging techniques.

5. *Equipment for Backscattering Measurements*

The scattering measurement device built up by Koppelmann (1972) is described in Section III.A2. The industrial applications in practice have been towards the nondestructive determination of the case-hardening depth on steel cylinders: the fine-grained hardened layer gives a low, slowly decreasing scattering amplitude, which leads (in the transfer region to the coarse-grained, ductile base material) to a maximum and then to a second part of the scattering curve with a steep decay. A conclusion can thus be drawn on the hardening depth from the time of flight and the sound path.

Due to the faster signal processing with digital equipment and the amplitude-modulated disadvantage of analogue averaging, the digital version is described in more detail (block diagram in Fig. 27): a frequency generator produces the frequency f with which the probe, working in either contact- or immersion-technique, is excited. A burst generator delivers the 1λ–99λ

long electric pulse, which operates the probe over a 50 dB power amplifier and through a transmit/receive circuit. With the frequency generator and the variable burst length, there are already two tuning devices on the transmitting side to give optimum transducer excitation. Experience has shown that in this way, with less electrical energy, the same acoustic result in pulse operation is obtained compared with the usual ultrasonic equipment, stimulating each probe of each frequency with the same electrical signal.

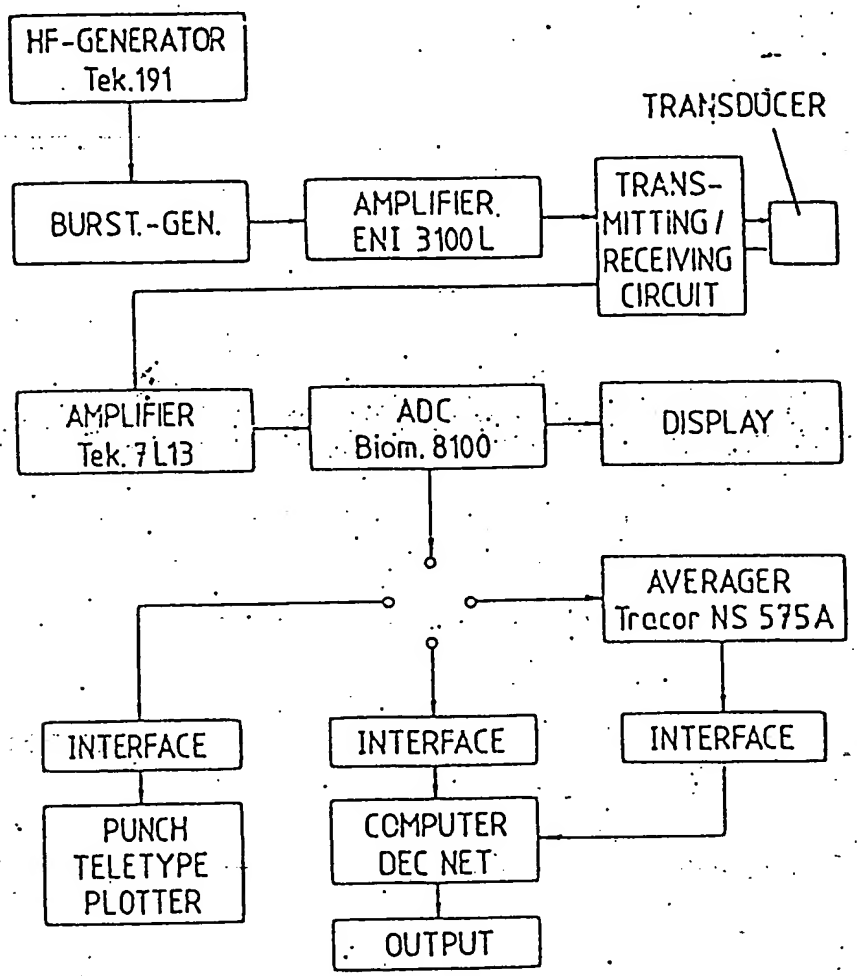

Fig. 27. Block diagram of the equipment for scattering measurements.

Because of the low scattering signal amplitudes, the receiving amplifier mus be of low noise and high gain; for quasi-monochromatic signals it must als have a small bandwidth. The receiving amplifier, used in Fig. 28, rectifies th scattering signals. Here too the central frequency of the measured signals ca be sensitively tuned.

The rectified scattering signals will be digitized by an analogue-to-digita converter (ADC) in order to be sent via a suitable interface directly to computer and be compressed, or they will be summed in a signal averag

for subsequent recording or transmission to the computer. Scattering curves, recorded on an x–y-recorder, can be evaluated manually. The usual processing method is conversion to a logarithmic scale in the computer followed by plotter recording. It is possible in this way to describe the homogeneity of the material or to state if multiple scattering is present. The software in the computer contains programmes for linear regression of the measuring points in order to find the attenuation coefficient α from the slope, using eqn (48), and to compute the mean grain size by the two-frequency method, using eqn (49).

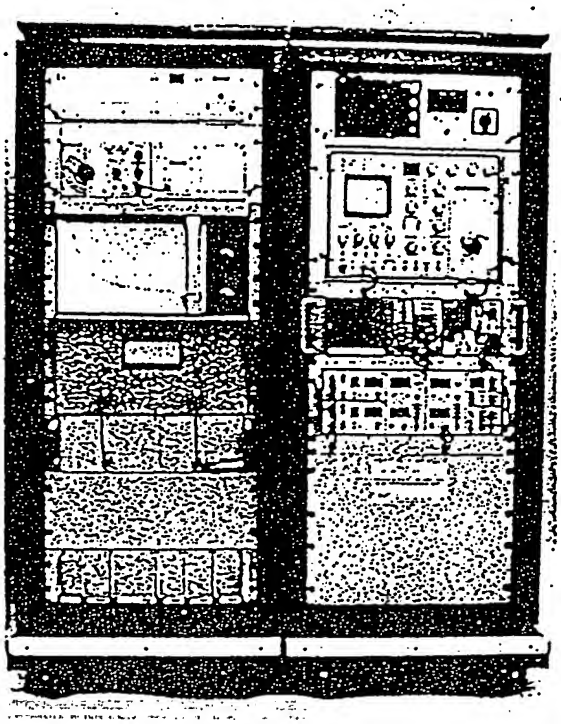

FIG. 28. Device for ultrasonic backscattering measurements.

Figure 28 is a photograph of the equipment described here for scattering measurements, which is mounted in two 19 in racks 1·50 m high. Spatial averaging which is most widely used is done with a sample- or probe-manipulator or, under difficult conditions on site, by hand.

Table VIII gives the technical specification of the equipment used at present. A prototype developed for grain size-determination for steel by means of ultrasonic backscattering measurements is independent of a large computer since all procedures (manipulation, measurement, evaluation) are controlled by microcomputer.

All equipment described here has been planned and built for pulse-echo and hence for backscattering measurements. It also enables one to work with

separated transmitters and receivers, thus analysing, for example, the angular dependence of the scattering.

TABLE VIII

Specification of the Equipment for Ultrasonic Scattering Measurements

Transmitter—frequency range	2–25 MHz (continuous)
—pulse length	1–99 λ (digital)
—power	50–100 Watt
—bandwidth	0.25—105 MHz
—impedance	50 Ω
—pulse repetition frequency	Single shot until 10 kHZ (continuous)
Receiver—impedance	50 Ω
—bandwidth (–3 dB)	3 MHz
—frequency range	2 MHz–1·8 GHz
—maximum amplification	80 dB
ADC—sample rate	⩽ 100 MHz
—resolution	8 bit
—memory	2k (2048)
Averager—memory	2k
—resolution	18 bit
—average velocity	⩽ 10 μs/address
Transducers	Any type

B. Applications

1. Grain Size Determination

An essential application of the backscattering measurement lies in non-destructive grain size determination (Goebbels, 1975, 1976; Goebbels and Höller, 1976, 1978). The three methods which can be applied (2*f*, 2*d*, multiple scattering) have been considered in Section IIIA. They have been used for grain size determinations in the regions ASTM 1–11 in ferritic and austenitic steels, in steels with mixed structures such as ferrite/pearlite, ferrite/bainite, and partly, too, in free machining steels. The use of shear waves in the Rayleigh region with the restriction

$$0{\cdot}03 \lesssim d/\lambda \lesssim 0{\cdot}3 \tag{54}$$

permitted the analysis of several hundred samples, using the scattering parameter $S_T = 0{\cdot}0131$ according to eqn (21). Shear waves were favoured because the scattering amplitude at the same wavelength is higher than for longitudinal waves (due to mode conversion L→T with the use of L-waves)

d because, in this way as well as in immersion techniques (reflection of the surface signal) and in contact techniques (dead time during the delay time in buffer), scattering amplitudes of the direct surface region can also be measured.

Measurements with the assistance of multiple scattering could also be extended into the region of stochastic scattering (Fig. 22), where the scattering parameter 0·007 $(mm/\mu s)^{-2}$ resulted. As stated in Section IIB, no theory exists for this region, which also takes the mode conversion in polycrystalline materials into account. Two-phase systems such as pearlite have not been analysed, as no theoretical basis yet exists.

Fine-grained structures with grain sizes below 10 μm had to be excepted as well, as this would have required the use of frequencies in excess of 20 MHz (which furthermore would not have permitted a reasonable correlation with d values determined light-microscopically by metallography), as well as grain sizes over 500 μm, because there are then no longer enough grains in the sound beam to guarantee a sufficient statistical orientation of the grains.

The comparison between grain sizes, determined metallographically and by means of ultrasonic scattering, is shown in Fig. 29. For operating within the range (except for some multiple scattering measurements) stated in eqn (54) for

$d \in$ ASTM 11–6 (9–50 μm)	frequencies between 10 and 20 MHz,
$d \in$ ASTM 6–4 (50–100 μm)	frequencies between 5 and 10 MHz, and
$d \in$ ASTM 1–4 (100–300 μm)	approximately 6 MHz

were used. The results (data of the samples in Table III) show a satisfactory agreement between the ultrasonic value and the metallographic value. The fluctuations of the single-value determinations are ±15%, corresponding to ± half an ASTM class. This agreement is all the more astonishing because the following simplifications are used:

(1) constant d^3f^4 law over the range, as per eqn (54);
(2) mean d- and f-values instead of d-, f-distributions;
(3) overproportional contributions of the larger grains with the d^3-law and higher frequency parts with the f^4-law;
(4) secondary phases (occasionally up to 30% pearlite) are completely neglected;
(5) the mean grain volume used is d^3 (= cube volume);
(6) the use of $S_T = 0{\cdot}0131$ for all calculations computed in the Rayleigh region;
(7) d (metallography) is a value biased towards small grain sizes, since the section through the volume does not cut all grains in their full diameter;

(8) all grain sizes determined by the two-frequencies method usually have been computed on the basis of a linear frequency dependen absorption.

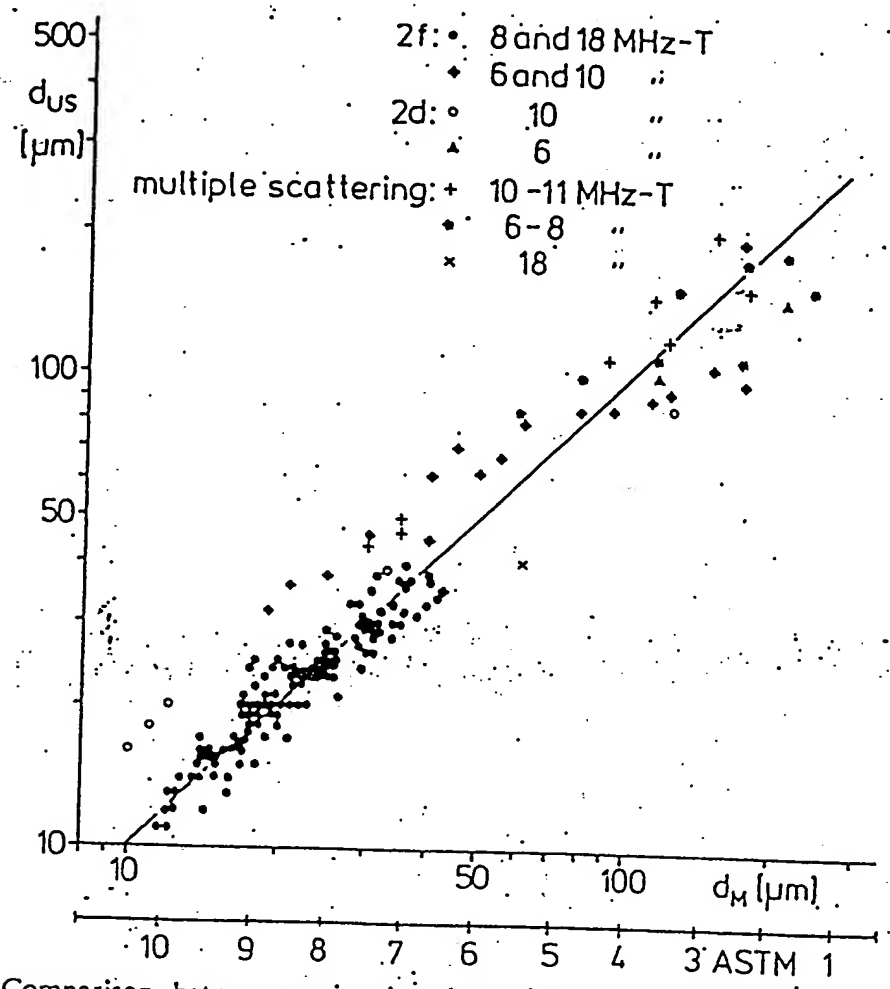

FIG. 29. Comparison between grain size determination by ultrasonic backscatte measurements (d_{US}) and by metallography (d_M).

The absorption coefficient will also be determined for each quantita determination of scattering coefficient. The behaviour of the absorpt coefficient under the above mentioned conditions and assumptions already been discussed in Section IB3 and in Fig. 4. It is surely of interes obtain more detailed information here although these tests have dem strated the possibility of backscattering measurement for the quantitat grain size determination in steel, independently of other methods.

2. *Structure Judgement*

The comparison between scattering and attenuation measurements in Ta IX shows clearly that the measurement of backscattering gives informati

about the structure inside the material with a resolution equal to the pulse length Δx. This is important since the homogeneity of a structure influences the mechanical and technological properties of a material and thus the decision concerning its application in practice. The following structure parameters are decisive for both metallic and non-metallic materials:

(1) grain size, grain size distribution, structure combination in mixed structures;
(2) secondary phases, segregations, inclusions, pores, microcracks, etc.;
(3) macroscopic lamellar tearing, texture and anisotropy;
(4) residual stresses.

TABLE IX

Comparison of Scattering Measurements and Attenuation Measurements

Problem	Backscattering measurement	Attenuation measurement by backwall echoes
Sample	Any shape, thickness $> \Delta x$ (pulse length)	Plane-parallel samples; deviations leading to additional losses
Surfaces	Any surfaces, as long as probes can be coupled in contact-technique or in immersion-technique	Very flat surfaces; deviations leading to additional losses
Coupling	Coupling and coupling disturbances of constant influence for the whole $A_s(x)$	Optimized coupling necessary; deviations leading to additional losses
Resolution	Axially: Δx	No resolution, measured value is integral over $\alpha(x)$ between surface and backwall
	laterally: $\approx 2 \times$ sound beam diameter	$1 \times$ sound beam diameter

Local or extended deviations from the mean structure are responsible for attenuation- and scattering-behaviour because grain size, other phases, and anisotropy enter directly into α_S. The semi-logarithmic presentation of backscattering measurements, $\ln A_S$ as a function of x, thus shows immediately whether a homogeneous structure is present, curve as per equation (48), or if measurable disturbances appear. The extension of these disturbances has to be comparable to the analysed volume element (Δx times sound beam cross-section).

Equation (44) formulates generally the curve of the scattering amplitudes for inhomogeneous structure. In Fig. 30 this is sketched for real values (fine-grained steel structure, 6 MHz T-waves), where

(1) the dimension of the regions of inhomogeneities (RoI) is large co
pared with Δx;
(2) the absorption is assumed to be constant;
(3) the scattering coefficient changes drastically upward by a factor 2 a
then takes up its former value after leaving the RoI.

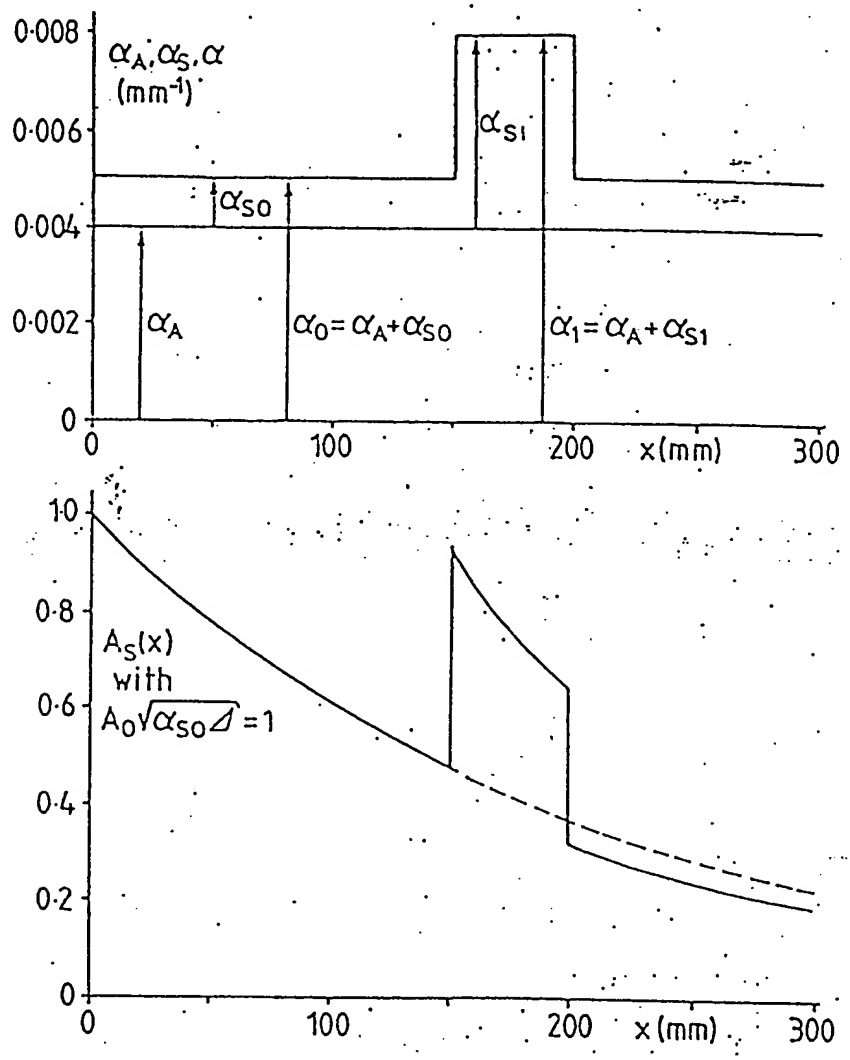

FIG. 30. Backscattering amplitude—schematic—for locally inhomogeneous structure.

All possibilities are given between the curve $A_S(x)$ in homogeneo
structures (the dotted line in Fig. 30) and the sketched scattering amplitu
curve in RoI (Goebbels and Höller, 1978; Goebbels *et al.*, 1978b).

$A_S(x)$ can vary by a small amount over an extended region from t
characteristic curve of homogeneous structure at different places in the sa
solid; locally, narrow high amplitude additional scattering (Fig. 31) ca
however, also occur.

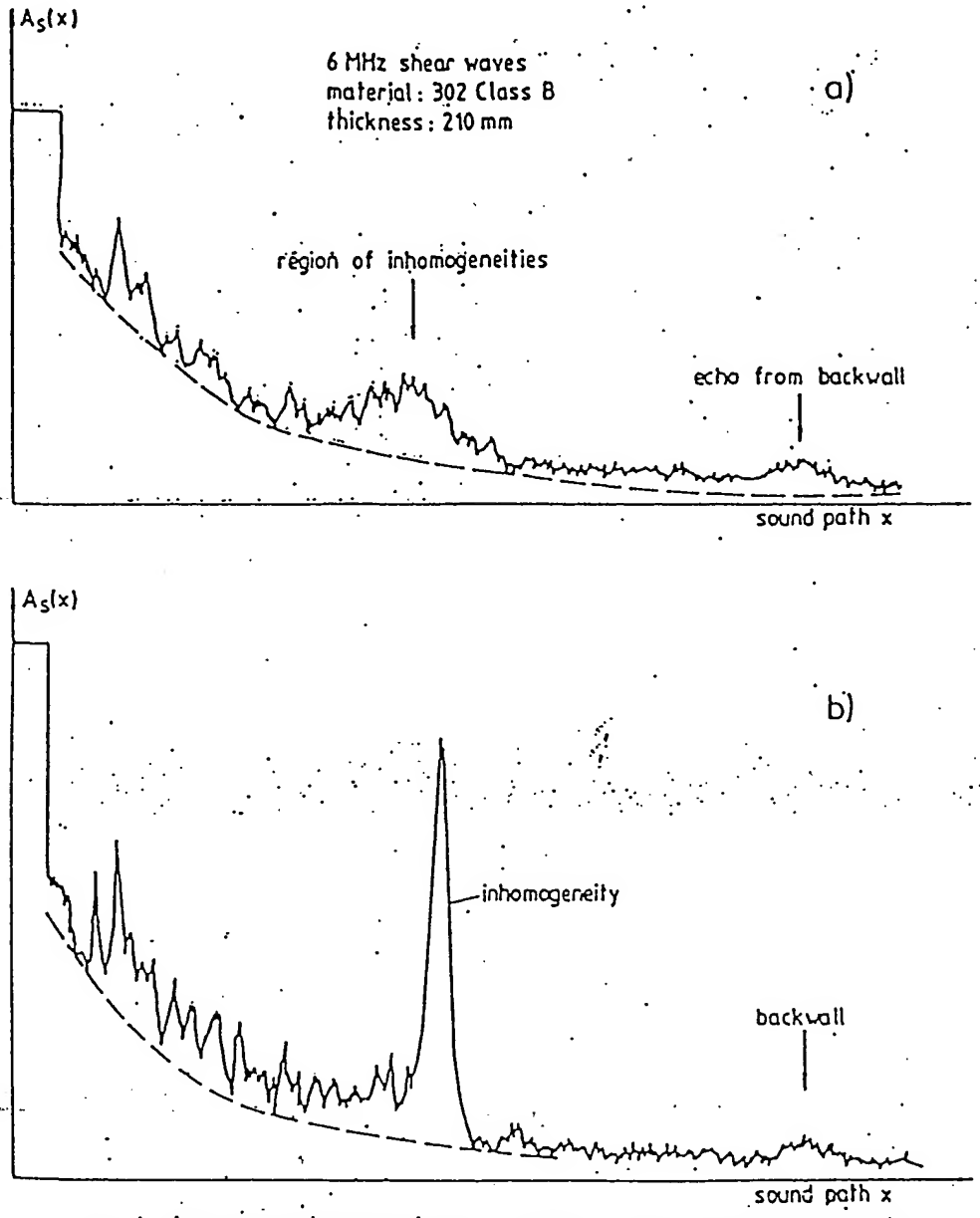

FIG. 31. Scattering indications from different types of heterogeneities.

In Fig. 32 there are three inhomogeneities, completely different from each other, identified by means of backscattering, whose metallographic analysis is shown in Fig. 33:

(a) Sheet with 0·16% C, 10 MHz, T-waves, 45°

Between the upper and lower surface of a 20 mm thick sheet, a narrow high-amplitude signal, which extends over several millimeters, appears in the middle of the sheet. As shown in Fig. 33(a), this derives from a pearlite segregation approximately 0·5 mm thick. In this case the extension of the measured function is larger than reality, because $\Delta x \gg \text{RoI}$. The oblique incidence of the divergent sound beam at the

segregation line must also be considered, i.e. informatio extension of the pulse length can also come from RoI of muc dimension. The high resolution in Fig. 32(a) is also due to th this pearlite segregation is extended over the complete sheet.

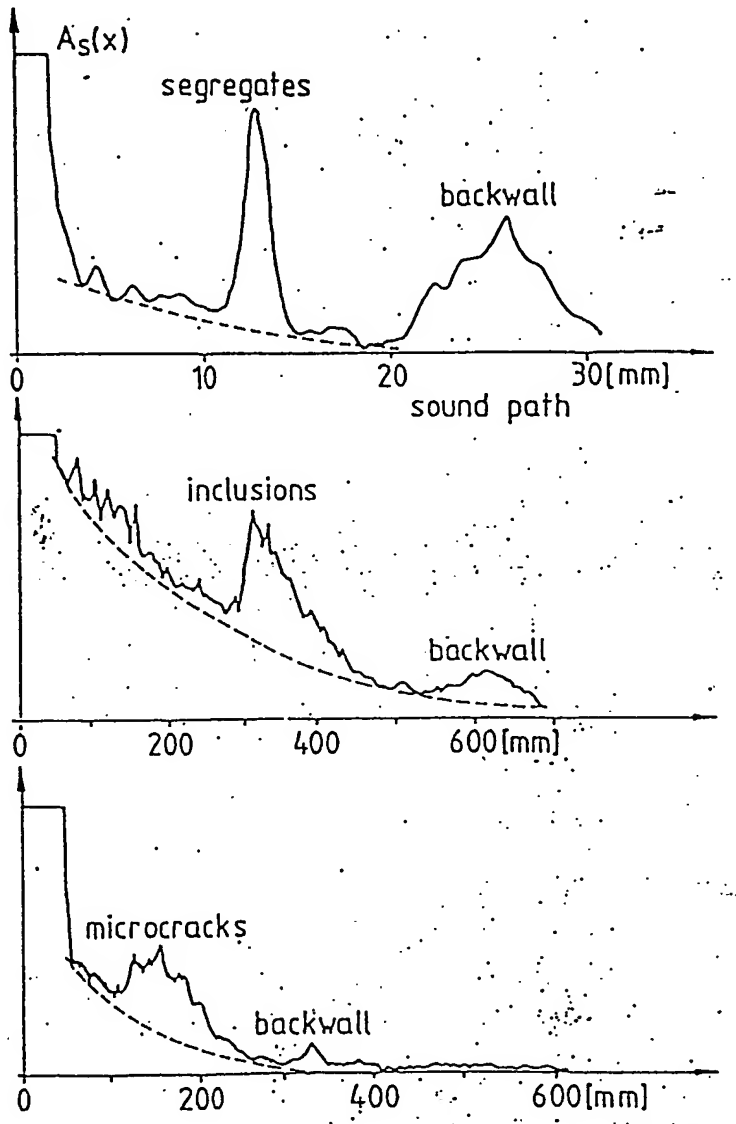

FIG. 32. Backscattering curves from inhomogeneous structures (6 MHz, shear waves)

(b) Sheet 22 NiMoCr 3 7, 6 MHz, T-waves, 45°
Approximately in the middle of the sheet of a sample of pressu vessel steel 22 NiMoCr 3 7, approximately 220 mm thick, scatteri indications extending over 50 mm are superimposed on the backgrou curve. The metallographic analysis (Fig. 33(b)) shows that a 40–50 m extended region with manganese sulphide inclusions appears relativ suddenly. In this case ($\Delta x \ll$ RoI) the backscattering measureme

provides an indication of the extent of the RoI quantitatively. While the sulphides have small dimensions and appear only isolated in the metallographic picture, they still lead in the scattering amplitude function to a connected (averaged) signal, superimposed upon the scattering of the basis structure.

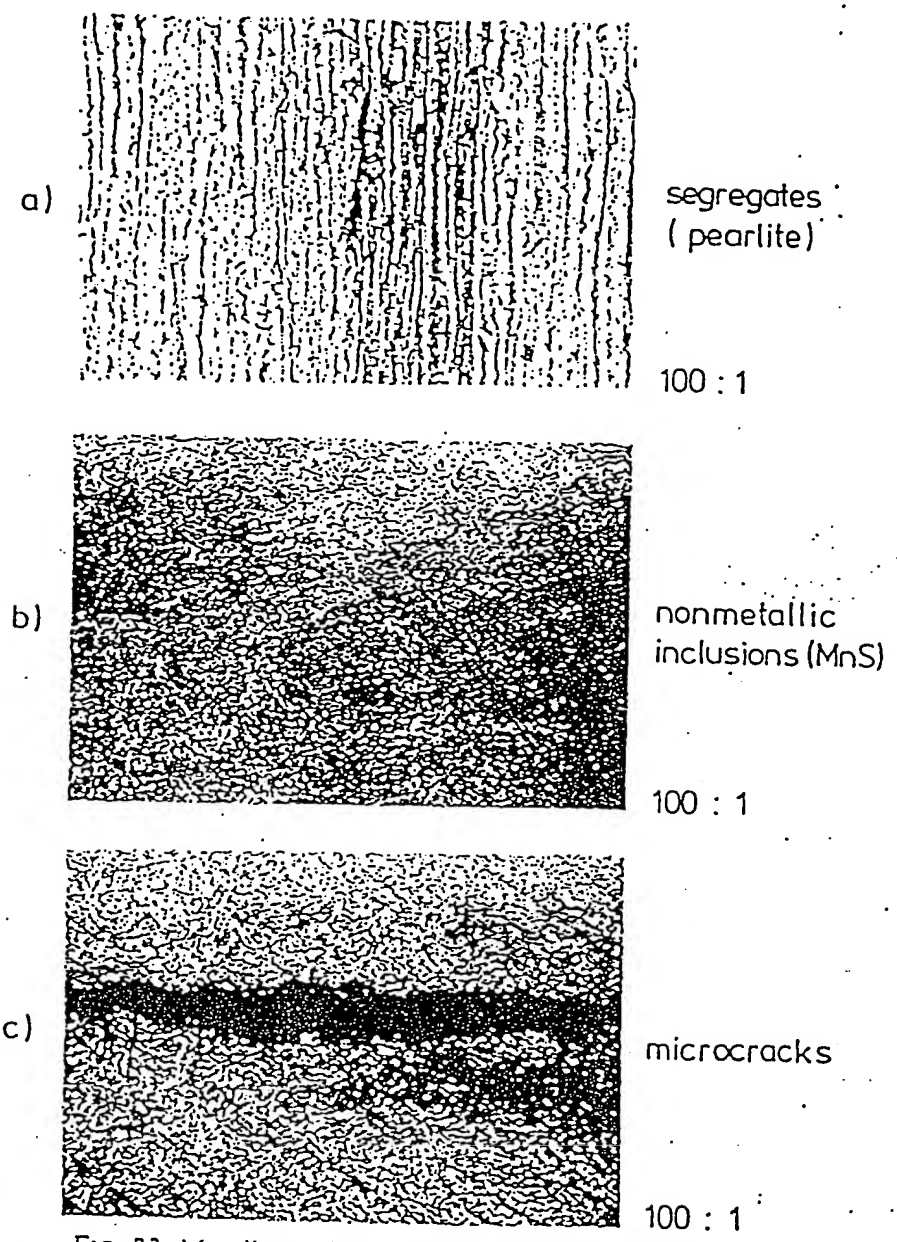

FIG. 33. Metallographic analysis of heterogeneities in steel.

(c) Sheet 22 NiMoCr 3 7, 6 MHz, T-waves, 45°

With another sheet, approximate thickness 130 mm, signals from a RoI were also registered in the middle of the sample over approximately 40 mm. The metallographic analysis (Fig. 33(c)) again confirms

the extension of the RoI; in this case, however, microcracks are the cause, with sizes between approximately 10 μm and 1 mm.

These examples show that quite different structure anomalies can lead to comparable results in the scattering amplitude function $A_S(x)$. The cause may be found in the fact that the parameters: type, geometry, magnitude orientation and concentration of inhomogeneities influence the measured scattering amplitude. Thus the jump $\Delta\rho v$ at the phase boundary matrix-scatterer is much smaller for MnS (as a non-metallic inclusion in steel) than for a pore; a planar "reflector" gives a higher scattering amplitude than a spherical one and so on. Finally, the overlapping range of scattering diffraction and reflection will be reached at single inhomogeneities, whereby the single contributions depend essentially on d/λ; for example.

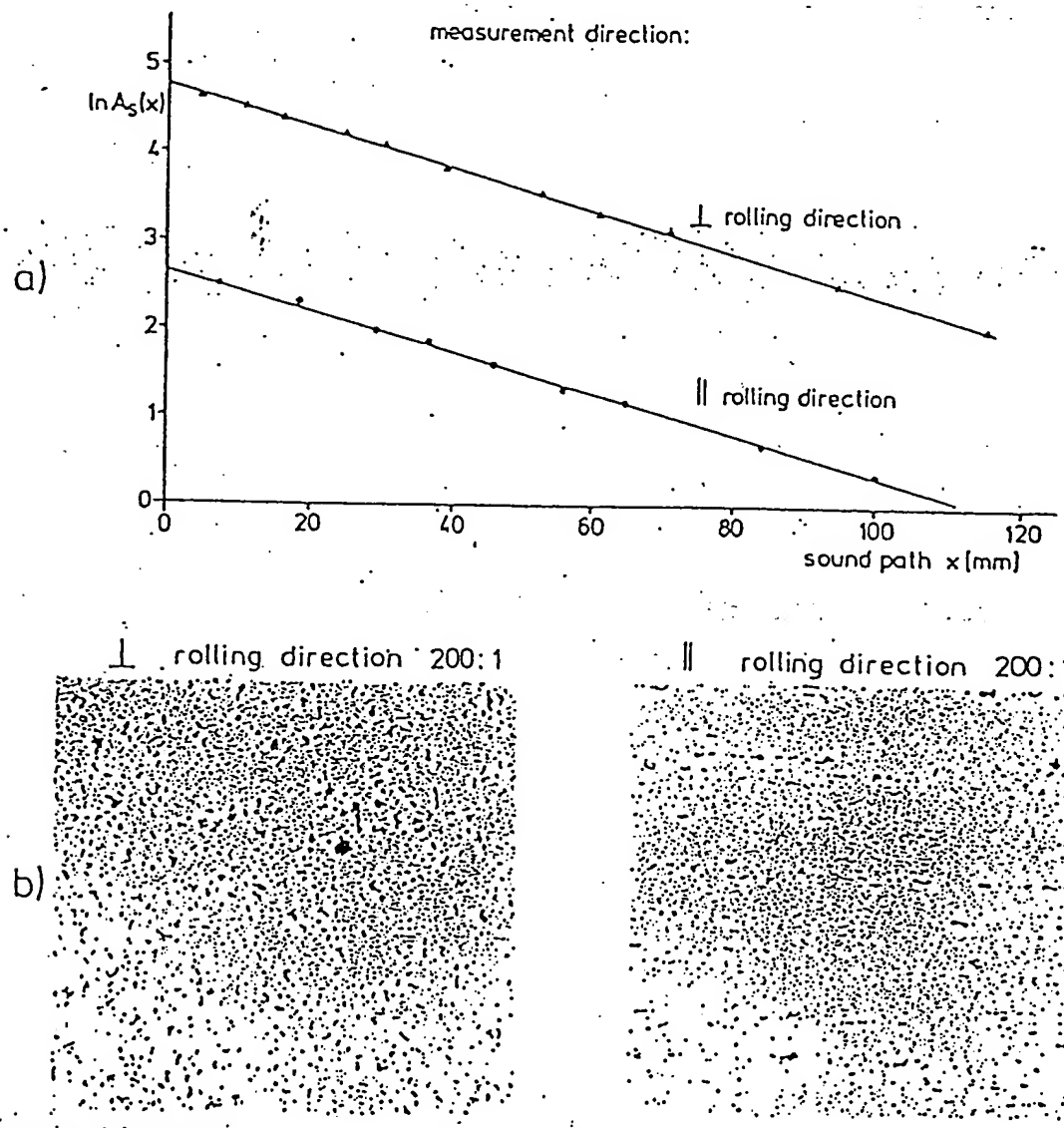

FIG. 34. Backscattering curves (half-logarithmic) and metallography for alloy AlCuMg.

All in all, it can be seen from this that scattering measurements give in a simple way qualitative information about RoI's; quantitative statements, however, are limited for the present to information on the extension of an identified RoI, on the transfer behaviour between undisturbed matrix and RoI (monotonic, abrupt) and on the relationship between RoI signal and scattering amplitude of the undisturbed structure. Further fundamental work on the scattering in multiphase materials with a polycrystalline base material is necessary.

Texture and anisotropy of materials resulting, for instance, from rolling or forging can also be considered in this context as inhomogeneous structures. Figure 34 gives structure views vertical and parallel to the rolling direction, and the corresponding scattering curves for an AlCuMg alloy.

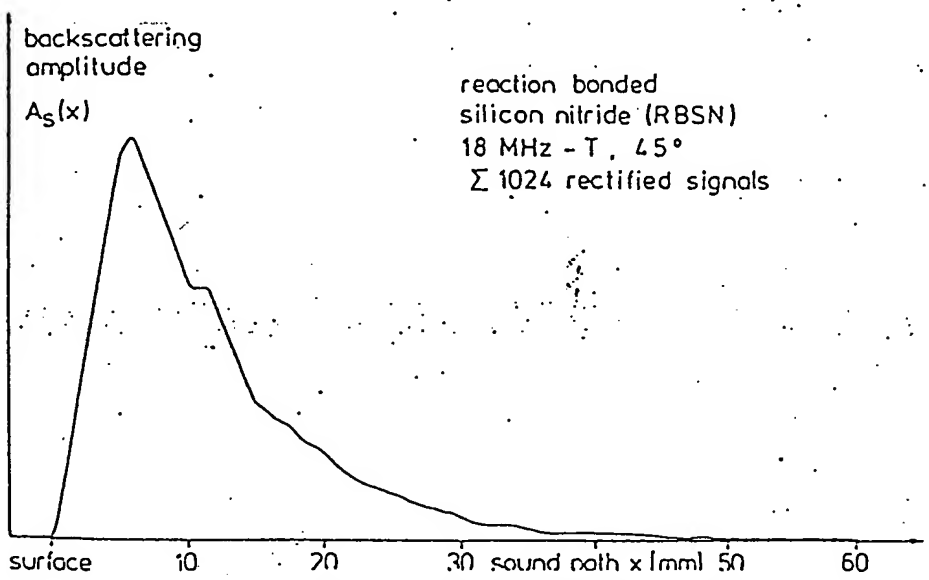

FIG. 35. Backscattering amplitude from RBSN.

High alloying grade, resulting in a structure with many different phase components as well as the deformation texture, means that in the two sound directions vertical to one another, scattering amplitudes occur differing by a factor of around 10, but with nearly equal attenuation coefficients (slope in the semi-logarithmic plot).

This nondestructive homogeneity evaluation, employed on metallic materials, can also be transferred to other materials that show scattering: for example to ceramics, composites, and also to biological tissues whose scattering has already been analysed in detail (Hill *et al.*; 1978; Sigelmann and Reid, 1973) but, due to the complexity of the tissue, is not yet completely understood.

Figure 35 gives an example for non-oxidic ceramics (Si_3N_4, SiC) as intended for use (Walzer *et al.*, 1976) in the high-temperature-vehicle-gas-turbine. At

a grain size of $\lesssim 1$ μm, and a sound velocity approximately 11 mm/μs for L-waves and 6 mm/μs for T-waves (resulting in small scattering parameters $S_{L,T}$ as per Figs 5 and 6), the scattering of hot pressed ceramics is only measurable in the frequency region around 200 MHz. Reaction-bonded Si_3N_4 or SiC, however, with a porosity up to 20%, pore size ≈ grain size ≈ 1 μm, presents a high scattering matrix even at around 10 MHz, caused by the large jump $\Delta\rho v$ at the phase boundary grain–pore.

3. *Welds*

Ferritic and austenitic welds, from a scattering point of view, act as inhomogeneity regions, extending from the heat affected zone (HAZ) to the weld material itself.

In the HAZ there is a microscopically changed structure in comparison with the base material, due to the heat transfer during welding and subsequent annealing. The absorption is particularly affected here by the segregation structure. Coarse- and fine-grained structures in the HAZ can be shown up by metallography fairly simply; scattering measurements, however, have not been successful up to now. The extension of these regions is small, $<\Delta x$, disturbances by the fusion line superimpose on one another, and—the most important point—a structure comparable to the one outside the coarse-grained zone lies in the inside of the coarse grain, representing the primary grain boundaries. The scattering therefore results mainly from the fine structure, not from the primary grain boundaries bordered with segregations.

At the fusion line the crystallographic structure of the weld leads to a jump in the sound impedance ρv not only for ferritic, but also for austenitic

TABLE X

Ultrasonic Wave Velocity in Steel, Mean Values and Single Crystal Values; Determination of the Coefficient of Reflection R

	(mm/μs)				(mm/μs)			
	Poly-crystalline	Single crystal			Poly-crystalline	Single crystal		
Material	$\langle v_L \rangle$	$v_{L,min}$	$v_{L,max}$	$R_{L,max}$	$\langle v_T \rangle$	$v_{T,min}$	$v_{T,max}$	$R_{T,max}$
α-Fe	5·90	5·48	7·08	0·09	3·23	2·47	3·84	0·13
X6 CrNi 18·11[1]	5·80	5·20	6·53	0·06	3·15	2·11	4·02	0·20
X6 CrNi 18·12	5·96	5·20	6·53	0·07	3·40	2·11	4·02	0·23
X CrNi 12·12	6·17	5·45	6·67	0·06	3·25	2·11	3·94	0·21[1]

[1] The values for the single crystal are taken from the row below:

$$R_{max} = \max \varepsilon \left[\left| \frac{v_{min} - \langle v \rangle}{v_{min} + \langle v \rangle} \right|, \left| \frac{v_{max} - \langle v \rangle}{v_{max} + \langle v \rangle} \right| \right].$$

eius. While the base material possesses a mean sound velocity $\langle v \rangle$ for andom distribution of the grain orientations, there is a particular velocity t the fusion line in the weld which results from the crystallographic orient-tion with respect to the sound propagation direction.

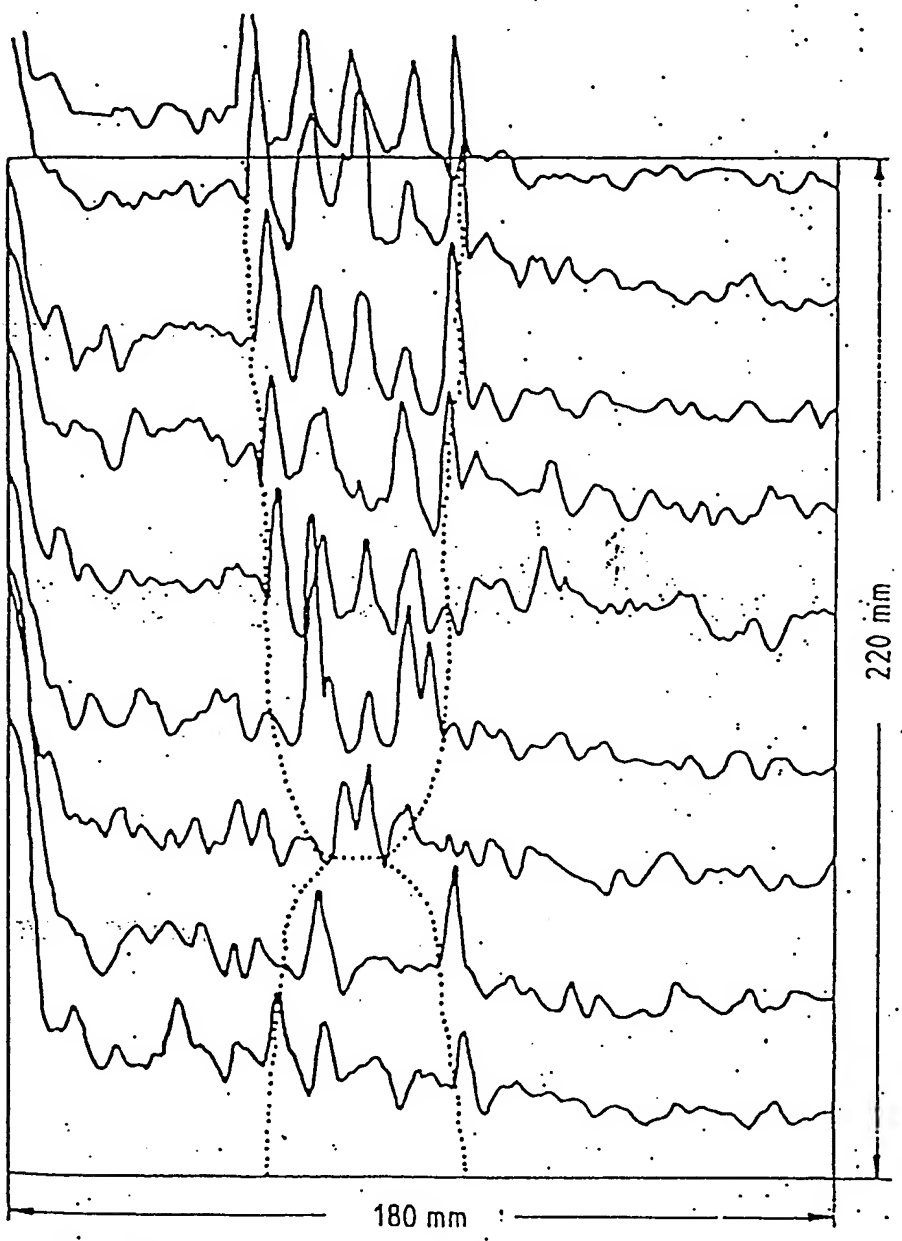

FIG. 36. Backscattering through ferritic weld (10 MHz, *L*-waves).

In Section IB1 the sound velocities in cubic single crystals have been iiscussed, and Table X shows which reflection coefficients R (assuming equal lensity) are to be expected in the extreme, for a vertical incident wave. Thus x :en 5 and 25% of the ultrasonic amplitude can be reflected at the fusion ine. Figure 36 gives an example of this (ferritic steel, 22 NiMoCr 3 7)

(10 MHz, L-waves, vertically through the weld). Scattering measurements can also be used in this way for the identification of welds.

The same situation is valid for the overlapping of the various passes in the weld itself. The curves plotted over each other in Fig. 36 allow the boundaries where the three passes of the weld come together to be clearly recognized. A quantitative computing of the scattering in the weld itself is not possible through the signals of the fusion lines and the passes. There results, however, qualitatively a valuable image of the structure inside welds and in their vicinity, as can be seen in Fig. 37 for a nozzle weld (Goebbels and Höller, 1978; Goebbels *et al.*, 1978b).

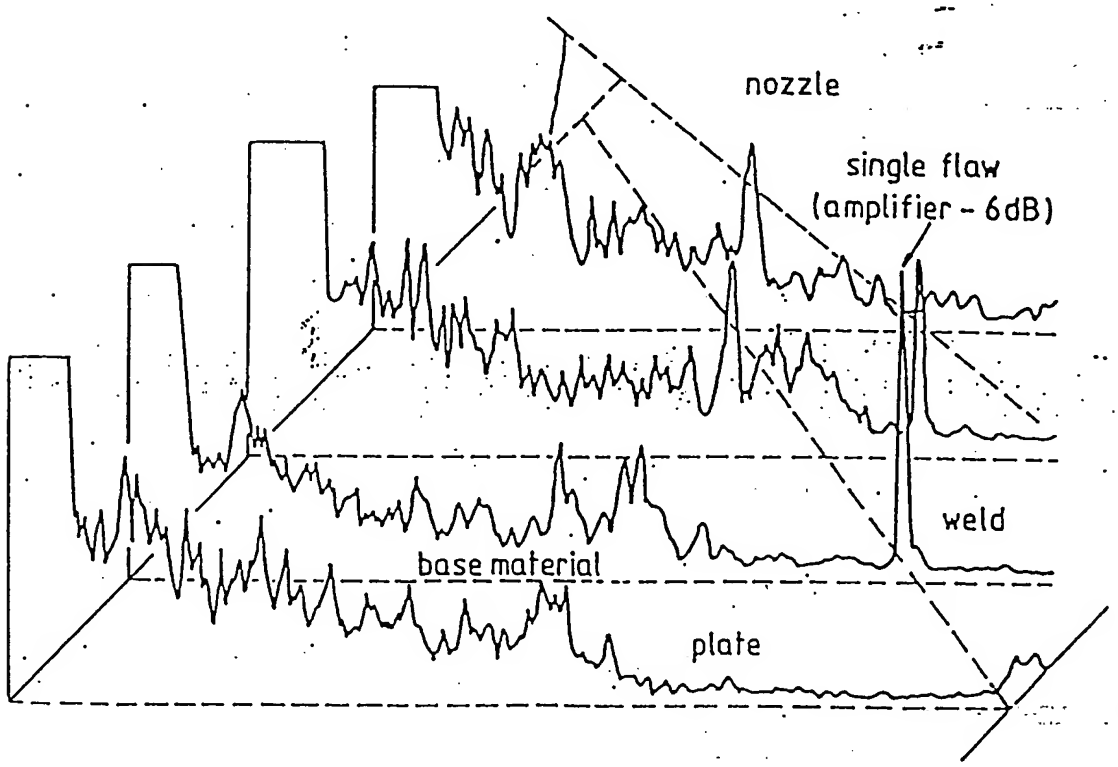

FIG. 37. Backscattering through base material and weld of a nozzle test piece (6 MHz shear waves).

4. *Signal-to-noise Ratio*

In coarse-grained materials (austenitic welds, castings) scattering signals occur at low frequencies (≈ 2 MHz) as well, rendering the detection of defects difficult. The single A-scan contains (besides the reflector signals) the high peaks of the scattering, resulting from the superimposing of the scattering processes from the grains in the sound beam (Fig. 26). Variation of the probe position by approximately one grain size alters this interference structure, and in Fig. 38(a) there are eight such A-scans plotted over each other (variation of position of the probe approximately 0·3 mm, corresponding to

one grain size). While the reflector signal—here a backwall echo with high amplitude—remains the same in amplitude and time of flight, the addition of the eight A-scans leads to a mean noise amplitude lying far below the single top values, so improving the signal-to-noise ratio. Figure 38(b) shows how it is possible to resolve more and more backwall echoes with an

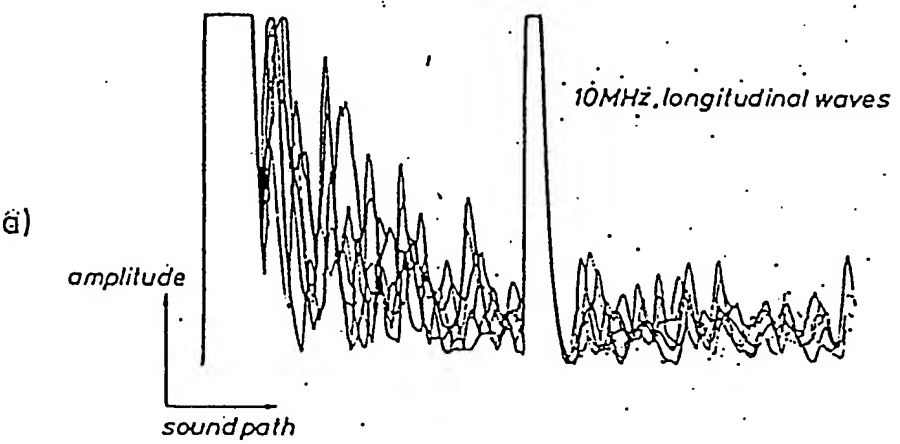

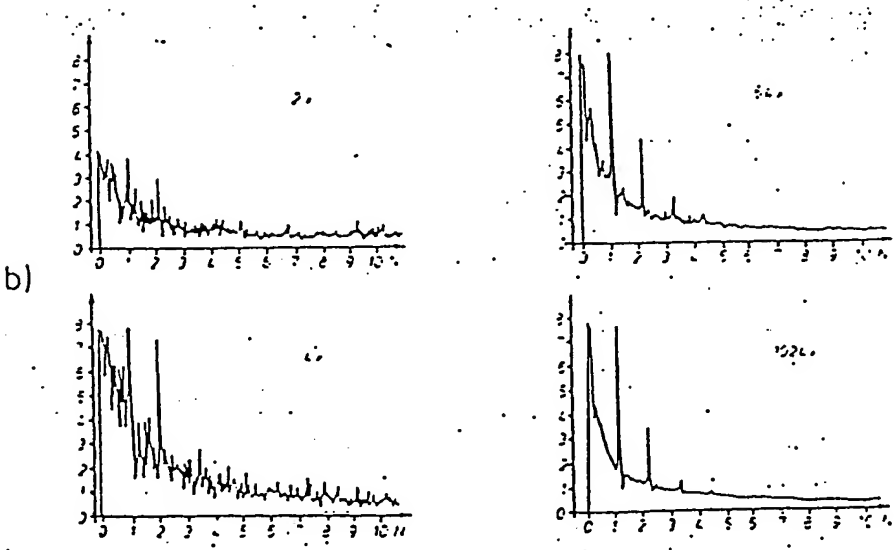

FIG. 38. Signal enhancement by increasing number of (spatial) averaging processes (N = nearfield length).

increasing number of averaging processes and the signal-to-noise ratio is entered in a distance–gain–size-diagram in Fig. 39. After approximately 256 processes, the optimum possible signal-to-noise ratio of $(\alpha_S \Delta x)^{-\frac{1}{2}}$ has been approached within a few dB. Increasing the number of processes to 1024 then brings only small improvements, although it progressively smoothes the curve of $A_S(x)$ between the single reflector signals (Kraus and Goebbels, 1977).

Principally this enhancement of signal-to-noise ratio is also valid for the detection of defects in a coarse-grained material. As long as the reflector size is larger than the grain size, an enhancement can be received over spatial and directional averaging at the defect (Goebbels *et al.*; 1978a; Kraus and Goebbels, 1977, 1978). The amplitude–locus curve (echodynamic) of the defect and its directional characteristic at the frequency averaging must be taken

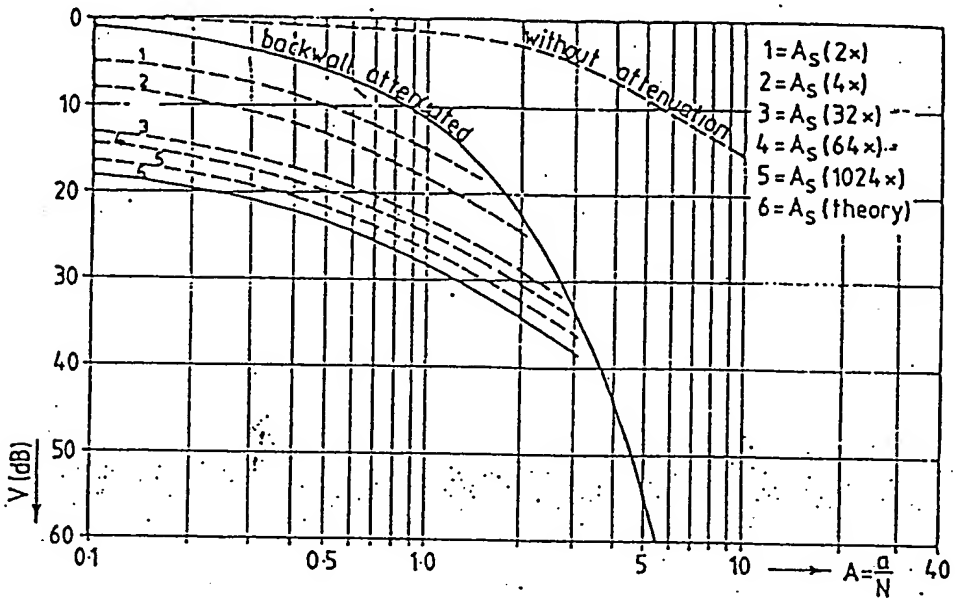

FIG. 39. DGS-diagram, number of averaging processes and improvement of signal-to-noise ratio.

into account according to the depth of the defect inside the material and the dimension of the defect, for instance by averaging in the amplitude fall for $\leqslant 6$ dB. Figure 40 contains three examples:

(a) Spatial averaging of a slag inclusion in an austenitic weld. The reflected amplitude after the averaging process corresponds to a side-drilled hole of 1 mm diameter.
(b) Directional averaging with 3 mm side-drilled hole in an austenitic weld.
(c) Frequency averaging of the same reflector as in Fig. 40(b).

Figure 41 shows that by signal averaging the signal-to-noise ratio not only can be improved, but it is also possible with a sufficient signal-to-noise ratio to identify signals which are completely lost in the noise in a single *A*-scan.

The development of fast ADCs and fast averagers therefore enables the use of signal averaging methods in the automatic on-line inspection of coarse-grained materials and welds.

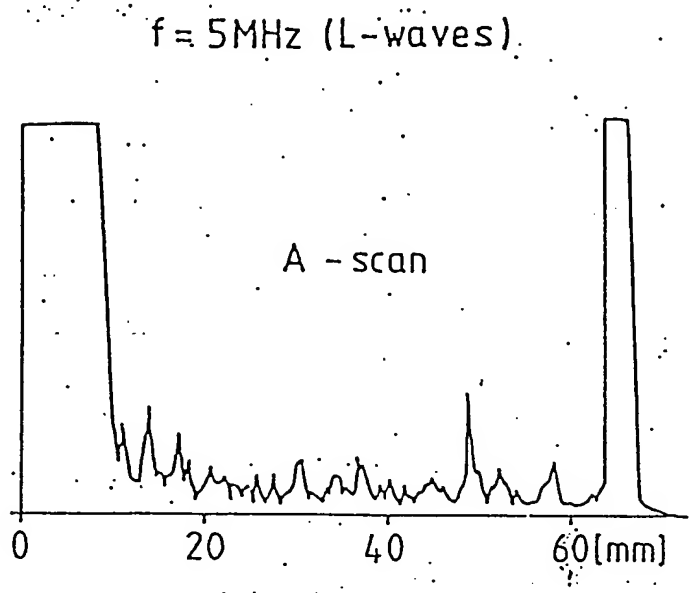

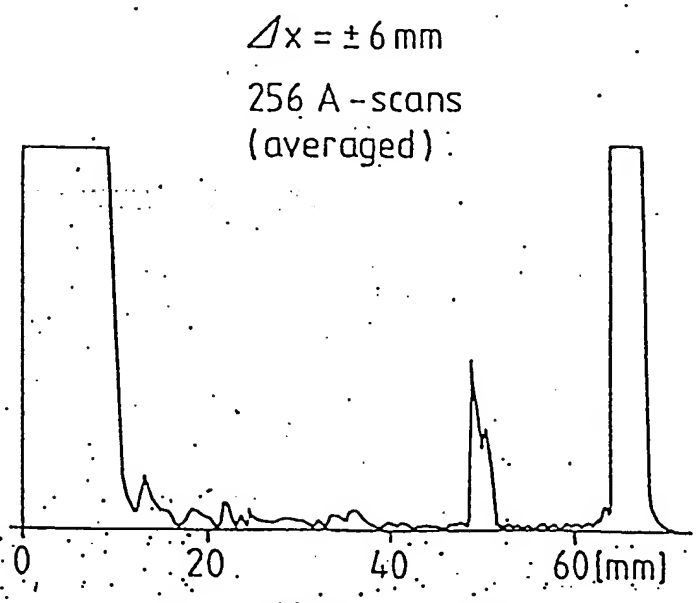

FIG. 40. (a) Spatial averaging.

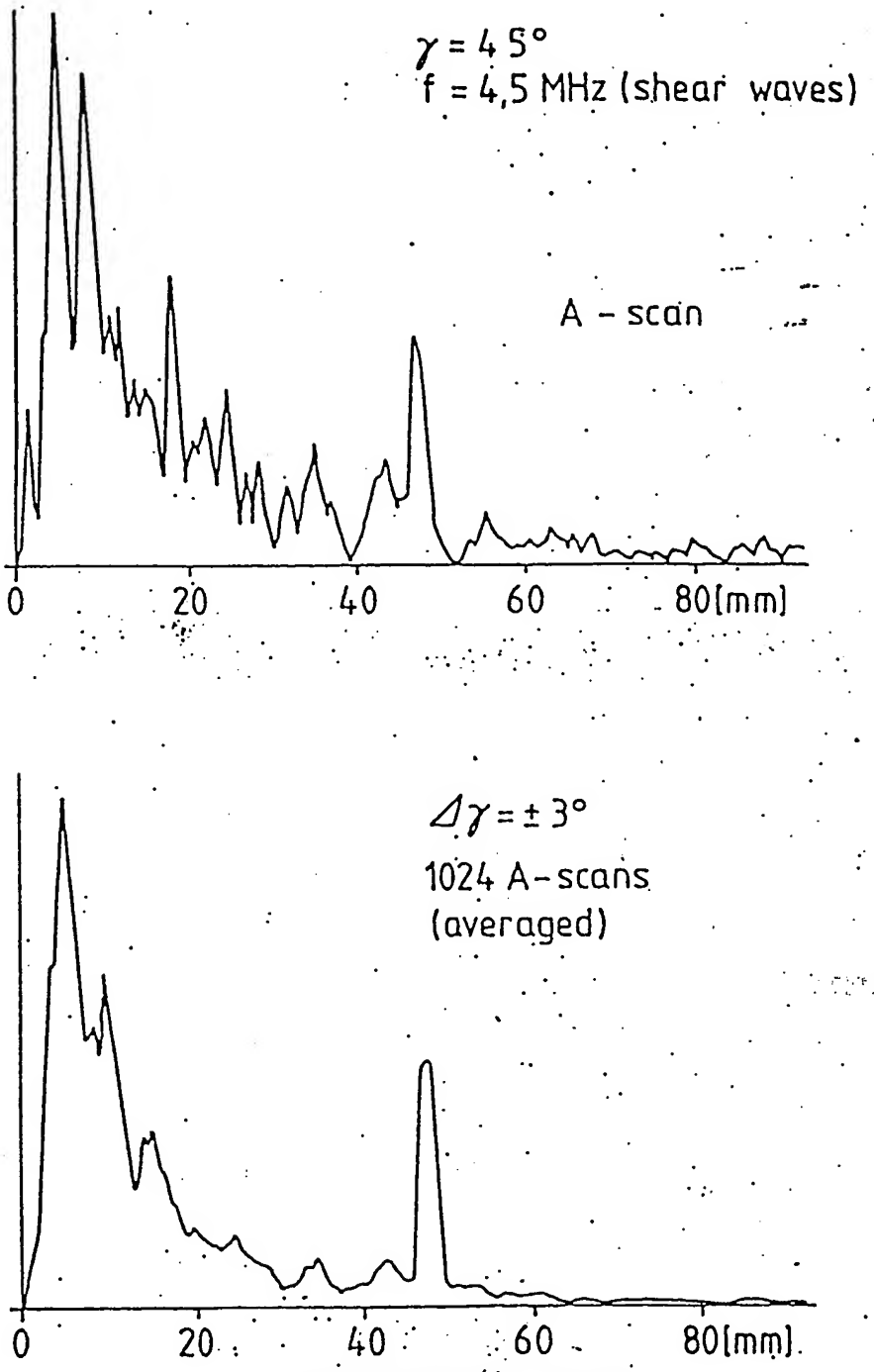

FIG. 40. (b) Directional averaging.

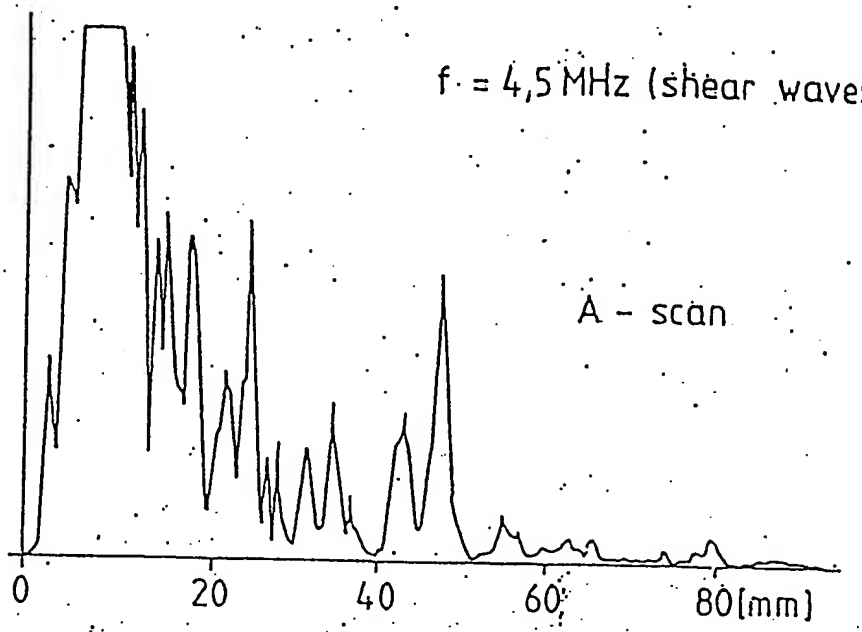

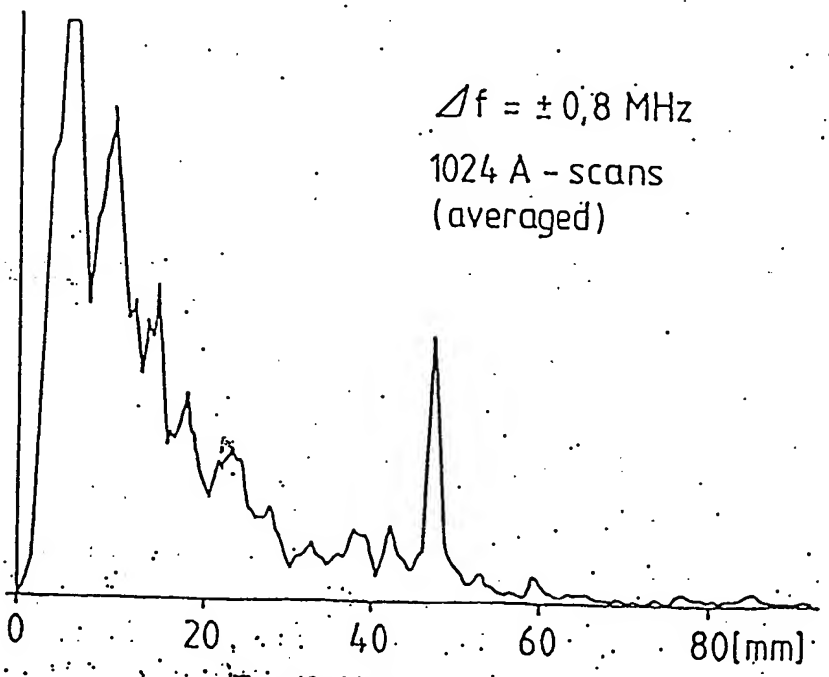

FIG. 40. (c) Frequency averaging.

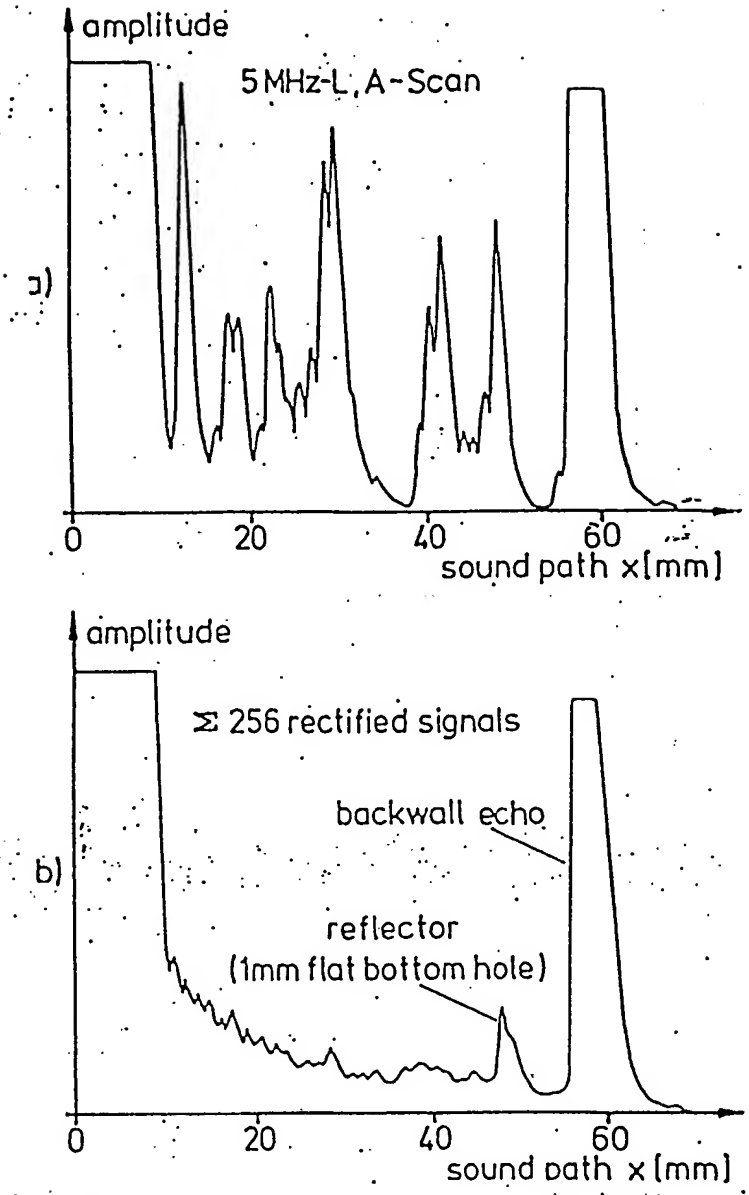

FIG. 41. Improvement of signal-to-noise ratio for a small reflector in a coarse-grain austenitic steel (ASTM 0).

IV. DISCUSSION AND FURTHER DEVELOPMENT

A. Theory

Although it is possible, at the present state of development, to use th scattering measurement for nondestructive structure characterization many materials, there are still many unsolved problems connected with th theoretical basis. The determination of the scattering coefficient for pol crystalline, monophasic systems according to Lifshits and Parkhomovsk (1948, 1950) and Bhatia and Moore (1959, 1969) can be assumed to be ful worked out in the Rayleigh region (Markgraf, 1963; Beecham, 196

elmann, 1967; Dunegan, 1964; DiGiacomo *et al.*, 1970; Szilard and cruton, 1973; Goebbels and Höller, 1976, 1978; Hill *et al.*, 1978). For tochastic and diffuse scattering, however, a corresponding theoretical eatment (which also takes into account mode conversion in the scattering rocess) has still to be found. The difficulty lies in selecting the type of catterer. It may be possible to develop corresponding solutions for models uch as spheres, cylinders (Varadan, 1978), discs, and strips, which have to egenerate in the case when $d \ll \lambda$ to the Rayleigh approximation, and in the ase when $d \gg \lambda$ to diffraction and geometrical reflection.

Ying and Truell (1956), Einspruch *et al.* (1960) and Truell *et al.* (1969) have robably completely solved the problem of scattering in two-phase structures ith isotropic phases and spherical scatterers, and this for any d/λ. Still nsolved, however, is the solution for any scatterer form. An approach xists for defining a scattering coefficient in two-phase systems with a poly-rystalline matrix, for instance, but as yet there are no experimental data. he scattering behaviour for macroscopic anisotropic structures (such as omposites) is completely unknown. Here is a wide-open field for further undamental investigation. Concerning multiple scattering it has been ossible to test successfully the works of Truell and co-workers (Waterman nd Truell, 1961; Truell *et al.*, 1969) by experiment (Latiff and Fiore, 1975; G bbels *et al.*, 1978b). The necessary limitation on "weak-scattering" in his case, i.e. $4\pi n_0 f(0)/k^2 \ll 1$ in eqn (31), has to be taken into consideration, nd for the diverging case there is still no practical solution in sight. The irection characteristic of the scattered ultrasound, depending on the icroscopic structure and d/λ, also seems to be an unsolved problem, as the ifferent functions of several authors in Fig. 15 show. A theory is necessary ere too, particularly because the directional characteristic can easily be omputed for the single scatterer under simplified boundary conditions Morse and Ingard, 1968; Malecki, 1969), but not for an assembly of andomly-oriented scatterers influencing each other, of equal or different orm and size.

B. Measurement Technique

There are no major difficulties with the mechanical and electronic design of equipment for scattering measurements. On the one hand, the development of electronic components is proceeding more rapidly (particularly ADCs and averagers, Linzer *et al.*, 1978; Kraus *et al.*, 1979) than practical realization is able to follow. On the other hand, the frequency region between 1 and 100 MHz, mostly used in nondestructive structural investigations, is more difficult to handle than low-frequency (kHz region) and very-high-frequency (-rowave) regions.

Resonant ultrasonic transducers are the only probes which can be used scattering measurements at present. Their phase sensitivity affects the cu of the scattering amplitudes $A_S(x)$ as in Figs 17 and 19, i.e. the scatteri information is contained in the interference pattern, but it can only be pul out by an averaging process. The development of a sensitive, phase-insensit transducer such as the acousto-electric transducer (Busse and Miller, 19 Heyman *et al.*, 1978) is, therefore, of great importance for scattering measu ments. It is expected that the backscattering measurement, from eqn (41) example, will be possible with this AET operating stationary. The accura and reproducibility of a scattering measurement are today relatively hi due to its many advantages over attenuation measurements. It can be ev further improved with an increasing number of averaging processes. Scatteri measurements taken on a large component at different "measurement poin must show, however, the same fluctuations as attenuation measuremer because small differences in structure produce large differences of α. Abso tion and scattering make equal contributions here.

C. Applications

Grain size determination by means of ultrasonic scattering measureme can be assumed to be reliable for practically any steels in the region AST 1–11 (Goebbels and Höller, 1978). This region includes—except for fi grained martensitic steels—the grain sizes existing in practice. Two-ph systems, such as pearlite, cannot be dealt with quantitatively at prese however. Similarly there is no possibility to describe quantitatively inhon geneous structures, with regard to type, geometry, dimension and conc tration of inhomogeneities, although their detection and also their qualitat interpretation are not difficult (Goebbels *et al.*, 1978b). The measurement backscattering presents an excellent nondestructive testing method h giving an insight into the material, even with a sound path of several hund millimetres, with good resolution.

The experience gained for steels can be transferred not only to ot metallic materials, but also to non-metallic materials such as ceramics a others. Complex multiphasic structures (e.g. composites) and orga materials including different kinds of medical tissues and emulsions are a open to scattering measurements.

For medical diagnosis, the qualitative problem of scattering measureme has been almost completely solved, and the different influencing parame are now known in principle (Hill *et al.*, 1978). A quantitative descripti however, is not yet possible. The directional characteristic of scattering the stochastic and diffuse region can be used to provide additional informat about microstructure; until now, however, this has not been used, pa because of fundamental lack of understanding.

V. Acknowledgements

The author would like to thank Professor P. Höller for his stimulating effect on this work. Major contributors are S. Kraus (signal averaging techniques) and S. Hirsekorn (two-phase systems). Their constructive criticism is gratefully acknowledged. The author would also like to express his appreciation to D. Bruche and to J. Maurer for performing the experimental measurements and for preparing the diagrams and Miss U. Brämer and Mrs Ch. Busch-Eicke for typing the manuscript.

References

Alers, G. A., Neighbours, J. R. and Sato, H. (1960). *J. Phys. Chem. Solids* 13, 40–55.
Aurich, D. and Martin, E. (1970). *Arch. Eisenhüttenwes.* 41, 282–291.
Beecham, D. (1966). *Ultrasonics* 4, 67–76.
Bhatia, A. B. (1959). *J. Acoust. Soc. Am.* 31, 16–23.
Bhatia, A. B. (1967). "Ultrasonic Absorption." Clarendon Press, Oxford.
Bhatia, A. B. and Moore, R. A. (1959). *J. Acoust. Soc. Am.* 31, 1140–1141.
Bradfield, G. (1964). *J. Iron Steel Inst.* 202, 616.
Bratina, W. J. (1971). *In* "Physics and Nondestructive Testing" (W. J. McGonnagle, ed.), pp. 117–139. Gordon and Breach, London, New York and Paris.
Busse, L. J. and Miller, J. G. (1978). III. Intern. Symp. Ultras. Imag. and Tissue Charact., Gaithersburg.
DiGiacomo, G., Ohlstein, G. and Jones, W. J. (1970). *Mat. Eval.* 28, 271–276.
Dunegan, H. L. (1964). *Mat. Eval.* 22, 353–359.
Einspruch, N. G. Witterholt, E. J. and Truell, R. (1960). *J. Appl. Phys.* 31, 806–818.
Ermolov, I. N. and Pilin, B. P. (1976). *NDT International* 9, 275–280.
Fay, B. (1973). *Acustica* 28, 354–357.
Fay, B. (1976a). *Arch. Eisenhüttenwes.* 47, 119–126.
Fay, B. (1976b). 1976 Ultras. Symp. Proc. IEEE, 51–53.
Foldy, L. L. (1945). *Phys. Rev.* 67, 107–119.
Franz, H. (1962). *Zeitschr. Metallkde* 53, 27–37.
Goebbels, K. (1975). *Materialprüf.* 17, 231–233.
Goebbels, K. (1976). *Materialprüf.* 18, 86–88.
Goebbels, K. and Höller, P. (1976). VIII WCNDT, Cannes, Paper 3F8.
Goebbels, K. and Höller, P. (1978). 1. Intern. Symp. Ultras. Materials Charact., Gaithersburg.
Goebbels, K., Deuster, G. and Greter, St.-E. (1974). Status Report "Ultrasonic Attenuation" (in German). IzfP Report No. 740209.
Goebbels, K., Greter, St.-E. and Höller, P. (1976). "Determination of Steel Structures by Means of Ultrasound." Report EUR-5776d, CEC, Luxembourg.
Goebbels, K., Kraus, S. and von Klot, R. (1978a). Seminar "ZfP in der Kernreaktortechnik"; Saarbrücken.
Goebbels, K., Kraus, S. and Zimmermann, W. (1978b). Europäische Tagung zfP, Mainz, Vortrag 47 Proc., pp. 403–410.
Granato, A. and Lücke, K. (1956). *J. Appl. Phys.* 27, 583–593.
Gubernatis, J. E., Domany, E. and Krumhansl, J. A. (1977). *J. Appl. Phys.* 48, 2804.
Hearmon, R. S. F. (1956). *Adv. Phys.* 5, 323–382.
Heyman, J. S., Cantrell, J. H. and Whitcomb, J. D. (1978). 1. Intern. Symp. Ultras. Materials Charact., Gaithersburg.

Hill, C. R., Chivers, R. C., Higgins, R. W. and Nicholas, D. (1978). *In* "Ultrasound: Its Application in Medicine and Biology" (F. J. Fry, ed.), Part I, pp. 441–493. Elsevier Scientific Publ. Co., Amsterdam.
Hirsekorn, S. (1979a). Izfp—Report 780157, Saarbrücken 1979.
Hirsekorn, S. (1979b). Izfp—Report 790218, Saarbrücken 1979.
Huntington, H. B. (1950). *J. Acoust. Soc. Am.* 22, 362–364.
Huntington, H. B. (1958). *Solid State Phys.* 7, 213–351.
Klinman, R., Webster, G. R., Marsh, F. J. and Stephenson, E. T. (1978). 1. Intern. Symp. Ultras. Materials Charact., Gaithersburg.
Kopec, B. (1975). *Ultrasonics* 13, 267–274.
Koppelmann, J. (1967). *Materialprüf.* 9, 401–436.
Koppelmann, J. (1971a). *Materialprüf.* 13, 382–387.
Koppelmann, J. (1971b). *Materialprüf.* 13, 289–291.
Koppelmann, J. (1972). *Materialprüf.* 14, 156–159.
Koppelmann, J. and Fay, B. (1973). *Acustica* 29, 297–302.
Kraus, S. and Goebbels, K. (1977). Izfp—Report 760717, Saarbrücken 1977.
Kraus, S. and Goebbels, K. (1978). 1. Intern. Symp. Ultras. Materials Charact., Gaithersburg.
Kraus, S., Neumann, R. and Goebbels, K. (1979). 9 WCNDT, Melbourne, Paper 445.
Krautkrämer, J. and Krautkrämer, H. (1975). "Werkstoffprüfung mit Ultraschall." Springer, Berlin.
Latiff, R. H. and Fiore, N. F. (1975). *J. Acoust. Soc. Am.* 57, 1441–1447.
Lax, M. (1952). *Phys. Rev.* 85, 621–629.
Lifshits, I. M. and Parkhomovskii, G. D. (1948). *Uc. Zap. Charkov Gos. Univ. Im.* 27, 25–35.
Lifshits, I. M. and Parkhomovskii, G. D. (1950). *Zh. Eksp. i Theor. Fiz.* 20, 175–182.
Linzer, M., Shideler, R. S. and Parks, S. I. (1978). 1. Intern. Symp. Ultras. Materials Charact., Gaithersburg.
Lord, A. E., Deisher, J. N. and Koerner, R. M. (1977). *Mat. Eval.* 35, 49–64.
Lücke, K. (1956). *J. Appl. Phys.* 27, 1433–1438.
Malecki, I. (1969). "Physical Foundations of Technical Acoustics." Pergamon Press, Oxford.
Markgraf, H. (1963). Dissertation, Humboldt-Universität, Berlin.
Martin, E. and Aurich, D. (1972). *Metall* 26, 791–801.
Martius, U. M. and Bratina, W. J. (1961). *J. Appl. Phys. Suppl.* 32, 280S-281S.
Mason, W. P. and McSkimin, H. J. (1947). *J. Acoust. Soc. Am.* 19, 464–473.
Mason, W. P. and McSkimin, H. J. (1948). *J. Appl. Phys.* 19, 940–946.
Mason, W. P. and McSkimin, H. J. (1949). *J. Appl. Phys.* 20, 228–229.
Mercier, N. (1975). *In* "Ultrasonics International 1975 Conference Proceedings", pp. 64–67. IPC, Guildford, U.K.
Merkulov, L. (1957a). *Sov. Phys.—Techn. Phys.* 1, 59–69.
Merkulov, L. (1957b). *Sov. Phys.—Techn. Phys.* 2, 953–957.
Merkulov, L. (1957c). *Sov. Phys.—Techn. Phys.* 2, 1282–1286.
Morse, P. M. and Ingard, K. U. (1968). "Theoretical Acoustics." McGraw-Hill, New York.
Papadakis, E. P. (1964). *J. Appl. Phys.* 35, 1474–1482.
Papadakis, E. P. (1965). *J. Acoust. Soc. Am.* 37, 703–710.
Papadakis, E. P. (1968). *J. Acoust. Soc. Am.* 43, 876–879.
Papadakis, E. P. and Reed, E. L. (1961). *J. Appl. Phys.* 32, 682–687.

3. *HF- and DC-averaging*

Another essential topic concerns the distinction between HF- and DC-averaging. The oscillating HF-scattering signal (Fig. 19) possesses positive and negative amplitude values. The averaging of this during spatial, directional, or frequency averaging thus results in the addition of positive and negative parts and ultimately in the disappearance of the scattering signals.

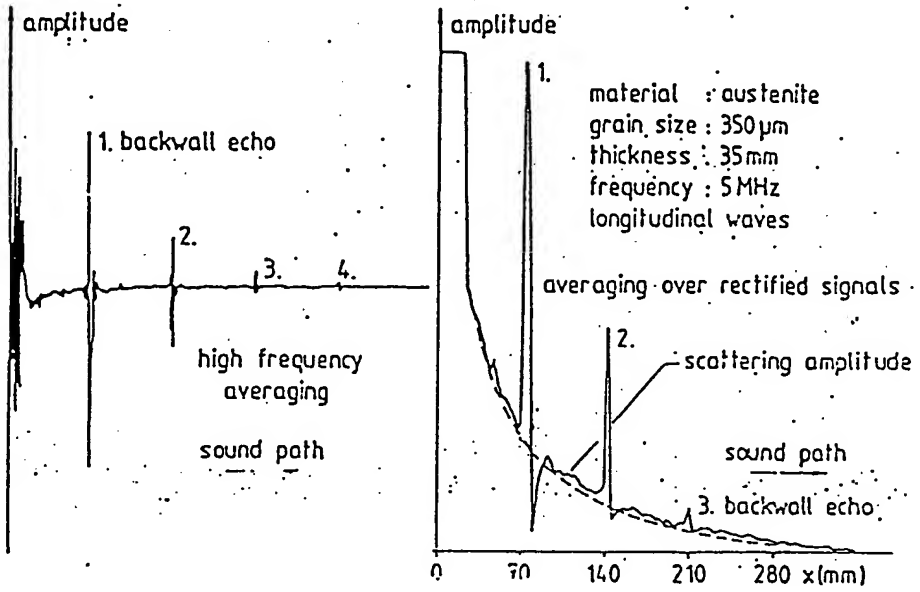

FIG. 25. Comparison between HF- and DC- averaging.

While HF-averaging cannot therefore be used for scattering measurements, this suppression of the coherent noise is of great advantage for the measurement of signals such as backwall echo sequences and flaw signals. Figure 25 shows how the HF-averaging resolves more backwall echoes and with higher signal-to-noise ratio than DC-averaging, the result of which is $A_S(x)$ according to eqn (41), with the superimposed backwall echo sequence. For the backwall echo sequence with constant sound path (flat, even parallel-sided sample) this advantage can be seen clearly. Rough surfaces, fluctuating coupling and differences in times of flight at different test locations, however, affect the detection of defects in the same way as they affect scattering: extinctions of the interesting defect signal will also result. For known geometric test conditions, the influence of the time of flight (amplitude locus curves) can be taken into account by the synthetic aperture approach to the detection of defects (Van den Broek *et al.*, 1978). Generally, in practice, the reliable (but, by some dB, smaller) resolution of DC-averaging is to be preferred to HF-averaging.

Pekeris, C. L. (1947). *Phys. Rev.* 71, 268–269.
Rayleigh (1945). "Theory of Sound", Vol. II, pp. 149–152. Dover Publishers, New York.
Richter, H.-U. (1965). Dissertation, TH Otto v. Guericke, Magdeburg.
Richter, H.-U. (1968). *Die Technik* 23, 610–619.
Rokhlin, L. L. (1972). *Sov. Phys.-Acoust.* 18, 71–75.
Roney, R. K. (1950). Dissertation, CALTEC, Pasadena.
Salmutter, K. and Stangler, F. (1960). *Zeitschr. Metallkde* 51, 544–548.
Seeger, A. and Schiller, P. (1962). *Acta Met.* 10, 348–357.
Seemann, H. J. and Bentz, W. (1954). *Zeitschr. Metallkde* 45, 663–669.
Serabian, S. and Williams, R. S. (1978). *Mat. Eval.* 36, 55–62.
Sigelmann, R. A. and Reid, J. M. (1973). *J. Acoust. Soc. Am.* 53, 1351–1355.
Skudrzyk, E. (1957). *J. Acoust. Soc. Am.* 29, 50–60.
Szilard, J. and Bihari, I. (1965). V. Congrès Intern, d'Acoustique, Liège, Paper D 12.
Szilard, J. and Scruton, G. (1973). *Ultrasonics* 11, 114–120.
Tietz, H. D. (1974). "Ultraschall-Messtechnik." Verlag Technik, Berlin.
Truell, R., Elbaum, C. and Chick, B. B. (1969). "Ultrasonic Methods in Solid State Physics." Academic Press, New York and London.
Van den Broek, C., Elzinga, M. B., Frederick, J. R. and Ganapathy, K. (1978). 1. Intern. Symp. Ultras. Materials. Charact., Gaithersburg.
Varadan, V. V. (1978). *J. Acoust. Soc. Am.* 63, 1014.
Varadan, V. V. and Pao, Y.-H. (1976). *J. Acoust. Soc. Am.* 60, 556.
Vary, A. (1978a). *Mat. Eval.* 35, 55–65.
Vary, A. (1978b). NASA Technical Memorandum TM–78905.
Walzer, P., Koehler, M. and Rottenkolber, P. (1976). *Motortechn. Z.* 37, 525–529.
Waterman, P. C. (1968). *J. Acoust. Soc. Am.* 45, 1417–1429.
Waterman, P. C. (1976). *J. Acoust. Soc. Am.* 60, 567.
Waterman, P. C. and Truell, R. (1961). *J. Math. Phys.* 2, 512–537.
Wüstenberg, J., Just, T., Möhrle, W. and Kutzner, J. (1977). *Materialpruf.* 19, 246–251.
Ying, C. F. and Truell, R. (1956). *J. Appl. Phys.* 27, 1086–1097.